DOCTORAL THESIS
Presented to the Department of Pharmacy
Graduate School of Pharmaceutical Science

The University of Naples Federico II
For the Degree of

DOCTOR OF PHILOSOPHY

MULTIFUNCTIONAL NANOPARTICLES FOR CANCER THERAPY

by

SARA MAIOLINO

APPROVED BY

Supervisor: Prof. Fabiana Quaglia
PhD Program Coordinator: Prof. Maria Valeria D'Auria

University of Naples Federico II, Naples, Italy
March, 2016

TABLE OF CONTENT

ABBREVIATIONS

ABC	ATP-binding cassette
ADCs	Antibody-drug conjugate
CLSM	Confocal laser scanner microscopy
CPT	Camptothecin
DOX	Doxorubicin
DTX	Docetaxel
ECM	Extracellular matrix
EPR	Enhanced Permeability and Retention Effect
FBS	Fetal bovin serum
FDA	Food and drugs administration
FRET	Fluorescence-guided resection
FU	Fluorouracil
GFP	Green Fluorescence Protein
HA	Hyaluronic acid
HARE	HA receptor for endocytosis
HER 2	Growth factor receptor 2
HYAL	Hyaluronidases
L-OHP	Oxaliplatinum
MDR	Multiple drug resistance
miRNA	Micro RNA
MPS	Malignant pleural mesothelioma
NO	Nitric oxide
NOPD	NO photodonors
NP	Nanoparticle
NR	Nile Red
PAA	Poly(acrylic acid)
PAAm	Poly(acrylamide)
PCL	Poly(caprolactone)
PDEAEMA	Poly(diethylaminoethyl methacrylate)
pDNA	Plasmid
PDT	Photodynamic therapy
PEG	Poly(ethyleneglycol)

PEI	Polyethyleneimine
PEO	Poly(ethyleneoxide)
Pgp	P-glycoprotein
PLA	Poly(lactic)acid
PLL	Poly-L-lysine
PLGA	Poly(lactic-co-glycolic acid)
PMA	Poly(methacrylic acid)
pNIPAM	Poly(N-isopropylacrylamide isopropylacrylamide).
PPO	Poly(propylene oxide
PS	Photosensitizing agent
PTT	Photothermal therapy
PTX	Paclitaxel
RES	Reticuloendothelial system
RHAMM	Receptor for Hyaluronan-mediated motility CD168
RHO	Rhodamine
ROS	Reactive oxygen species
shRNA	Short hairpin RNA
siRNA	Small interfering RNA
SRB	Sorafenib
TLR	Toll-like receptor
TNF	Tumour necrosis factor
TPPS	Tetraphenylporphirine
VP	Verteporfin
VEGF	Vascular endothelial growth factor

Chapter 1
Introduction and aim

Chapter 1

1 Drawbacks in cancer chemotherapy

Cancers figure among the leading causes of morbidity and mortality worldwide and consist in an uncontrolled and fast cellular proliferation due to a combination of different mutation. This is coupled to a chaotic irregular generation of blood vessels which give nutrients and oxygen to tumor tissues, and a degradation of the extracellular matrix (ECM) which confines the stromal mass of solid tumor.[1]Metastasis, the spread of cancer from primary tumors to secondary tumors in distant sites, is one of the main issue to manage in cancer treatments. For many patients, when cancer is detected, metastases have just developed. Although cancer therapies are improving, many drugs are not reaching the site of metastases, and doubt remains over the efficacy of those that do.[2]

Cancer treatment is currently based on a combination of surgery, radiotherapy, chemotherapy, and more recently immunotherapy. Each treatment modality bears advantages and drawbacks and needs to be established depending on tumor location, stage of tumor growth, and presence of metastasis. Chemotherapy is one of the principal modes of treatment for cancer. The main Achilles‘ heel in a chemotherapeutic regimen resides in poor selectivity of the treatment that generates severe side effects, contributing to decrease patient compliance and quality of life.[3]Indeed, the vast majority of chemotherapeutics are administered by the intravenous route, distribute in the whole body according to their physical chemical features – which drive interactions with plasma proteins – and reach, besides diseased tissue, also healthy organs. Furthermore, several conventional chemotherapeutics, such as taxanes, are poorly water-soluble and are formulated in pharmaceutical vehicles including synthetic solvents (polysorbate 80 or castor oil) that directly

[1]A. K. Iyer, A. Singh, S. Ganta, and M. M. Amiji, "Role of integrated cancer nanomedicine in overcoming drug resistance," *Advanced Drug Delivery Reviews* 65, no. 13-14 (2013).

[2]A. Schroeder, D. A. Heller, M. M. Winslow, J. E. Dahlman, G. W. Pratt, R. Langer, T. Jacks, and D. G. Anderson, "Treating metastatic cancer with nanotechnology," *Nature Reviews Cancer* 12, no. 1 (2012).

[3]S. P. Egusquiaguirre, M. Igartua, R. M. Hernandez, and J. L. Pedraz, "Nanoparticle delivery systems for cancer therapy: advances in clinical and preclinical research," *Clinical & Translational Oncology* 14, no. 2 (2012).

contribute to adverse effects.[4] Thus, a fine balance between therapeutic and toxic effects needs to be found for each patient adapting standard combination protocols time by time.

The effectiveness of a chemotherapy is also limited by intrinsic or acquired drug resistance.[5,6] Upon treatment, tumor develops drug resistance mechanisms, which can be roughly grouped into five categories: i) induction of drug transporters, ii) DNA repair, iii) change in drug metabolism, iv) gene amplification or mutation of target proteins, v) changes in survival/apoptotic pathways. The overexpression of multidrug transporters and the altered apoptosis are the major mechanisms of drug resistance. In particular, the up-regulation of transmembrane drug efflux pumps under the ATP-binding cassette (ABC) superfamily actively pump the drug out of the cancer cell which reduces drug intracellular concentration and activity as well. These transporters act on a variety of anticancer drugs, such as a glycoprotein (P-gp)which is over-expressed in liver cancers and can pump out Doxorubicin (DOX) and paclitaxel (PTX).[7]

Although the knowledge of molecular, cellular, and physiological mechanisms involved in the initiation and progression of cancer has been significant refined, the benefit of cancer treatments remains mainly confined to an increased survival of patients while ensuring a sufficiently good quality of life.[8]

[4]R. K. Jain and T. Stylianopoulos, "Delivering nanomedicine to solid tumors," *Nat.Rev.Clin.Oncol.* 7, no. 11 (2010).

[5]C. Holohan, S. Van Schaeybroeck, D. B. Longley, and P. G. Johnston, "Cancer drug resistance: an evolving paradigm," *Nature Reviews Cancer* 13, no. 10 (2013).

[6]Q. Wu, Z. P. Yang, Y. Z. Nie, Y. Q. Shi, and D. M. Fan, "Multi-drug resistance in cancer chemotherapeutics: Mechanisms and lab approaches," *Cancer Letters* 347, no. 2 (2014).

[7]H. Y. Yuan, X. Li, J. F. Wu, J. P. Li, X. J. Qu, W. F. Xu, and W. Tang, "Strategies to overcome or circumvent P-glycoprotein mediated multidrug resistance," *Current Medicinal Chemistry* 15, no. 5 (2008).

[8]Rebecca A. Burrell, Nicholas McGranahan, Jiri Bartek, and Charles Swanton, "The causes and consequences of genetic heterogeneity in cancer evolution," *Nature* 501, no. 7467 (2013).

2 Nanocarriers for cancer therapy

2.1 Generalities

In the past twenty years, nanotherapeutics have been introduced in the clinical practice for treating tumors with the goal to improve therapeutic outcome of conventional pharmacological therapies and to alleviate their toxicity as well as to overcome multidrug resistance (MDR).[9,10,11,12]

Nanomedicine is described as the application of nanotechnology to medicine and healthcare, nanotechnology consist of engineering materials and systems on the nanometer scale (10-200 nm).Nanoscale delivery system scarrying an anticancer drug can in theory offer the advantages of drug protection from degradation, efficient control of pharmacokinetics and accumulation in tumor tissue, thus limiting drug interaction with healthy cells and as a consequence side effects.

In the attempt to improve the rate of success of a cancer therapy, chemotherapeutics should i) be able to reach the desired tumor tissues through the penetration of barriers in the body with minimal loss of activity in the bloodstream; ii) drugs should have the ability to selectively kill tumor cells without affecting normal cells and extend their effect over time.

The delivery of chemotherapeutics through nanocarriers has been mainly focused on intravenous route to reach remote sites in the body through blood system.[13]In fact, the unique properties of tumor vasculature and microenvironment result in a natural tendency of a nanocarrier bearing a drug cargo to accumulate in solid tumors referred

[9]K. K. Jain, "Advances in the field of nanooncology," *BMC.Med.* 8 (2010).

[10]A. Z. Wang, R. Langer, and O. C. Farokhzad, "Nanoparticle delivery of cancer drugs," *Annu.Rev.Med.* 63 (2012).

[11]J. L. Markman, A. Rekechenetskiy, E. Holler, and J. Y. Ljubimova, "Nanomedicine therapeutic approaches to overcome cancer drug resistance," *Adv.Drug Deliv.Rev.* 65, no. 13-14 (2013).

[12]Srinath Palakurthi, Venkata Kashyap Yellepeddi, and Kiran Kumar Vangara, "Recent trends in cancer drug resistance reversal strategies using nanoparticles," *Expert Opinion on Drug Delivery* 9, no. 3 (2012).

[13]D. M. Webster, P. Sundaram, and M. E. Byrne, "Injectable nanomaterials for drug delivery: Carriers, targeting moieties, and therapeutics," *Eur.J.Pharm.Biopharm.* (2013).

as passive targeting.[14,15] Architectural defectiveness and high degree of vascular density generate abnormal ―leaky" tumor vessels, aberrant branching and blind loops of twisted shape. Blood vessels in tumor present an irregular architecture compared with those in normal tissue. Tumor vessels are heterogeneous in their spatial distribution, dilated and tortuous, leaving a vascular spaces of various size. In addition, in tumors, vassel-wall structure is abnormal with interendothelial junctions, present an abnormally thick or thin basement membrane, large numbers of fenestrae and transendothelial channels formed by vesicles, and maximum pore diameters as large as several hundred nanometers (Fig. 1).

[14]Hiroshi Maeda, "Macromolecular therapeutics in cancer treatment: The EPR effect and beyond," *Journal of Controlled Release* 164, no. 2 (2012).

[15]Jun Fang, Hideaki Nakamura, and Hiroshi Maeda, "The EPR effect: Unique features of tumor blood vessels for drug delivery, factors involved, and limitations and augmentation of the effect," *Advanced Drug Delivery Reviews* 63, no. 3 (2011).

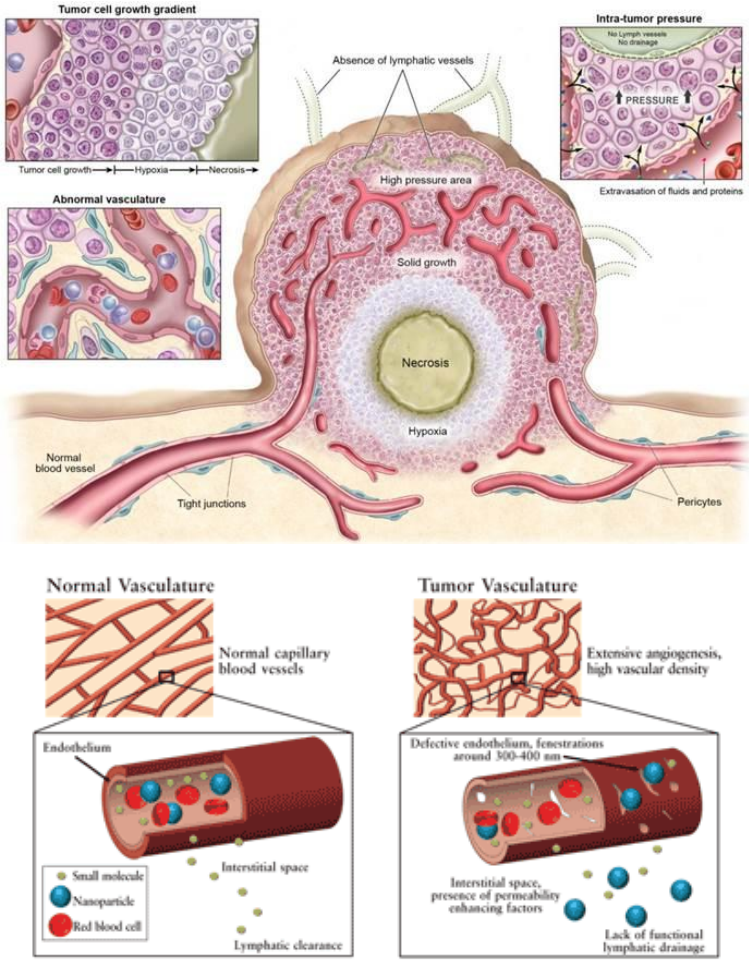

Fig. 1. (Top) Main features of a solid tumor relevant for nanodelivery. **(Bottom)** Enhanced Permeability and retention (EPR) effect Hisataka Kobayashi, ―Improving conventional EPR effects; what is the appropriate target? ―*Theranostics,* 4 (2014). The accumulation of a drug delivery platform by the EPR effect requires high sustained plasma concentrations. Minimizing accumulation in peripheral tissue by transendothelial or paracellular transport is important in maintaining high plasma concentrations (*http://www.uspharmacist.com/content/s/197/c/33020/*).

Moreover, normal lymphatic network drains excess fluid from tissue in order to maintain tissue interstitial fluid balance. In tumor tissue the proliferating cancer cells compress lymphatic vessels, particularly at the center of the tumor, causing their collapse. Impaired lymphatic drainage

decreases the clearance of locally resident macromolecules. Blood flow behavior, such as direction of blood flow, is also irregular or inconsistent in these vessels. The pore size of tumor vessels varies from 100 nm to almost 1 mm in diameter, depending upon the anatomic location of the tumors and the stage of tumor growth.

EPR effect enables nanocarriers to extravasate through the hyperpermeable tumor blood vessels into extravascular spaces and to accumulate inside tumor tissues (Fig.2).

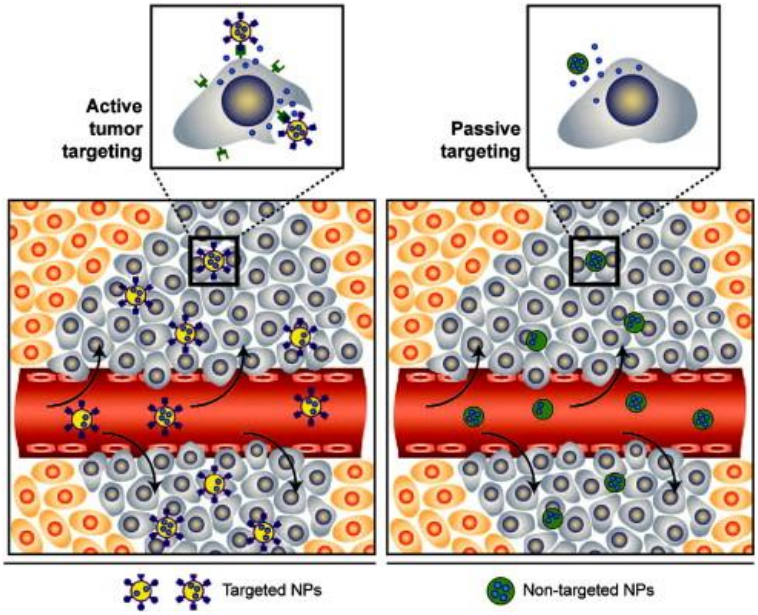

Fig. 2. Passive *vs* active targeting. (Right) NPs tend to passively (by their biophysicochemical properties) extravasate through the inflammated vasculature; (Left) Once NPs have extravasated in the target tissue, the presence of targeting ligands (e.g. proteins) on the NP surface. Morteza Mahmoudi, ―Superparamagnetic iron oxide nanoparticles (SPIONs): Development, surface modification and application in chemotherapy, ―*Advanced Drug Delivery Reviews* 63, no 24-46 (2011).

Furthermore, nanocarrier decoration with ligands that specifically recognize peculiar elements on the membrane of tumor cells has been considered the most favourable option to increase accumulation in cancer tissue, an approach known as active targeting (Fig. 2). These two basic strategies are expected to simultaneously increase the intracellular concentration of drugs and to reduce dose-limiting toxicities finally improving patient survival and quality of life. Nevertheless, exploiting

EPR effect is complicated by the presence of physiological elimination processes, including both renal clearance and mononuclear phagocyte system (MPS) uptake.

Nanocarriers can be designed also with exquisite responsiveness to tumor environment (pH, temperature, redox potential) or external stimuli (light, magnetic field, ultrasound, temperature), which can in theory trigger drug release only at tumor level.[16,17,18,19,20,21,22.]

Over recent decades, several nanosized carriers made of different materials such as lipids, polymers, metals, inorganic materials have been proposed in the biomedical field as therapeutic and diagnostic tools (Fig.3).

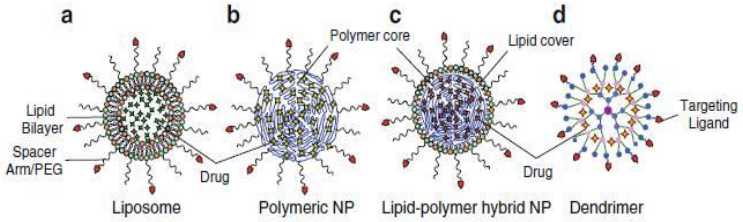

Fig. 3. Examples of nanoplatforms used in drug development Archana Swami, ―Nanoparticles for targeted and temporally controlled drug delivery" *Springer* (2012)

[16]C. S. Kim, B. Duncan, B. Creran, and V. M. Rotello, "Triggered Nanoparticles as Therapeutics," *Nano.Today.* 8, no. 4 (2013).

[17]V. Torchilin, "Multifunctional and stimuli-sensitive pharmaceutical nanocarriers," *Eur.J.Pharm.Biopharm.* 71, no. 3 (2009).

[18]S. Mura, J. Nicolas, and P. Couvreur, "Stimuli-responsive nanocarriers for drug delivery," *Nat.Mater.* 12, no. 11 (2013).

[19]Weiwei Gao, Juliana M. Chan, and Omid C. Farokhzad, "pH-Responsive Nanoparticles for Drug Delivery," *Mol.Pharmaceutics* 7, no. 6 (2010).

[20]J. Z. Du, C. Q. Mao, Y. Y. Yuan, X. Z. Yang, and J. Wang, "Tumor extracellular acidity-activated nanoparticles as drug delivery systems for enhanced cancer therapy," *Biotechnol.Adv.* 32, no. 4 (2013).

[21]S. Nowag and R. Haag, "pH-Responsive Micro- and Nanocarrier Systems," *Angew.Chem.Int.Ed Engl.* 53, no. 1 (2014).

[22]S. R. Abulateefeh, S. G. Spain, J. W. Aylott, W. C. Chan, M. C. Garnett, and C. Alexander, "Thermoresponsive polymer colloids for drug delivery and cancer therapy," *Macromol.Biosci.* 11, no. 12 (2011).

There are currently six FDA-approved nanomedicine (Table 1): brentuximab vedotin and trastuzumab amtansine, Doxil, DaunoXome, Marquibo and Abraxane.[23]

Table 1. FDA-approved nanomedicines.

Platform	class	drug	Size (nm)	Issue addressed
Brentuximab Vedotin®	ADC	Monomethyl auristan E	10	Drug is too toxic to be used alone
Trastuzumab Emtansine®	ADC	Mertansine	10	Drug is too toxic to be used alone
Myocet	Liposome	Doxorubicin	100	Cardiac side effect
Doxil®	Liposome	Doxorubicin	100	Cardiac side effect
DaunoXome®	liposome	Daunorubicine	50	Cardiac side effect
Marqibo®	liposome	Vincristine	100	Cardiac side effect
Abraxane®	Protein carrier	Paclitaxel	130	Overcome very slow solubiliy of drug

Brentuximab, Vedotin and Trastuzumab emtansine are antibody-drug conjugate (ADCs), conceptually engineered for targeting molecule respectively to the CD30 protein and growth factor receptor 2 (HER2). This drugs are too toxic to be used alone. Doxil, DaunoXome and Marquibo are liposomal nanomedicines. Doxil is a pegylated liposome about 100 nm in diameter and encapsulating about 10.000 DOX molecules.[24]Encapsulation minimizes side effects, such as cardiotixicity associated with high dose of DOX. DaunoXome and Marqibo are liposomal formulation of Daunorubicin and Vincristine, respectivetly.In contrast to Doxil the design strategy for DaunoXome and Marqibo is to promote uptake by MPS, proving a reservoir from which the free drug can enter circulation, similar to slow infusion. DaunoXome is about 50

[23]C. M. Dawidczyk, C. Kim, J. H. Park, L. M. Russell, K. H. Lee, M. G. Pomper, and P. C. Searson, "State-of-the-art in design rules for drug delivery platforms: Lessons learned from FDA-approved nanomedicines," *Journal of Controlled Release* 187 (2014).

[24]Y. Barenholz, "Doxil (R) - The first FDA-approved nano-drug: Lessons learned," *Journal of Controlled Release* 160, no. 2 (2012).

nm in diameter and Marqibo 100 nm.[25,26]Myocet works analogously to those latters. Abraxane or nab-paclitaxel (nanoparticle albumin bound) is lyophilized human serum albumin non-specifically bound to paclitaxel. Paclitaxel has very low solubility and is administered ina toxic non-ionic solvent which gives allergic reaction. The diameter of nab-paclitaxel is 130 nm and it contains 10.000 Paclitaxel molecules per nanoparticle.[27]

2.2 Nanocarriers in cancer: biologically driven design rules

To take benefit of EPR effect, nanocarriers need to escape from filtration through the glomerular capillary wall (filtration-size threshold) which depends on molecular weight and allows molecules with a diameter larger than 15 nm to remain in the circulation. Opsonin adsorption on nanocarrier surface mediates MPS recognition and is considered a key factor to control nanocarrier biodistribution in the body.[28] Due to opsonizations, nanocarriers fast disappearance from blood circulation and accumulation in the MPS organs (liver, spleen, bone marrow) occurs. Accumulation in the liver can be of benefit for the chemotherapeutic treatment of MPS localized tumors (e.g. hepatocarcinoma or hepatic metastasis arising from digestive tract or gynecological cancers, bronchopulmonary tumors) but undesirable when trying to target other body compartments (Fig.4).

In order to overcome opsonization, a number of strategies have been investigated to make a nanocarrier ~~–s~~tealth", that is able to evade MPS and long-circulating. Coating with a hydrophilic shell can form a cloud on nanocarrier surface which repels opsonins giving decreased levels of

[25]P. S. Gill, J. Wernz, D. T. Scadden, P. Cohen, G. M. Mukwaya, J. H. vonRoenn, M. Jacobs, S. Kempin, I. Silverberg, G. Gonzales, M. U. Rarick, A. M. Myers, F. Shepherd, C. Sawka, M. C. Pike, and M. E. Ross, "Randomized phase III trial of liposomal daunorubicin versus doxorubicin, bleomycin, and vincristine in AIDS-related Kaposi's sarcoma," *Journal of Clinical Oncology* 14, no. 8 (1996).

[26]J. A. Silverman and S. R. Deitcher, "Marqibo (R) (vincristine sulfate liposome injection) improves the pharmacokinetics and pharmacodynamics of vincristine," *Cancer Chemotherapy and Pharmacology* 71, no. 3 (2013).

[27]E. Miele, G. P. Spinelli, E. Miele, F. Tomao, and S. Tomao, "Albumin-bound formulation of paclitaxel (Abraxane (R) ABI-007) in the treatment of breast cancer," *International Journal of Nanomedicine* 4, no. 1 (2009).

[28]M. P. Monopoli, C. Aberg, A. Salvati, and K. A. Dawson, "Biomolecular coronas provide the biological identity of nanosized materials," *Nat Nanotechnol.* 7, no. 12 (2012).

uptake by the MPS and longevity in the blood, finally promoting nanocarrier accumulation in solid tumors through EPR mechanism.[29] Engineering a nanocarrier with a biomimetic shell of polyethylenglycol (PEG) is the most explored strategy to obtain long-circulating NPs[30] although other alternatives polymers are under investigation. Thus, nanocarriers with hydrophobic surfaces will preferentially be taken in MPS organs while long-circulating nanocarriers fulfilling size requirements (less than 100 nm) can accumulate at tumor level.

By exploiting passive mechanisms, only a limited nanocarrier fraction can reach tumor site.[31] Recent findings highlight that variation of nanocarrier dimension in the scale length > 100 nm can heavily affect blood circulation time, whereas the role of geometry in driving in vivo biodistribution has not been clarified yet.[32,33] Only an amount around 10% of the injected dose benefits of EPR effect while the remnant is accumulated in spleen, liver and bone marrow. Drug cargo can be after released systemically or inside tumors and this is found to allow a significant decrease of side effects. Current research efforts are focused on finding strategies to increase tumor to healthy tissue ratio and to improve tumor response. Targeting endothelial cells in defective tumor vasculature (i.e. integrin receptor) is one of the most advanced strategies under investigation .

Although extracellular matrix itself seems not an evident obstacle to NP passage, tissue neighboring tumor cells are surrounded by coagulation-derived matrix gel (fibrin gel or stromal tissues) representing a further barrier to drug transport. Nevertheless, penetration in the remote area of a solid tumor (hypoxic zones) is strictly related to

[29]Z. Amoozgar and Y. Yeo, "Recent advances in stealth coating of nanoparticle drug delivery systems," *Wiley Interdiscip.Rev Nanomed Nanobiotechnol* 4, no. 2 (2012).

[30]R. Gref, A. Domb, P. Quellec, T. Blunk, R. H. Muller, J. M. Verbavatz, and R. Langer, "The controlled intravenous delivery of drugs using PEG-coated sterically stabilized nanospheres," *Advanced Drug Delivery Reviews* 64 (2012).

[31]F. Alexis, E. Pridgen, L. K. Molnar, and O. C. Farokhzad, "Factors affecting the clearance and biodistribution of polymeric nanoparticles," *Mol.Pharm.* 5, no. 4 (2008).

[32]Larken E. Euliss, Julie A. DuPont, Stephanie Gratton, and Joseph DeSimone, "Imparting size, shape, and composition control of materials for nanomedicine," *Chem.Soc.Rev.* 35, no. 11 (2006).

[33]P. Decuzzi, R. Pasqualini, W. Arap, and M. Ferrari, "Intravascular Delivery of Particulate Systems: Does Geometry Really Matter?," *Pharmaceutical Research* 26, no. 1 (2009).

size for drugs, i.e. small drugs penetrates better than a high molecular weight antibody.[34]

The presence of a hydrophilic coating allows NP escape from MPS recognition but decreases the rate and extent of NP uptake inside cancer cells.[35]A strategy to encourage nanocarrier internalization in solid tumors resides in surface decoration with ligands recognizing typical or overexpressed receptors in tumor microenvironment, which can promote its transport through receptor-mediated endocytosis. Different chemical motifs interacting with specific receptors overexpressed in cancer cells (folate, CD44, transferrin, EGF and some others) can be exploited to this purpose. This approach, known as active targeting, can aid selective nanocarrier accumulation inside cancer cells while avoiding healthy cells, thus decreasing treatment toxicity. Nevertheless, it has been recently demonstrated that targeted NPs can paradoxically lose targeting ability in a biological environment due to interaction with different high-affinity proteins or confine their activity to perivascular regions of a tumor (binding site barrier).[36] Cell cycling also plays a role in NP uptake rate and amount of NPs internalized by cells due to splitting between daughter cells when the parent cell divides.[37] Thus, proper understanding of NP properties at biointerface is a critical issue needing future investigational efforts.[38]

An added sophistication to selective delivery of drug cargo in cancer cells can be brought about by utilizing certain cues inherently characteristic of the tumor microenvironment or by applying certain stimuli to this region from outside the body. Stimuli-sensitive

---

[34]T. Fujimori, K. Harada, T. Yoshimura, Y. Yamano, T. Ogawa, and Y. Ikeda, "Good Correlation Between Anti-Platelet Effect and Intraplatelet Content of Orally-Administered E-5510 in Human Healthy-Volunteers," *Thrombosis and Haemostasis* 62, no. 1 (1989).

[35]K. Kettler, K. Veltman, D. van de Meent, A. van Wezel, and A. J. Hendriks, "Cellular uptake of nanoparticles as determined by particle properties, experimental conditions, and cell type," *Environmental Toxicology and Chemistry* 33, no. 3 (2014).

[36]H. Lee, H. Fonge, B. Hoang, R. M. Reilly, and C. Allen, "The effects of particle size and molecular targeting on the intratumoral and subcellular distribution of polymeric nanoparticles," *Mol.Pharm* 7, no. 4 (2010).

[37]J. A. Kim, C. Aberg, A. Salvati, and K. A. Dawson, "Role of cell cycle on the cellular uptake and dilution of nanoparticles in a cell population," *Nat Nanotechnol.* 7, no. 1 (2012).

[38]Eugene Mahon, Anna Salvati, Francesca Baldelli Bombelli, Iseult Lynch, and Kenneth A. Dawson, "Designing the nanoparticle-biomolecule interface for targeting and therapeutic delivery," *Journal of Controlled Release* 161, no. 2 (2012).

nanocarriers based on tailor-made materials can indeed be designed to deliver drug payload sharply and ―on-demand" by undergoing structural modifications under internal or external stimuli of chemical, biochemical and physical origin. Internal stimuli typical of solid tumors include mainly pH, temperature and reductive conditions. In fact, as compared to normal/host tissues, pH value in tumor interstitium is lower with an average value of 6.84 due to up-regulated glycolysis producing lactates and protons.[39] Furthermore, once NPs are internalized through endocytic pathways involving lysosomes, pH progressively decreases from early endosomes (pH 5-6) to more acidiclate endosomes[40] (pH 4-5) which can strongly alter nanocarrier stability and release features. pH sensitiveness has been widely employed to trigger NP disassembly and drug release.[41] Certain tumor microenvironments are also characterized by mild hyperthermia (1-2°C above healthy tissues) and some treatment modalities implies rising temperature which, together with pH sensitiveness, can be of help for triggering drug release. In addition, extracellular space is considered oxidative in comparison with intracellular compartment (≈100-1000 folds), mainly in the hypoxic area of tumors, due to different concentration levels of glutathione. Finally, an array of tumor-associated enzymes, either extracellular or intracellular, can be used as biochemical trigger of drug release to attain a fine control on spatial distribution of the delivered cargo.

[39]L. Tian and Y. H. Bae, "Cancer nanomedicines targeting tumor extracellular pH," *Colloids and Surfaces B-Biointerfaces* 99 (2012).

[40]S. Mukherjee, R. N. Ghosh, and F. R. Maxfield, "Endocytosis," *Physiological Reviews* 77, no. 3 (1997).

[41]E. Fleige, M. A. Quadir, and R. Haag, "Stimuli-responsive polymeric nanocarriers for the controlled transport of active compounds: Concepts and applications," *Advanced Drug Delivery Reviews* 64, no. 9 (2012).

2.3 Polymer Nanoparticles for Cancer Therapy

2.3.1 Generalities

Polymer-based nanoparticles (NPs) are at limelight in the burgeoning field of nanomedicine due to the advantage to manipulate their properties by selecting polymer type and mode of carrier assembly.[42]In fact, the advances in polymer chemistry makes it possible to produce an almost infinite number of sophisticated structures which can be engineered in light of strictly defined biological rules. Thus, not only those features affecting distribution of drug dose in the body and interaction with target cells can be controlled, but also spatio-temporal release of the delivered drug can be finely tuned.

Polymer-based NPs are matrix-type submicron-sized particles prepared from biodegradable or non-biodegradable materials. In some cases they can be nanocapsules (NCs), where an oily or aqueous core is surrounded by a polymeric shell. The main advantage of polymeric NPs is the fact that their features (size, surface properties, and release rate of drug cargo) can be easily tuned by selecting appropriate materials among a vast variety of commercially available candidates as well as by synthesizing novel tailor-made materials. Depending on the type of base material, some NPs are biodegradable/bioeliminable and can be administered by the parenteral route while others are not and thus useful only for local applications, assuming that no systemic NP absorption occurs. When dealing with NP entering the systemic circulation, degradability of the polymer is of utmost importance since polymer accumulation in the body above a certain molecular weight can occur. Drug biopharmaceutical properties (solubility, stability, charge, molecular weight, etc.) also guide nanocarrier design and suggest the needs of specific release features (triggered, sustained) as well as preferential location inside or outside cancer cells.

In their simplest architecture, passively, actively and physically targeted NPs can be formed by: i) nanostructuring (self-assembly) of

[42]N. Kamaly, Z. Y. Xiao, P. M. Valencia, A. F. Radovic-Moreno, and O. C. Farokhzad, "Targeted polymeric therapeutic nanoparticles: design, development and clinical translation," *Chemical Society Reviews* 41, no. 7 (2012).

amphiphilic all-in-one copolymers; ii) physical adsorption of a shell-forming material on preformed polymeric NPs acting as a core template.

Polymers that are insoluble in water form the core template of NPs, which is then coated by one or more than one layer of hydrophilic materials/phospholipids to impart tailored properties to the shells (biomimetic and targeted shells). Hydrophilic polymers can be used also as core template after crosslinking with either low molecular weight molecules or an interacting hydrophilic polymer with opposite charge, thus providing nanogels. Amid shell-forming hydrophilic polymers giving long-circulating NPs, PEG is undoubtedly the most common material employed to modify hydrophobic NPs, although several others have been proposed.

A wide array of currently-available materials and their possible combinations can be employed to fabricate submicron NPs spanning from simple biomimetic systems for passive targeting to more sophisticated structures integrating specificity and multifunctionality. Biodegradability and effective elimination of the polymer is a key prerequisite that should be taken into account when developing injectable NPs especially when considering novel materials.

The main biomaterials employed in injectable biodegradable NPs are summarized in Table 2 and span from natural materials (polysaccharide, proteins, polyaminoacids) to synthetic polymers (polyesters and PEGylated polyesters, poloxamers, acrylic polymers, polyammines). Stimuli-responsive polymers, referred to as "environmentally-sensitive", "smart" or "intelligent" polymers are a huge class of chemically diverse structures that respond sharply to small changes in physical or chemical conditions with relatively large phase or property changes mainly used in the cancer field to trigger drug release at tumor level.

Each polymer presents peculiar solubility features which, coupled with drug physico-chemical profile, specific needing for surface engineering and drug release rate, drive toward specific fabrication methods to attain core/shell NPs.

Table 2. Main synthetic polymers employed to prepare polymeric NPs for cancer therapy.

Polymer type	Location in NPs	Key Features
Polyesters (PLGA, PLA, PCL)	core	Hydrophobic and soluble in common organic solvents Biodegraded in the body Encapsulation of hydrophilic/hydrophobic drugs as well as macromolecules Protection of drug cargo Sustained release as a function of polymer properties.[43]
PEGylated polyesters (PLGA-PEG, PLA-PEG, PCL-PEG)	Core-shell	Amphiphilic non-ionic copolymers with different segment lengths and architectures forming NPs with a biomimetic/stabilizing shell Shielding ability depends on molecular weight, architecture and surface density Biodegraded in the body Hydrophilic/hydrophobic ratio and fabrication method control the mode of aggregation (micelles, polymersomes, NPs) Molecular weight affects NP size Molecular weight and hydrophobicity of lipophilic segments affect drug loading and stability inside NPs Surface decoration with targeting ligands Low molecular weight copolymers (< 500 Da) can revert MDR.[44,45]
Pluronics	Core-shell	Amphiphilic non-ionic copolymers with different block length. Able to form small micelles entrapping hydrophobic drugs. Mixed micelles of different Pluronic types can be formed. Unimers act on P-gp and allow to overcome MDR[46,47]

[43]F. Danhier, O. Feron, and V. Preat, "To exploit the tumor microenvironment: Passive and active tumor targeting of nanocarriers for anti-cancer drug delivery," *Journal of Controlled Release* 148, no. 2 (2010).

[44]H. Sah, L. A. Thoma, H. R. Desu, E. Sah, and G. C. Wood, "Concepts and practices used to develop functional PLGA-based nanoparticulate systems," *International Journal of Nanomedicine* 8 (2013).

[45]C. Conte, I. D'Angelo, A. Miro, F. Ungaro, and F. Quaglia, "PEGylated Polyester-Based Nanoncologicals," *Current Topics in Medicinal Chemistry* 14, no. 9 (2014).

[46]Daria Y. Alakhova and Alexander V. Kabanov, "Pluronics and MDR Reversal: An Update," *Mol.Pharmaceutics* 11, no. 8 (2014).

[47]E. V. Batrakova and A. V. Kabanov, "Pluronic block copolymers: evolution of drug delivery concept from inert nanocarriers to biological response modifiers," *J Control Release* 130, no. 2 (2008).

PAA PAAm PMA PDEAEMA	Core	Obtained by cross-linking different monomer types to form nanogels Molecular weight and cross-linker chemistry affect their elimination from the body Some derivatives are protonating/deprotonating polymers with charge shift from either anionic to neutral or from neutral to cationic Acrylic derivatives with hydrazine, hydrazide and acetal linkages swells or collapses for electrostatic reasons and can be employed to get pH-sensitive sheddable coatings.[48]
PEI/PLL	Shell	Decoration of negatively-charged NPs via electrostatic interactions Need of a further polymer coating to shield positive charge of the NP shell For PEI, enhanced tumoricidal capacity of tumor associated macrophages through Toll-like receptor signaling.[49,50,51]
pNIPAM and derivatives	Core	Temperature-controlled self-assembly Collapse in the hyperthermic tumour environment Release depending on the MW and nature of the polymer hydrophobic block Encapsulation of both hydrophobic/hydrophilic drugs.
Polymers sensitive to pH or enzymes-various	Core/Shell	Contain group(s) susceptible to pH variations ( )or enzyme degradation (ester or carbamates for proteases, disulfide for reductase) Enzyme- or pH-sensitive sheddable coatings can be designed.

[48]T. Thambi, V. G. Deepagan, H. Ko, Y. D. Suh, G. R. Yi, J. Y. Lee, D. S. Lee, and J. H. Park, "Biostable and bioreducible polymersomes for intracellular delivery of doxorubicin," *Polymer Chemistry* 5, no. 16 (2014).

[49]Y. Kaneda, "Update on non-viral delivery methods for cancer therapy: possibilities of a drug delivery system with anticancer activities beyond delivery as a new therapeutic tool," *Expert Opinion on Drug Delivery* 7, no. 9 (2010).

[50]Z. Huang, Y. Yang, Y. Jiang, J. Shao, X. Sun, J. Chen, L. Dong, and J. Zhang, "Anti-tumor immune responses of tumor-associated macrophages via toll-like receptor 4 triggered by cationic polymers," *Biomaterials* 34, no. 3 (2013).

[51]P. Hammond, "Nano approaches to using nucleic acids," *ACS Nano.* 7, no. 5 (2013).

2.3.2 Fabricating biocompatible nanoparticles for cancer

When developing NPs for cancer therapy, a rational design should be planned taking into account specific needs dictated by i) disease features (tissue, stage, vascularization extent, presence of metastases); ii) the strategy selected to accumulate the highest dose fraction at tumor level (pharmacokinetics) and to deliver the drug (intracellular/tumor interstitium, sustained or pulsed release); iii) physical-chemical properties of the drug (solubility profile, stability); iv) achievement of a product with satisfactory shelf-life (preferably a solid). This is certainly the most critical step in NP development where a multidisciplinary approach at interface between pharmaceutical technology, biology and medicine should be carried out.

Drugs can be loaded in NPs through encapsulation, covalent linkage or post-loading. Encapsulation relies on physical entrapment of a drug in NP core or shell based on hydrophobic or electrostatic interactions and hydrogen bond formation. Drug loading in the core of NPs can contribute to achieve a sustained release rate in the biological environment while timing of drug release can be finely tuned by allocating different drugs in the core or the shell, that is especially important in combination therapies. In the post-loading method, drug is added to preformed NPs by equilibrium in solution. Covalent binding of a drug to NPs is difficult to attain and requires either covalent attachment of the drug to monomers that are then polymerized or self-assembled in NPs or post-modification of preformed NPs.

In general, NPs are prepared by bottom-up approaches, primarily using monomers or preformed polymers that are then nanostructured by techniques such as emulsification/solvent evaporation, interfacial deposition after solvent displacement, dialysis or salting-out.[52,53,54]

Layer-by-layer deposition method has been recently introduced as NP preparation technique to give multifunctional NPs (matrix or reservoir

[52]Madaswamy S. Muthu and Barnabas Wilson, "Challenges posed by the scale-up of nanomedicines," *Nanomedicine* 7, no. 3 (2012).

[53]S. Saraf, "Process optimization for the production of nanoparticles for drug delivery applications," *Expert Opinion on Drug Delivery* 6, no. 2 (2009).

[54]N. Anton, J. P. Benoit, and P. Saulnier, "Design and production of nanoparticles formulated from nano-emulsion templates-a review," *J.Control Release* 128, no. 3 (2008).

type).Layer-by-layer technique consists in sequentially depositing oppositely charged polymers on a nanotemplate to build a stable multilayer NPs. For each depositing step, NPs are incubated with a polymeric water solution, then centrifuged to eliminate non-adsorbed polymer and redispersed to allow the next absorption step. Charged polymers have to sequential adsorb with precision over the previously deposited layer and can eventually embed a drug. These advantages, combined with the ability to incorporate a broad range of therapeutics and materials with diverse functionalities, greatly facilitate the development of drug delivery platforms with sophisticated control over the spatial and temporal release of constituents. Many Layer-by-layer NPs has been recently studied in order to delivery different drugs. For example based only on electrostatic interactions, core-shell PLGA NPs prepared by stepwise modification through several sequential layering of positive and negative polymers such as chitosan/alginate, polylysine/alginate and polylysine/HA has been found successful to achieve physically stable NPs.

It is worth noting that properties of NPs are strictly dictated by the production method, which is especially critical when specific targeting elements have to be exposed on the surface.

From a therapeutic standpoint, timing of drug release is important not only to drive administration scheme (number of administrations, frequency) but also useful to optimize therapeutic outcome. For example, sustained extracellular release can be expected to amplify cell response to some chemotherapeutics and to extend activity to hypoxic zones of certain tumors resembling a metronomic therapy(subactive doses for longer time frames) whereas responsiveness to external or internal stimuli can be useful to trigger drug release at specific subcellular level. Nevertheless, timing of drug release can be finely tuned by allocating different drugs in the core or the shell, that is of utmost importance in drug-nucleic acid combination therapies. In all the cases, drug amount released from NPs should be reasonably low in the circulation and regulated at tumor level to obtain the optimal therapeutic response.

The unique nano-scale structure of NPs provides significant increases in surface area to volume ratio which results in high propensity to aggregation during manufacturing, storage and shipping. This aspect remains a very challenging issue during pharmaceutical product

development. The freeze-drying process is the most diffused method to handle and stabilize NPs, avoiding undesirable changes upon storage. However, freeze-drying also induce aggregation, which mainly affect dispersability in a pharmaceutical vehicle for intravenous administration. Sugars such as trehalose, glucose, sucrose, fructose and sorbitol have been proposed as cryoprotectants to minimize NPs collapse upon freeze-drying, although papers focusing on this aspects are very few.[55]

2.4 PLGA nanoparticles in cancer therapy

2.4.1 *Generalities of PLGA nanoparticles*

Many biocompatible and biodegradable polymers, such as poly-(D,L-lactide-co-glycolide) (PLGA), poly(lactic acid) (PLA), poly(caprolactone) (PCL) provide safe and non-toxic NPs for in vivo administration. In recent years, PLGA derivatives have shown a great potential for engineering drug delivery system. PLGA is one of the most successfully used biodegradable polymers in the biomedical field due to well-recognized biocompatibility. After hydrolysis in the body, it gives as metabolites constituting monomers, lactic acid and glycolic acid, which are easily metabolized by the body via the Krebs‘cycle. PLGA is approved by the US FDA and EMA in various drug delivery systems (Fig. 4).

[55]Pedro Fonte, Sandra Soares, Fl+ívia Sousa, Ana Costa, V. + Seabra, Salette Reis, and Bruno Sarmento, "Stability Study Perspective of the Effect of Freeze-Drying Using Cryoprotectants on the Structure of Insulin Loaded into PLGA Nanoparticles," *Biomacromolecules* 15, no. 10 (2014).

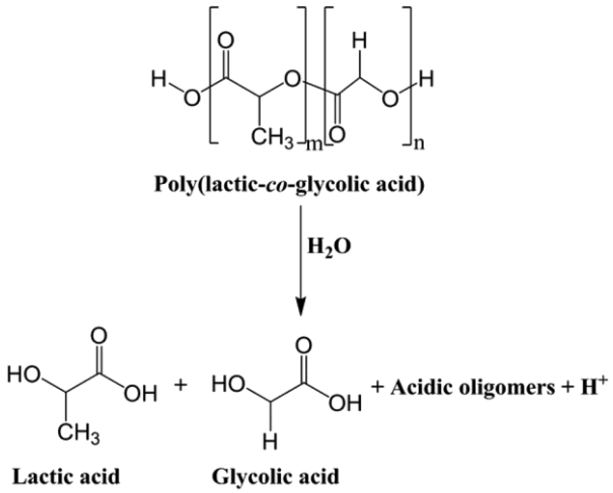

Fig. 4. Chemical structure of poly(lactic-*co*-glycolic acid) and the products of its hydrolytic degradation. In a PLGA copolymer, *m* and *n* refer to the amounts of lactide and glycolide monomer units,A.C.Dumitru, F.M. Espinosa, ~~–~~In situ nanomechanical characterization of the early stages of swelling and degradation of a biodegradable polymer" *Nanoscale,* n 7 (2015).

The polymers are commercially available with different molecular weights and copolymer compositions. The degradation time depends on the copolymer composition.

PLGA NPs have been widely employed for the loading or encapsulation of a variety of anticancer drugs, ranging from hydrophilic drugs such as DOX,5-Flurouracil,and cisplatin to hydrophobic drugs such as Paclitaxel. A variety of methods have been employed to prepare drug-loaded PLGA based nanoformulations. A brief summary of these methods is provided in Table 3 as reported by Jain et al.[56]

[56]A. K. Jain, M. Das, N. K. Swarnakar, and S. Jain, "Engineered PLGA nanoparticles: an emerging delivery tool in cancer therapeutics," *Crit Rev Ther.Drug Carrier Syst.* 28, no. 1 (2011).

Table 3. Fabrication methods of PLGA NPs.

Method of Preparation	Brief Description	Drug(s) Incorporated	Remarks
Emulsion-evaporation	Drug and polymer dissolved in organic solvents and emulsified in aqueous solution of emulsifier/stabilizer. The resulting emulsion droplet size is reduced by high-energy source either by sonication and homogenization. Then organic phase is evaporated under reduced pressure. The nanoparticles are collected by ultracentrifugation and freeze-dried.[146]	Paclitaxel[39,148]	Particle size can be controlled by stirring rate and other conditions[148]; high efficiency for lipophilic drugs.[39]
Double-emulsion evaporation	Addition of aqueous drug solution to the polymer solution under vigorous stirring conditions to form a water/oil emulsion, which is added into the stabilizer solution with stirring to form a water/oil/water emulsion. The resulting double emulsion is subjected to solvent evaporation.[149]	Cisplatin[38]	Optimization parameters include percentage of drug loading, concentration of stabilizer, polymer concentration, and volume of external phase.
Salting-out	Solution of polymer and drug in acetone is added to aqueous solution contacting the stabilizers and salting-out reagent under mechanical stirring. Emulsion is diluted with water, which leads to the diffusion of acetone. Cross-flow filtration is employed to remove the acetone and salting-out reagent.[151]	9-Nitrocamptothecin[152]	Optimization parameters include stirring rate, concentration of stabilizer, polymer concentration, and type of electrolyte concentration.
Emulsification-diffusion	Addition of polymer solution in a partially water-miscible solvent such as ethyl acetate, benzyl alcohol, or propylene carbonate, which is added to the stabilizer solution under stirring conditions. Water is added to the system, which leads to destabilization. The solvent diffuses into the external phase and is ultimately evaporated, leading to the formation of nanoparticles.[147]	–	Provides more intensive purification step, suffers from the lower entrapment efficiency of hydrophilic drugs, increased by addition of medium-chain glyceride into the aqueous phase.
Solvent displacement/ nanoprecipitation	Solution of polymer, drug, and lipophilic surfactant in semipolar solvent such as acetone and ethanol injected into aqueous containing the stabilizers under magnetic stirring. Nanoparticles are formed by rapid solvent diffusion, and the solvent is removed under the reduced pressure.[37]	Paclitaxel,[59] docetaxel[103,148,153]	Particle size is affected by the injection rate of organic solvent into aqueous solution; narrow particle size for different formulations.

The most common technique used for the preparation of PLGA NPs is the emulsification-solvent evaporation technique. Polymer and drugs are dissolved in an organic solvent (dichloromethane)e; the emulsion oil

(O) in water (W) is prepared by adding water and surfactant (Pluronic F68) to the polymeric solution. NPs are homogenized, centrifugated and collected. NPs can also formed by precipitation method also called the interfacial deposition method. The polymer and the drug are co-dissolved in an organic phase (such as acetone) and added dropwise to a water solution, after the evaporation of solvent, NPs are collected and purified by centrifugation step.

2.4.2 Engineering PLGA nanoparticles for cancer therapy

The limits of intravenous PLGA NPs are well know; hydrophobic particles are recognized as foreign by body and the reticulo-endothelial system (RES) quickly eliminates these from blood stream and takes them up in the liver or the spleen. The possibility to modify the surface of NPs has been investigated to produce NPs not recognized by the RES. The most common surface modification is the covalent conjugation of PLGA with the hydrophilic and non-ionic polymer PEG that increases the blood circulation half-life of bare PLGA NPs.[57] Stealth functionality imparted to NPs is found to be strongly influenced by PEG length and surface density on NPs surfaces. The length and density of PEG can influence the mushroom or brush-like conformation of PEG onto NPs: long PEG favors mushroom conformation while short PEG favors brush-like conformation. Generally, higher surface coverage of PEG increases the circulation time of NPs, and PEG with a molecular weight of 5000 Da provides the ideal surface coating for stealth functionalization.[58]

Surface charge of NPs also plays an important role on their interaction with cells and on their uptake. It has been shown that positively charged NPs seem to allow higher internalization in cells due tothe ionic interaction between positively-charged particles and negatively-charged cell membranes. In principle, negative charge of

[57]F. Danhier, E. Ansorena, J. M. Silva, R. Coco, A. Le Breton, and V. Preat, "PLGA-based nanoparticles: An overview of biomedical applications," *Journal of Controlled Release* 161, no. 2 (2012).

[58]I. Hamad, O. Al-Hanbali, A. C. Hunter, K. J. Rutt, T. L. Andresen, and S. M. Moghimi, "Distinct Polymer Architecture Mediates Switching of Complement Activation Pathways at the Nanosphere-Serum Interface: Implications for Stealth Nanoparticle Engineering," *Acs Nano* 4, no. 11 (2010).

PLGA NPs can be shifted to positive charge by surface adsorption of surfactants and polymers.

It has been already discussed that cancer cells, unlike normal cells, proliferate rapidly. One mechanism underlying this growth is the overexpression of receptors, which allows the uptake of growth factors via receptor-mediated endocytosis to proceed more efficiently than in normal cells. This mechanism could be used as a "Trojan horse" for site-specific delivery of anticancer agents, and is executable by decorating the surface of NPs with antibodies or ligands that specifically bind to these receptors. This modification mainly relies on chemical conjugation of PLGA or PEG-PLGA NPs with different targeting moieties such as antibodies, aptamers, peptides, or small ligands. Very few is known on the possibility to modify NP surface through supramolecular chemistry.

2.5 Active targeting of NPs through CD44 receptor

CD44 receptor is a transmembrane glycoprotein (85 kDa) playing a role in a lot of cellular functions, including cell orientation, adhesion, migration, and matrix-cell signaling processes.[59] CD44 is overexpressed in many solid tumor cells: lung, breast, colorectal, gastric, pancreatic cancer. Additionally, CD44 is also considered as a common marker for several cancer stem cells and exhibit highly malignant and chemo-resistant properties.

The ligand for CD44 receptor is the extracellular matrix Hyaluronan or hyaluronic acid (HA) which is a linear negatively-charged polysaccharide formed by alternating D-glucuronic acid and N-acetyl-D-glucosamine (Fig. 4). In addition to CD44 receptor, HA can also interact with other receptor including RHAMM (receptor for Hyaluronan-mediated motility CD168), HARE (HA receptor for endocytosis) and Toll-like receptor 2 and 4.

The binding of HA molecule to multiple CD44 receptors (Fig. 5) induce the extracellular clustering of the receptors which regulates intracellular organization of cytoskeleton, this mechanism giving the activation of diverse kinases. The second signaling pathway finally

[59]H. S. S. Qhattal and X. L. Liu, "Characterization of CD44-Mediated Cancer Cell Uptake and Intracellular Distribution of Hyaluronan-Grafted Liposomes," *Molecular Pharmaceutics* 8, no. 4 (2011).

induces subsequent changes in cellular behavior. The molecular weight of HA is a key factor in CD44-mediated signaling.

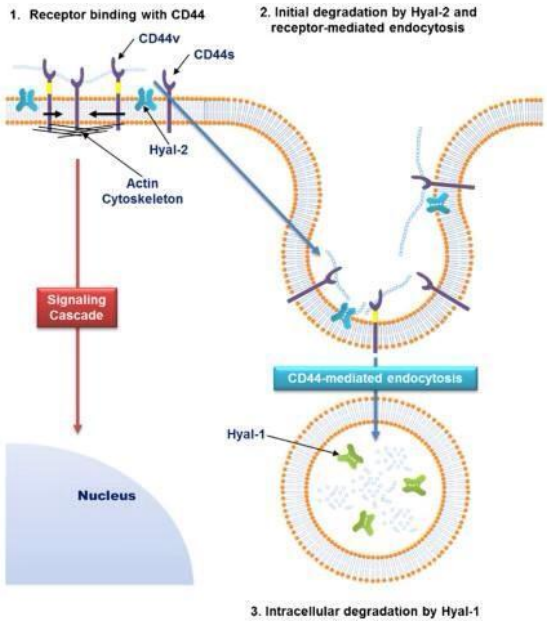

Fig. 5. (Top) Structure of hyaluronic acid. **(Bottom)**Schematic illustration of CD44-mediates signal transduction and cellular uptake Ki Young Choi, ―Hyaluronic acid-based nanocarrier for intracellular targeting: Interfacial interactions with proteins in cancer", *Colloids and Surfaces B: Biointerfaces*. 99, n 82-94 (2012).

For example it has been demonstrated that low molecular weight HA fragments but not high native molecular weight HA can activate cell-signaling pathways and induce expression of tumor necrosis factor.[60]

HA is internalized into cells that overexpress CD44 receptor via receptor-mediate endocytosis and is compartimentalized in the lysosome where it is degraded by lysosomal enzyme called Hyaluronidases 1 (Hyal1).

A variety of HA-based nanocarriers have been developed for targeting drugs to cancer cells, generally encompassing covalent conjugates with chemotherapeutics. For example PLGA based NPs for

[60]K. Y. Choi, G. Saravanakumar, J. H. Park, and K. Park, "Hyaluronic acid-based nanocarriers for intracellular targeting: interfacial interactions with proteins in cancer," *Colloids Surf.B Biointerfaces.* 99:82-94. doi: 10.1016/j.colsurfb.2011.10.029. Epub@2011 Oct@20. (2012).

delivering of DOX in particular DOX-loaded HA-g-PLGA micelle NPs exhibited higher cellular uptake and greater cytotoxicity than free DOX for HCT-116 cells that over-expressed HA receptor, suggesting that they were taken up by the cells via HA receptor-mediated endocytosis.[61]In another studies HA coated docetaxel-loaded vesicles performance in vivo and in vitro several advances including the high selectivity to CD44 overexpressing tumor cells, passive target via EPR effect and the extremely low cytotoxicity to the normal cells shown that self-assembled HA NPs were taken up in MDA-MB-231 cells by CD44-mediate endocytosis via an energy-dependent endocytic pathway and compared uptake in two cell line with different CD44 expression to elucidate the enhanced uptake mediated HA-CD44 interaction (Fig. 5).

2.6 Combining different treatment modalities through tailored NPs

Combination therapy has been introduced in clinical practice to overcome problems associated with single chemotherapeutic cancer treatments, that is MDR, significant toxicity and undesirable side effects. Generally combination therapy consists in the administration of two or more than two therapeutic agents co-delivered simultaneously or a combination of different strategies, such as chemotherapy, hormone therapy, immunotherapy and radiotherapy.[62] In the past few years, the rationale for this approach has been centered on targeted drugs acting on specific biochemical pathways. In fact it has been hypothesized that one-dimensional mechanism of action of a single chemotherapeutic, often determines the activation of alternative pathways, which determines failure of therapy or tumor recurrence.

Accumulating clinical experience, supported by animal studies, suggests that chemotherapy is most effective when given in combination to give an additive effect as compared to the individual pharmacological activity of single compound. Moreover co-encapsulation of drugs with

[61]A. Almalik, S. Karimi, S. Ouasti, R. Donno, C. Wandrey, P. J. Day, and N. Tirelli, "Hyaluronic acid (HA) presentation as a tool to modulate and control the receptor-mediated uptake of HA-coated nanoparticles," *Biomaterials* 34, no. 21 (2013).

[62]P. Parhi, C. Mohanty, and S. K. Sahoo, "Nanotechnology-based combinational drug delivery: an emerging approach for cancer therapy," *Drug Discovery Today* 17, no. 17-18 (2012).

different pharmacokinetics properties at the same body site allows to give a temporal sequencing of drug release. The fact that the two agents or more act on different signaling pathways synergistically is very promising to overcome the compensatory mechanisms induced in the cancer cells. Furthermore, low dosage of each compound or the access to context-specific multi-target mechanisms consent to avoid the use of high drug doses which are associated to a toxic effects.[63] Furthermore, the possibility to administer multiple drugs with different molecular targets consent to modulate the genetic barrier which are responsible of cell mutations and the cancer adaptation process which often causes the failure of therapy. These advantages of drugs in combination are expected to be greater than the sum of the effects of drugs individually. The best drug combination with maximal antitumor efficacy can be calculated by multiple drug effect/combination index isobologram analysis, an effective way to demonstrate that drugs are working synergistically.[64] In addition, co-treatment tumor modulators which are involved in MDR(P-glycoprotein inhibitors)is an important strategy.

Nanotechnology-based strategies to deliver drug combinations offer the advantage to improve pharmacokinetics increasing drug fraction available at tumor site through EPR effect and to overcome the systemic toxicity toward normal tissue (Fig. 6). NPs give also the possibility to co-delivery multiple drugs at a predetermined ratio, that maximizes the combination efficacy. In fact, the ratio of two or more drugs has been found to influence the efficacy of combination therapy.[65] The degree of synergism and antagonism is strongly affect to the relative concentration between the combined drugs in combinatorial NPs.[66,67]

[63]J. Lehar, A. S. Krueger, W. Avery, A. M. Heilbut, L. M. Johansen, E. R. Price, R. J. Rickles, G. F. Short, J. E. Staunton, X. W. Jin, M. S. Lee, G. R. Zimmermann, and A. A. Borisy, "Synergistic drug combinations tend to improve therapeutically relevant selectivity," *Nature Biotechnology* 27, no. 7 (2009).

[64]T. C. Chou, "Drug Combination Studies and Their Synergy Quantification Using the Chou-Talalay Method," *Cancer Research* 70, no. 2 (2010).

[65]C. M. J. Hu and L. F. Zhang, "Nanoparticle-based combination therapy toward overcoming drug resistance in cancer," *Biochemical Pharmacology* 83, no. 8 (2012).

[66]V. Pavillard, D. Kherfellah, S. Richard, J. Robert, and D. Montaudon, "Effects of the combination of camptothecin and doxorubicin or etoposide on rat glioma cells and camptothecin-resistant variants," *British Journal of Cancer* 85, no. 7 (2001).

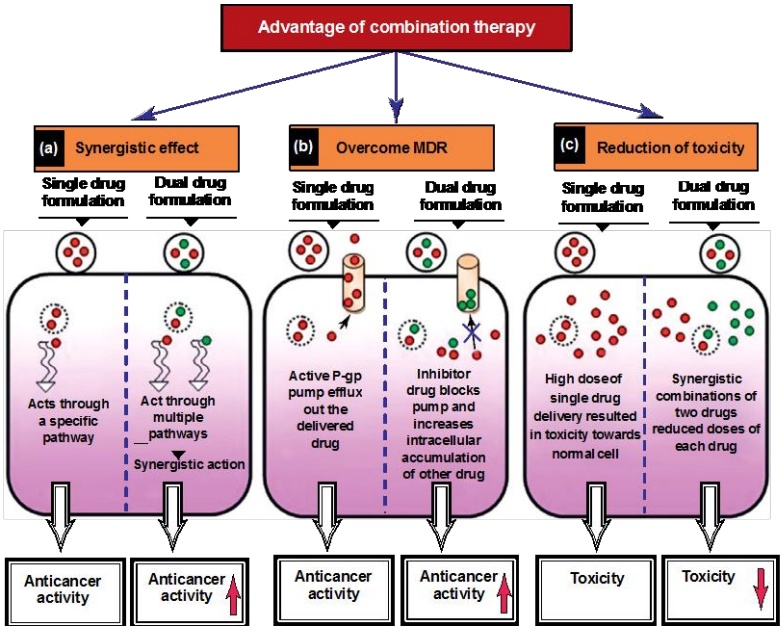

Fig.6 Schematicrepresentationdepictingvariousadvantagesshownbycombinationdrug Delivery for cancer therapy Che-Ming Jack Hu, "Nanoparticles-based combination therapy toward overcoming drug resistance in cancer", *Biochemical Pharmacology* 83, no 1104-1111 (2012).

For example, dual-drugs liposomes with precise molar ratio have been prepared to deliver cytarabine and daunorubicin in ratio 5:1 for leukemia treatment [68,69] and irinotecan and floxuridine formulation in ratio 1:1 for colon-rectal cancer treatment.[70] These combinations

[67]M. Raitanen, V. Rantanen, J. Kulmala, H. Helenius, R. Grenman, and S. Grenman, "Supra-additive effect with concurrent paclitaxel and cisplatin in vulvar squamous cell carcinoma in vitro," *International Journal of Cancer* 100, no. 2 (2002).

[68]W. S. Lim, P. G. Tardi, N. Dos Santos, X. W. Xie, M. N. Fan, B. D. Liboiron, X. P. Huang, T. O. Harasym, D. Bermudes, and L. D. Mayer, "Leukemia-selective uptake and cytotoxicity of CPX-351, a synergistic fixed-ratio cytarabine:daunorubicin formulation, in bone marrow xenografts," *Leukemia Research* 34, no. 9 (2010).

[69]E. J. Feldman, J. E. Lancet, J. E. Kolitz, E. K. Ritchie, G. J. Roboz, A. F. List, S. L. Allen, E. Asatiani, L. D. Mayer, C. Swenson, and A. C. Louie, "First-In-Man Study of CPX-351: A Liposomal Carrier Containing Cytarabine and Daunorubicin in a Fixed 5:1 Molar Ratio for the Treatment of Relapsed and Refractory Acute Myeloid Leukemia," *Journal of Clinical Oncology* 29, no. 8 (2011).

[70]G. Batist, K. A. Gelmon, K. N. Chi, W. H. Miller, S. K. L. Chia, L. D. Mayer, C. E. Swenson, A. S. Janoff, and A. C. Louie, "Safety, Pharmacokinetics, and Efficacy of CPX-1 Liposome Injection in Patients with Advanced Solid Tumors," *Clinical Cancer Research* 15, no. 2 (2009).

demonstrate the ability to maintain the synergistic ratio in vivo and are more effective than the cocktail administration of the free drugs.
Another important aspect refers to the possibility of a temporal control on sequenced drug release in the attempt to deliver the biochemical agents at the appropriate cellular stage. Many chemotherapeutics are more potent in specific cell cycle state, and, therefore, improper sequencing could lead to unintended cell cycle arrest and diminished response to the subsequent drugs.[71]

2.6.1 Combining chemotherapy with light-activated therapies

The rapid delivery of biologically relevant species with precise spatiotemporal control is a hot topic in life science.[72] Light is the most on/off trigger to support these criteria. In fact, the fast response of the photochemical reactions and their instantaneous initiation/stopping represent a powerful tool for the introduction of given amounts of "photocaged" chemical entities in biological systems in non-invasive way. In addition, the use of photons as external impulse offer the advantage of not affecting important physiological parameters, such as pH, temperature and ionic strength, which is a critical condition for bio-applications.

Amid light-activated therapies, Photodynamic therapy (PDT) is an emergent and selective therapy for the management of a variety of solid tumors including colon, breast, prostate and ovarian cancer. PDT is based on photochemical processes where an exogenous and non-toxic photosensitizer (PS), after irradiation with light at specific wavelength preferentially corresponding at PS maximum absorption, usually visible (VIS) or near-infrared (NIR), is able to generate oxygen-based molecular species which produce many effects at cell and tissue level.[73,74](Fig. 7).

---

[71]M. A. Shah and G. K. Schwartz, "Cell cycle-mediated drug resistance: An emerging concept in cancer therapy," *Clinical Cancer Research* 7, no. 8 (2001).
[72]E. Vittorino, M. T. Sciortino, G. Siracusano, and S. Sortino, "Light-Activated Release of Nitric Oxide with Fluorescence Reporting in Living Cells," *Chemmedchem* 6, no. 9 (2011).
[73]A. P. Castano, P. Mroz, and M. R. Hamblin, "Photodynamic therapy and anti-tumour immunity," *Nature Reviews Cancer* 6, no. 7 (2006).
[74]P. Agostinis, K. Berg, K. A. Cengel, T. H. Foster, A. W. Girotti, S. O. Gollnick, S. M. Hahn, M. R. Hamblin, A. Juzeniene, D. Kessel, M. Korbelik, J. Moan, P. Mroz, D. Nowis, J. Piette, B. C. Wilson, and J. Golab, "Photodynamic therapy of cancer: an update," *CA Cancer J.Clin.* 61, no. 4 (2011).

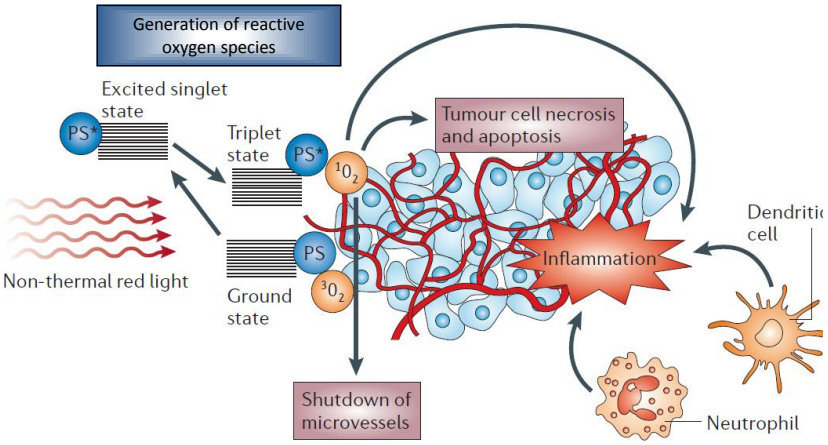

Fig. 7. The mechanism of action on tumours in photodynamic therapy. The photosensitizer (PS) absorbs light and an electron moves to the first short-lived excited singlet state. This is followed by intersystem crossing, in which the excited electron changes its spin and produces a longer-lived triplet state. The PS triplet transfers energy to ground-state triplet oxygen, which produces reactive singlet oxygen ($^1O_2$). $^1O_2$ can directly kill tumour cells by the induction of necrosis and/or apoptosis, can cause destruction of tumour vasculature and produces an acute inflammatory response that attracts leukocytes such as dendritic cells and neutrophils. A.P. Castano, *"Photodynamic therapy and anti-tumour immunity",Nature Reviews Cancer*6 (2006).

There are several technical difficulties in the application of PDT in cancer, partly shared by most clinically relevant chemotherapeutics. First is the difficulty in preparing pharmaceutical formulations that allow parenteral administration because most existing PSs are hydrophobic, aggregate easily under physiological condition and partly lose their photophysical properties.

Although second generation PSs show lower toxicity, most of them exhibit poor solubility in aqueous media, complicating intravenous delivery into the bloodstream because the use of vehicles (Chremophor®, propylenglycol) can give allergy, hypersensitivity and toxicity.[75] Several hydrophobic PSs tend to aggregate in physiological conditions via the strong attractive interactions between π-systems of the

[75]H. Gelderblom, J. Verweij, K. Nooter, and A. Sparreboom, "Cremophor EL: the drawbacks and advantages of vehicle selection for drug formulation," *European Journal of Cancer* 37, no. 13 (2001).

polyaromatic macrocycles and, as a consequence, to produce singlet oxygen with very low yields.[76]

Aggregation is one of the determining factors which can cause a loss of PS efficacy in vivo by decreasing its bioavailability and limiting its capacity to absorb light.[77] Second is the selective accumulation in diseased tissues, which is often not high enough for clinical use. Foscan®, a first-generation PS, has failed FDA approval for the treatment of head and neck cancer due to poor tumor selectivity resulting in serious skin burns arising from photosensitivity. A third aspect is related to light-activation of PS that generally occurs at a wavelength where radiation is poorly penetrating and unable to reach deep tissues.

Nanotechnological approaches in PDT (nanoPDT) can offer many advantages to deliver a PS and to solve at least part of these issues. Development of nanoscale-carrier to deliver a PS agent can result in optimized pharmacokinetics, enhancing the treatment ability to target and kill cancer cells of diseased tissue/organ while affecting as few healthy cells as possible.[78,79] Furthermore, nanocarriers offer the possibility to deliver therapeutic concentrations of PS in the diseased tissue at specific subcellular location and to overcome solubility and tendency to aggregation of PSs. Nanocarriers also serve as a multimodal platform to bind/include a great variety of molecules, such as tumor-specific targeting ligands for targeted nanoPDT and/or imaging agents integrating in a single platform the unique opportunity for concurrent diagnostic and treatment of cancer tumors, the so-called theranostic. Recently, several multifunctional theranostic systems have been developed for real-time imaging-guided PDT of cancer.[80]

---

[76]L. P. F. Aggarwal and I. E. Borissevitch, "On the dynamics of the TPPS4 aggregation in aqueous solutions - Successive formation of H and J aggregates," *Spectrochimica Acta Part A-Molecular and Biomolecular Spectroscopy* 63, no. 1 (2006).

[77]D. Gabrielli, E. Belisle, D. Severino, A. J. Kowaltowski, and M. S. Baptista, "Binding, aggregation and photochemical properties of methylene blue in mitochondrial suspensions," *Photochemistry and Photobiology* 79, no. 3 (2004).

[78]D. K. Chatterjee, L. S. Fong, and Y. Zhang, "Nanoparticles in photodynamic therapy: an emerging paradigm," *Adv.Drug Deliv.Rev.* 60, no. 15 (2008).

[79]M. E. Davis, Z. Chen, and D. M. Shin, "Nanoparticle therapeutics: an emerging treatment modality for cancer," *Nature Reviews Drug Discovery* 7, no. 9 (2008).

[80]S. Mallidi, B. Q. Spring, S. Chang, B. Vakoc, and T. Hasan, "Optical Imaging, Photodynamic Therapy and Optically Triggered Combination Treatments," *Cancer Journal* 21, no. 3 (2015).

Strategies to deliver PDT agents and chemotherapeutics have been recently revised.[81]

2.6.2 Combination of chemotherapy with NO release

In the past twenty years, nanotechnology has offered a valuable tool to target bioactive molecules to solid tumors with the goal to improve response to conventional pharmacological therapies, to alleviate anticancer drug toxicity as well as to overcome multidrug resistance (MDR). In recent studies nitric oxide (NO) has been demonstrated a promising anticancer activity.[82] NO radical is a able to attack biological substrates of different nature like plasma membrane,[83] mithocondria,[84] and the cell nucleus.[85] Moreover NO represents a multitarget cytotoxic agent, which does not suffer MDR problems encountered with target-specific –conventional" anticancer drugs. Evidence of NO-induced death in various cell types, both by apoptosis and necrosis, is discussed in relevant reviews.[86] Furthermore, the short half-life in blood (<1s), the lack of charge, the god lipophilicity and the small size, allow NO to easily diffuse in the cellular environment over short distances (<200 nm) confining the region of action without inflicting systemic side effects common to several chemotherapeutics. An additional advantage of NO is allow toxicity towards healthy cells, especially at concentrations toxic to cancer cells. However concentration and dose of NO strictly dictate its biologic effects.[87] Light represent a powerful and minimally invasive

[81]C. Conte, S. Maiolino, D. S. Pellosi, A. Miro, F. Ungaro, and F. Quaglia, "Polymeric Nanoparticles for Cancer Photodynamic Therapy," *Light-Responsive Nanostructured Systems for Applications in Nanomedicine* 370 (2016).

[82]D. Fukumura, S. Kashiwagi, and R. K. Jain, "The role of nitric oxide in tumour progression," *Nature Reviews Cancer* 6, no. 7 (2006)..

[83]S. Gupta, C. Mcarthur, C. Grady, and N. B. Ruderman, "Stimulation of Vascular Na+-K+-Atpase Activity by Nitric-Oxide - A Cgmp-Independent Effect," *American Journal of Physiology* 266, no. 5 (1994).

[84]M. Nishikawa, E. F. Sato, K. Utsumi, and M. Inoue, "Oxygen-dependent regulation of energy metabolism in ascites tumor cells by nitric oxide," *Cancer Research* 56, no. 19 (1996).

[85]M. N. Routledge, D. A. Wink, L. K. Keefer, and A. Dipple, "Dna-Sequence Changes Induced by 2 Nitric-Oxide Donor Drugs in the Supf Assay," *Chemical Research in Toxicology* 7, no. 5 (1994).

[86]Peter C. Ford, "Polychromophoric metal complexes for generating the bioregulatory agent nitric oxide by single- and two-photon excitation," *Accounts of Chemical Research* 41, no. 2 (2008).

[87]Alexis W. Carpenter and Mark H. Schoenfisch, "Nitric oxide release: Part II. Therapeutic applications," 41, no. 10 (2012).

trigger for the release of NO in biological systems with a superb spatiotemporal accuracy by using NO photodonors[88] (Fig. 8).

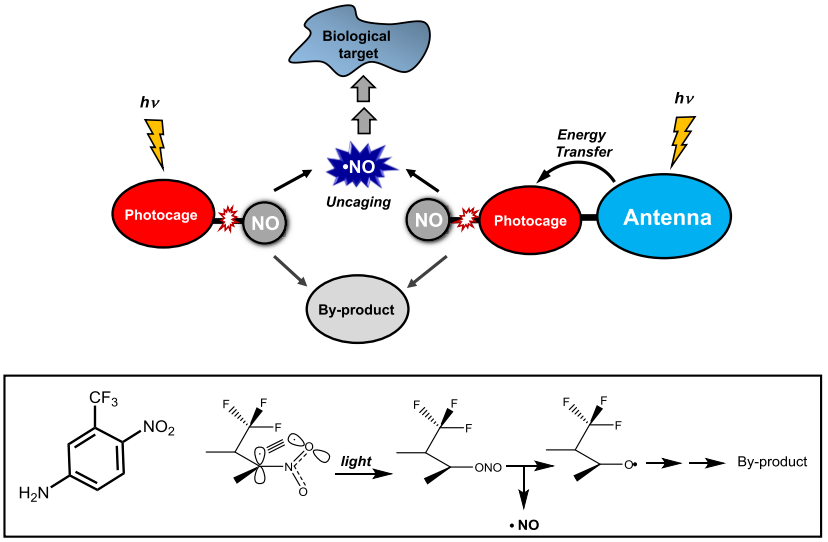

Fig. 8. (Top) The photouncaging process: light excitation of the photocage triggers cleavage of the covalent bond with the caged and unactive NO molecule, releasing it in its active form; alternatively, photoexcitation of an antenna chromophore encourages the NO uncaging upon intramolecular energy transfer to the photocage. **(Bottom)** Molecular structure of a nitroaniline-based photocage and sketch of the mechanism for its NO photorelease.

A number of molecular and macromolecular scaffolds and nanomaterials able to deliver NO with some control have been developed over the last years.[89,90] The working principle of a NO photochemical precursor bases on the concept of "photocaging". This term refers, in general, to the momentary inactivation of a biologically active molecule by its covalent incorporation within the molecular skeleton of a photoresponsive chromogenic centre (the photocage).[91]The photosensitive moiety exploits the absorbed excitation light to break a

[88]Salvatore Sortino, "Light-controlled nitric oxide delivering molecular assemblies," *Chemical Society Reviews* 39, no. 8 (2010).

[89]{Riccio, 2012 737 /id

[90]{Kim, 2014 776 /id}

[91]Petr Klan, Tomas Solomek, Christian G. Bochet, Aurelien Blanc, Richard Givens, Marina Rubina, Vladimir Popik, Alexey Kostikov, and Jakob Wirz, "Photoremovable Protecting Groups in Chemistry and Biology: Reaction Mechanisms and Efficacy," *Chemical Reviews* 113, no. 1 (2013).

chemical bond, releasing the "caged" molecule, *i.e*. NO, in its active form. This strategy permits to confine the site of action of NO at the irradiated area with an exquisite spatial precision and to control its dosage with great accuracy by tuning the light intensity and/or duration as needed.

Furthermore, the simple structure of these NO photoprecursors makes them suitable for derivatization *via* simple synthetic procedures.

In view of image-guided NO-based phototherapies, the visualization of the NO photodonor in a cellular environment through fluorescence techniques represents an indispensable requisite. This permits to produce a highly localized "burst" of NO precisely at the desired sites. Differently to photosensitizers used in PDT, which are intrinsically fluorescent, the combination of fluorescent imaging and phototherapeutic capacity in the same structure is less common in the case of NO photodonors.[92] Of course, in the case of NO photocages lacking of emissive properties, fluorescent character can be imposed by their covalent combination with suitable flurogenic centers. In this case, inter-chromophoric interactions (*i.e.* energy or electron transfer) between the fluorophoric unit and the NO photocage need to be intentionally avoided with a careful choice of chromophoric groups by taking into account the energy of the lowest excited states of the components as well as their redox potential. Under these conditions, the fluorophoric center and the NO photocage can act in tandem even under condition of co-absorption of the excitation light.

While combinations of NO and singlet oxygen photorelease have been investigated,[93] the effect of combining NO release with conventional chemotherapy is practically unexplored.

---

[92]A. Fraix and S. Sortino, "Photoactivable Platforms for Nitric Oxide Delivery with Fluorescence Imaging," *Chemistry-An Asian Journal* 10, no. 5 (2015).

[93]F. Quaglia and S. Sortino, "Polymer Nanoparticles for Cancer Photodynamic Therapy Combined with Nitric Oxide Photorelease and Chemotherapy," in *Applied Photochemistry: when light meets molecules*, ed. G. Bergamini and S. Silvi. Springer, 2016).

2.6.3 Combination of gene therapy with chemotherapy

The use of combination therapy involving both gene therapy and chemotherapy has resulted in enhanced anti-cancer effects and has become an increasingly important strategy in medicine. Gene therapy consists in the delivery of genes in the form of plasmid DNA (pDNA), to supplement down-regulated or to replace mutated genes, and/or nucleic acid fragments in the form of small interfering RNA (siRNA), short hairpin RNA (shRNA) or micro RNA (miRNA) able to interfere with the expression of any gene of interest.

The majority of research in this area has been focused on the co-delivery of a drug and a gene using separate carriers to the same target tissue. Often this method has failed encouraging the development of nanoplatforms combining the gene and drug in one system thus overcoming differences in the physicochemical properties, such as hydrophobicity, molecular weight and metabolic stability. As a consequence this may results in sub-optimal gene transfection/expression efficiencies and drug release in target cells.[94,95] Moreover, the use of polymeric NPs consent to condense and pack pDNA, to protect pDNA/nucleic acid fragments from degradation by serum nuclease in the extracellular medium, and to neutralize their negative charge to avoid repulsion by anionic plasma membrane.

Several types of multifunctional NPs have been reported in the literature where the potential of this approach has been evaluated.[96]

[94]Jessica A. Kemp, Min Suk Shim, Chan Yeong Heo, and Young Jik Kwon, ""Combo" nanomedicine: Co-delivery of multi-modal therapeutics for efficient, targeted, and safe cancer therapy," *Advanced Drug Delivery Reviews* 98 (2016).

[95]Pei Yun Teo, Wei Cheng, James L. Hedrick, and Yi Yan Yang, "Co-delivery of drugs and plasmid DNA for cancer therapy," *Advanced Drug Delivery Reviews* 98 (2016).

[96]Lin Kang, Zhonggao Gao, Wei Huang, Mingji Jin, and Qiming Wang, "Nanocarrier-mediated co-delivery of chemotherapeutic drugs and gene agents for cancer treatment," *Acta Pharmaceutica Sinica B* 5, no. 3 (2015).

2.7 Aim of the work and outline of thesis contents

Based on this background, in an attempt to engineer multifunctional NPs for cancer therapy, we develop novel double-coated NPs through a layer-by-layer deposition technique. The aim was to test different combinations of bioactive species and to deliver NPs selectively to cancer cell overexpressing CD44 receptor to potentiate chemotherapeutic activity. On a technological standpoint, we designed biodegradable NPs with sustained delivery of the entrapped drug and surface-decorated with polymer layers by electrostatic interactions able to embed ionic drugs and to allow NP targeting.

Core NPs were made of PLGA and entrapped hydrophobic drug preferentially. Then a first polycationic layer made of Polyethyleneimine and a second decorating polyanionic layer of low molecular weight HA are envisaged.

Branched Polyethyleneimine (PEI) is a cationic polymer that contains primary, secondary and tertiary amino groups. It was selected as a bridging layer for several reasons. First, PEI has been found to induce anticancer effects through toll-like receptors (TLRs) and considered a potential therapeutic agents for cancer immunotherapy.[97] Second, HA-decorated NPs are expected to lose partly the HA layer due to the presence of hyaluronidases and to operate as cationic PEI-covered NPs with the advantage of i) increased accumulation in cancer cell via electrostatic interaction between the NPs and the plasma membrane;ii) inhibition of tumor growth through necrosis; iii) deep penetration into remote tumor area because the necrosis caused by NPs reduces cell density, thus allowing the anticancer drug to diffuse into deep tissue.[98]In addition, the activity of PEI as transfecting agents can be of help in delivering nucleic acids.[99]

The research activity has been summarized in five chapters and two annexes:

[97]P. Balakumar and M. Singh, "Anti-tumour necrosis factor-alpha therapy in heart failure: Future directions," *Basic & Clinical Pharmacology & Toxicology* 99, no. 6 (2006).

[98]H. Yim, S. J. Park, Y. H. Bae, and K. Na, "Biodegradable cationic nanoparticles loaded with an anticancer drug for deep penetration of heterogeneous tumours," *Biomaterials* 34, no. 31 (2013).

[99]A. Ediriwickrema, J. B. Zhou, Y. Deng, and W. M. Saltzman, "Multi-layered nanoparticles for combination gene and drug delivery to tumors," *Biomaterials* 35, no. 34 (2014).

- Biodegradable NPs sequentially decorated with Polyethyleneimine and Hyaluronan for the targeted delivery of docetaxel (DTX) to airway cancer cells (Chapter 2). This part reports the development of double coated NPs (dcNPs) delivering DTX and compares colloidal and biological properties of PEI-coated PLGA NPs to those of HA/PEI-coated PLGA NPs.
- Hyaluronan-decorated polymer NPs targeting CD44 receptor for the combined photo/chemo-therapy of cancer (Chapter 3).Here, we try to potentiate DTX activity combining a Tetraphenylporphirine ($TPPS_4$) to DTX in dcNPs.
- PLGA NPs for the delivery of a doxorubicin-nitric oxide photodonor molecular hybrid to overcome multidrug resistance (Chapter 4). To this purpose, a Doxorubicin-NO photodonor conjugates (DOX/NO) was entrapped in dc-NPs and its photochemical properties studied. This part of work has been carried out at the University of Catania under the supervision of Prof. Salvatore Sortino.
- Combining chemotherapy and gene therapy through nanoparticles decorated with a Polyethyleneimine -hyaluronan sequential layer (Chapter 5).We based this strategy on a preliminary cellular studies which showed that cytotoxicity of 5-Fluorouracil (5FU) was increased by a high level of rpL3 ribosomal protein. 5-FU and a plasmid of L3 protein were entrapped in dcNPs and their colloidal and biological properties deeply explored.

In the two annexes the development of Pluronic micelles for drug delivery is reported. In Annex I the combination Sorafenib-Verteporfin is formulated as a supplementary example of coupling chemotherapy to photodynamic therapy while in the Annex II the potential of Pluronic micelles as pulmonary delivery platform is explored.

Part of the work has been carried in collaboration with colleagues at Department of Pharmacy and Chemistry (University of Napoli Federico II, Italy), Department of Biology (University of

Padova, Italy), Department of Drug Science (University of Catania, Italy) and Department of Chemistry (University of Maringa, Brazil).

Chapter 2
Biodegradable nanoparticles sequentially decorated with Polyethyleneimine and Hyaluronan for the targeted delivery of docetaxel to airway cancer cells

Published as:
Sara Maiolino, Annapina Russo, Valentina Pagliara, Claudia Conte, Francesca Ungaro, Giulia Russoand Fabiana Quaglia

J Nanobiotechnology3 (2015) 13-29

Chapter 2

Abstract

Background; Novel polymeric nanoparticles (NPs) specifically designed for delivering chemotherapeutics in the body and aimed at improving treatment activity and selectivity, cover a very relevant area in the field of nanomedicine. Here, we describe how to build a bioresponsive polymer shell of Hyaluronan (HA) and Polyethyleneimine (PEI) on biodegradable NPs of poly(lactic-co-glycolic) acid (PLGA) through electrostatic interactions and to achieve NPs with unique features of CD44 targeting as well as sustained delivery of a docetaxel (DTX) drug cargo.

Results; A stable HA/PEI shell could be obtained by careful selection of layering conditions. NPs with exquisite stability in salt and protein-rich media, with size and surface charge matching biological requirements for intravenous injection and endowed with sustained DTX release could be obtained. Since cationic NPs can be formed by degradation/dissociation of the surface HA because of the excess hyaluronidasess that are overexpressed in tumour interstitium, cytotoxicity, uptake and activity of NPs in CD44(+) (A549) and CD44(-) (Calu-3) lung cancer cells were evaluated on both PLGA/PEI/HA and PLGA/PEI NPs. There was no statistically significant cytotoxic effect of PLGA/PEI/HA and PLGA/PEI NPs in either A549 or Calu-3 cell lines, thus suggesting that introduction of PEI in NP shell was not hampered by its toxicity. Intracellular trafficking of fluorescently labeled RHO-PLGA/PEI/HA and RHO-PLGA/PEI NPs demonstrated an increased time-dependent uptake only for RHO-PLGA/PEI/HA NPs in A549 cells as compared to Calu-3. As expected, RHO-PLGA/PEI NP uptake in A549 cells was comparable to that observed in Calu-3 cells. RHO-PLGA/PEI/HA NPs internalized into A549 cells demonstrated a preferential perinuclear localization. Cytotoxicity data suggest that the delivery of DTX through PLGA/PEI/HA NPs allowed a much more potent antiproliferative activity than free DTX in A549 cells. Furthermore, DTX-PLGA/PEI NPs, as hypothetical result of hyaluronidases-mediated degradation in tumor interstitium, were still able to improve the cytotoxic activity of free DTX.

Conclusions; Taken together, results lead us to hypothesize that biodegradable NPs coated with a PEI/HA shell represent a very

promising system to treat CD44 overexpressing lung cancer. In principle, this novel nanocarrier can be extended to different single drugs and drug combinations taking advantage of the shell and core properties.

1 Introduction

In the past twenty years, nanotherapeutics have been introduced in the clinical practice for treating tumors with the goal to improve therapeutic outcome of conventional pharmacological therapies, to alleviate their toxicity as well as to overcome multidrug resistance [1-8]. By providing a protective housing for the drug, nanoscale delivery system can in theory offer the advantages of drug protection from degradation, efficient control of pharmacokinetics and accumulation in tumor tissue, thus limiting drug interaction with healthy cells and as a consequence side effects. Polymer-based nanoparticles (NPs) specifically designed for cancer treatment cover a very relevant and widely explored area in the field of nanotechnology [9-11]. The main advantages of polymer NPs reside in the opportunity to readily manipulate their properties by selecting polymer type and mode of carrier preparation. As a consequence, not only those surface features which affect biological behavior (spatial distribution of drug dose in the body) are controlled, but also timing of drug release (temporal control of drug availability to target) is predetermined. Due to their well-established biocompatibility and safety profile, nano-oncologicals made of polyesters such as poly(lactic-co-glycolic) acid (PLGA) can be considered one of the most interesting materials for this application and are greatly emerging in the field [2]. To be used as an effective nanomedicine, PLGA NPs need to be surface-engineered according to specific technological and therapeutic needs [12]. Core-shell architecture represents an effective way to attain multiple functionalities on a nanoscopic length scale. Indeed, a core (template) generally carrying a chemotherapeutic agent can be surrounded by a shell with different composition and configuration that provides a functional and interacting interface with biological environment [13]. The shell is also responsible of colloidal stability of the system "in the bottle" (shelf life) and in biologically relevant media. A wide array of currently-available materials and possible combinations can be used to fabricate core-shell NPs spanning from tailored amphiphilic polymers, able to form nanoassemblies in aqueous media, to nanostructures where electrostatic or hydrophobic interactions drive shell deposition on a core template. The latter approach is very attractive since no complicate synthetic steps to attain polymer functionalization are required. In the construction of layered

NPs, an emerging aspect in nanotechnology is represented by the use of polymers with specific functions for cancer treatment. Two relevant examples are Polyethyleneimine (PEI) and Hyaluronan (HA). PEI is a cationic polymer widely employed for transfection due to its capacity to complex polyanionic DNA and oligonucleotides (decoy, siRNA, miRNA)[14]. Recently, it has been demonstrated that PEI can induce anticancer effects via electrostatic interaction with cell membranes [15,16]. Furthermore, it has been observed that intratumoral injection of different cationic polymers evokes a robust infiltration of Th 1 and NK cells into the tumor site, reversing the tumor microenvironment from immunosuppressive to immunostimulatory and inducing massive tumor necrosis [17]. In other studies, PEI triggered APC activation via TLR-signaling and exerted direct tumoricidal activity in a mouse model of ovarian tumors [18]. Cationic NPs are considered intriguing systems to promote deep penetration in tumor tissues [19,20]. Nevertheless, cationic NPs induce rapid formation of complex aggregates with negatively charged serum molecules or membranes of cellular components, which are then cleared by the reticuloendothelial system (RES). More importantly, many cationic vectors developed so far exhibit substantial toxicity [21], which has limited their clinical applicability thus demanding strategies to reversibly shield their surface with biomimetic coatings. A functional anionic polymer such as hyaluronan (HA) can perfectly fit the purpose to cover cationic NPs through electrostatic interactions and to form a bioresponsive shell. HA is a negatively-charged polysaccharide with a relevant role in cancer since its receptors (CD44, RHAMN) are overexpressed on the surface of a broad variety of cancer cells [22]. Recently, combination of chemotherapeutic drugs with HA NPs for selectively targeting CD44-overexpressed cancer cells has received increasing attention to improve specificity of the drug and alleviate side effects [23]. In fact, receptor-mediated endocytosis of HA-decorated NPs facilitates drug transport inside the cells and contributes to enhance drug cytotoxicity [24]. Nevertheless, HA is involved in ECM remodeling of cancer tissues since HA degradation by interstitium hyaluronidases is a process at basis of facilitated metastasis formation [23]. Although based only on electrostatic interactions, core-shell PLGA NPs prepared by stepwise modification through several sequential layering of positive and negative polymers such as chitosan/alginate,

polylysine/alginate and polylysine/HA [25] has been found successful to achieve physically stable NPs for the co-delivery of different drugs with nucleic acid fragments [26]. In this paper, we describe how to build a bioresponsive shell on biodegradable PLGA NPs through PEI/HA electrostatic interactions and achieve NPs with unique features of CD44 targeting, tumor penetration after HA shedding as well as sustained delivery of the hydrophobic anticancer drug docetaxel (DTX). After a formulation study aimed at optimizing preparation conditions of NPs, a powder for injection was obtained and characterized for release properties and stability in media with different ions and protein contents. HA-decorated NPs were tested for trafficking and activity in CD44(+) and CD44(-) lung cancer cells and potential contribute of HA shedding highlighted.

2 Materials and methods

Docetaxel (DTX, MW=807.88) was purchased from LC laboratories (USA). Poly(lactic-co-glycolic) acid (PLGA) (D,L-lactic, 50:50 Resomer RG 502H, inherent viscosity 0.16 - 0.24 dl/g) was purchased from Boehringer Ingelheim (Ingelheim, Germany). Rhodamine B (RHO), trehalose, polyethyleneimine (PEI, MW= 25 kDa branched), copper (II) sulphate (MW= 63.55), hexadecyltrimethyl-ammonium bromide, poloxamer 188 (Pluronic® F68), sodium acetate, sodium chloride, sodium hydroxide, glacial acetic acid and trifluoracetic acid (TFA) were purchased from Sigma-Aldrich. Acetonitrile and acetone were purchased from Carlo Erba Reagenti (Milan, Italy).DMEM and Fetal Bovine Serum (FBS) were purchased from GibcoLife Technologies. Hyaluronan (HA, MW <10 kDa) was a kind gift of Magaldi Life S.r.l. Ultrapure water was used throughout the study.

2.1 Preparation of DTX-PLGA/PEI/HA NPs

NPs were prepared through a layer-by-layer deposition method. In a first step, DTX-PLGA NPs were prepared by nanoprecipitation. PLGA 502H (5 mg) and DTX (5,10,15 and 20 % w/w) were co-dissolved in acetone(1 mL) and added drop-wise to 2 mL of an aqueous phase containing Pluronic F68 (0.1% w/v) under magnetic stirring. The organic solvent was then evaporated under vacuum using a rotary evaporator for 15 min, Thereafter, NP dispersion was splitted in 4 Eppendorf® tubes and centrifuged at 5000 x g for 15 min (Mikro 20 Zentrifugen). In the second step, NP pellet in each Eppendorf® tube was disperded in 1 mL of ultrapure water (final PLGA NP concentration was 1.5 mg/mL) and in each sample 125 μL of a PEI solution in water (0.5, 1.0 and 1.5 mg/mL) were added under stirring for 15 min. Thereafter, the sample was centrifuged again (2.800 x g for 10 min) to eliminate un adsorbed PEI and redispersed in 1 mL of ultrapure water (DTX-PLGA/PEI). In the third step,100 μL of a HA solution (1 mg/mL) were added to PLGA/PEI NPs under stirring for 15 min (DTX-PLGA/PEI/HA). Final NPs were freeze-dried for 24 h with trehalose as cryoprotectant (30 mg in each vial) and kept at 4 °C. Recovery yield of production process was evaluated on an aliquot of DTX-PLGA/PEI/HA NPs (without cryoprotectant) by weighting the solid residue after freeze-drying.

Results are expressed as the ratio of the actual NPs weight to the theoretical polymer weight×100. Fluorescent NPs were prepared analogously by incorporating a 20% w/w of PLGA-RHO to PLGA NP core.

2.2 Characterization of DTX-PLGA/PEI/HA nanoparticles

2.2.1 Size, surface charge and morphology

Hydrodynamic diameter, polydispersity index (PI) and Zeta potential of NPs after each preparation step were determined on a ZetasizerNano Z (Malvern Instruments Ltd., UK). Results are reported as mean of three separate measurements of three different batches (n=9) ± SD.

Particle morphology was analyzed by scanning electron microscopy (SEM) (Leica S440, Germany) after gold sputtering.

2.2.2 DTX entrapment efficiency

DTX loading inside DTX-PLGA/PEI/HA NPs was assessed by placing 0.5 mg of freeze-dried NPs or 30.5 mg of NPs freeze-dried with trehalose in 500 μL of DCM under stirring and dried. Thereafter, 500 μL of water and 500 μL of acetonitrile were added under stirring and the sample was finally filtered through a 0.45 μm filter (RC, Chemtek, Italy). DTX was analyzed by HPLC on a Shimadzu apparatus equipped with a LC-10ADvp pump, a SIL-10ADvp autoinjector, a SPD-10Avp UV–Vis detector and a C-R6 integrator. The analysis was performed on a Supelco 5 μm, C18 column (250×4.6 mm, Å). The mobile phase was a55:45 (v/v) mixture of water with TFA 0,1 % and acetonitrile pumped at a flow rate of 1 mL/min. The UV detector was set at 227 nm. A calibration curve for DTX in ethanol was constructed in the concentration range 0.980–196 μg/mL. The limits of quantification (LOQ) and detection (LOD) were 1.29 and 0.39 μg/mL, respectively.

2.2.3 PEI amount in NPs

PEI was quantified by a colorimetric method developed by us [33].To evaluate the amount of PEI in DTX-PLGA/PEI/HA NPs, 0.5 mg of freeze-dried NPs (with and without 30 mg of cryoprotectant) were treated with 1mL of NaOH 1 M and stirred overnight. The sample (0.5 mL) was diluted with 0.5 mL of 1 M acetic acid. The resulting solution

(0.5 mL)was added to 1 mL of acetate buffer 0.1 M at pH 5.4, and complexed with 0.25 mL of a copper (II) sulphate water solution (0.1%w/v).The absorbance value of each solution was recorded at 281nm (Shimadzu, UV 1800). A calibration curve was constructed in the same condition in the PEI concentration range 15–380 μg/mL.

2.2.4 HA amount in NPs

To evaluate the extent of HA adsorption onto DTX-PLGA/PEI/HA NPs, 0.5 mg of NPs were centrifuged at 13000 x g for 15 min, the supernatant was withdrawn and freeze-dried. The solid residue was then dissolved in 1mL of 0.2 M acetate buffer (0.2 M sodium acetate and 0.15 M sodium chloride) at pH 6. Thereafter,2mL of cetyltrimethylammonium bromide reagent (2 g sodium hydroxide, 1 g hexadecyltrimethylammonium bromide in 100 mL water) was added and the sample was analyzed at 350nm. A calibration curve was constructed in same condition in HA concentration range 10–200 μg/mL.

2.2.5 Stability in different media

30.5 mg of freeze-dried DTX-PLGA/PEI and DTX-PLGA/PEI/HA NPs powder (corresponding to 0.5 mg of NPs) were dispersed in glucose 5%, NaCl 0.9%, DMEM without and with FBS 10% (1 mL). Size, polydispersity index and zeta potential of the samples were evaluated.

2.2.6 In vitro release studies

In vitro release of DTX from NPs was assessed in 10 mM phosphate buffer containing NaCl (137 mM) and KCl (2.7 mM) at pH 7.4 (PBS) by a dialysis method. Around 100 mg of DTX-PLGA/PEI and DTX-PLGA/PEI/HA freeze-dried powder (corresponding to 2 mg of NPs) was dispersed in 0.5 mL of DMEM with 10% FBS and placed in a dialysis bag (MWCO=3500 Da,Spectra/Por®). The sample was plunged in PBS and kept at 37 °C up to 72 h. At selected time intervals, 1 mL of release medium was withdrawn and replaced with an equal volume of fresh medium. DTX quantitative analysis was performed as described above. Release profile of free DTX dissolved in EtOH (10 μL, 2 μg/μL) and added to 0.5 mL of medium was assessed for comparison. Results are expressed as % release over time ± SD of three experiments.

2.3 Cell cultures and treatments

The A549 and Calu-3cell lines were cultured in Dulbecco‘s Modified Eagle‘s Medium (DMEM) supplemented with 10% heat-inactivated fetal bovine serum (FBS) (Invitrogen, Life Technologies, Italy), 1.5 mM L-glutamine, 100 units/ml penicillin, and 100 μg/ml streptomycin under humidified atmosphere of 5% CO2 at 37°C. Treatments of cells were performed replacing the culture medium with those containing increasing concentrations of DTX (0.1 ng-2 μg), unloaded and DTX-loaded PLGA/PEI and PLGA/PEI/HA NPs (0.1 mg–2 NPs, 0.1 ng-2 μg DTX). DMSO 0.1% (v/v) was used as vehicle for DTX.

2.3.1 MTT assay

A549 and Calu-3 cells were seeded onto 96-well plates (2 × 104 cells/well) and incubated with NPs for 24 h and 72 h. Then, cell viability was evaluated as mitochondrial activity using the MTT [34]. The absorbance measured at 540 nm using a microplate reader (LabsystemsMultiskan, MS).

2.3.2 LDH assay

LDH leakage into the media, an indicator of cell injury, was detected using using the cytotoxicity assay, CytoTox 96® (Promega, USA), according to the manufacturer‘s instructions, as described [35].Samples from clarified medium of treated and untreated A549 and Calu-3 cells were taken after 24 h and 72 h of incubation and the LDH activity was measured.

2.3.3 Confocal microscopy

A549 cells and Calu-3 cells were plated on coverslips at a density of 2 × 104 cells per well in 12-well plates as previously reported (Russo et al., 2006). Images of fluorescence-labeled cells were captured with a Zeiss LSM 510 meta confocal microscope equipped with an oil immersion plan Apochromat 100× objective 1.4 NA.The laser line was set at 553 nm for RHO and 405 nm for DAPI. Images were acquired simultaneously in red and blue channels, and as z- stack. A gallery of optical slices was collected and xz, yz composites were processed using ImageJ Software to reconstruct the x-axis projection using stack images.

The scale bars on all the images correspond to 10 μm. The uptake of NPs was evaluated by measuring the incorporation of the fluorescent probe RHO in A549 and Calu-3 cells. Briefly, cells (2 × 104 cells per well in 12-well plates) were collected and analysed by fluorimetry. The fluorescence was measured with a Cary Eclipse fluorescence spectrophotometer (Varian). Excitation and emission wavelengths were 553 and 627 nm, respectively.

3 Results and discussion

To improve DTX activity and selectivity to cancer cells, we tried to engineer biodegradable PLGA NPs with a PEI/HA shell endowed with ability to interact with CD44 receptor thus improving NP accumulation in cancer cells. An anionic non end-capped PLGA nanoparticle template entrapping the model anticancer drug DTX was covered with a polycationic layer of PEI (25 kDa, branched) followed by a finishing layer of low molecular weight HA (<10 kDa). We first developed a robust layering procedure to obtain NPs and characterized the system in biologically-relevant media. Next, we assessed cytotoxicity, uptake and activity of NPs in CD44(+) and CD44(-) lung cancer cells also considering a possible HA shedding and generation of PEI-coated NPs.

3.1 Layering procedure

Preparation of DTX-loaded PLGA/PEI/HA NPs is a multistep process comprising i) the preparation of a PLGA core template; ii) the absorption of a positive PEI layer; iii) the absorption of a negative bioresponsive layer of HA (Fig. 1A).

DTX-PLGA NPs were prepared by nanoprecipitation of a PLGA acetone solution in a Pluronic F68 water solution. The size of unloaded PLGA NPs was only slightly affected by PLGA concentration while the surface was always negative (Fig. 2A). Thus, a PLGA concentration of 5 mg/mL was selected for all further experiments. After a washing step to eliminate surface-adsorbed Pluronic F68, around 60% of NPs with the original size/zeta potential could be recovered. Then, a first positive layer of PEI was adsorbed through electrostatic interactions by incubating NPs with a PEI water solution.

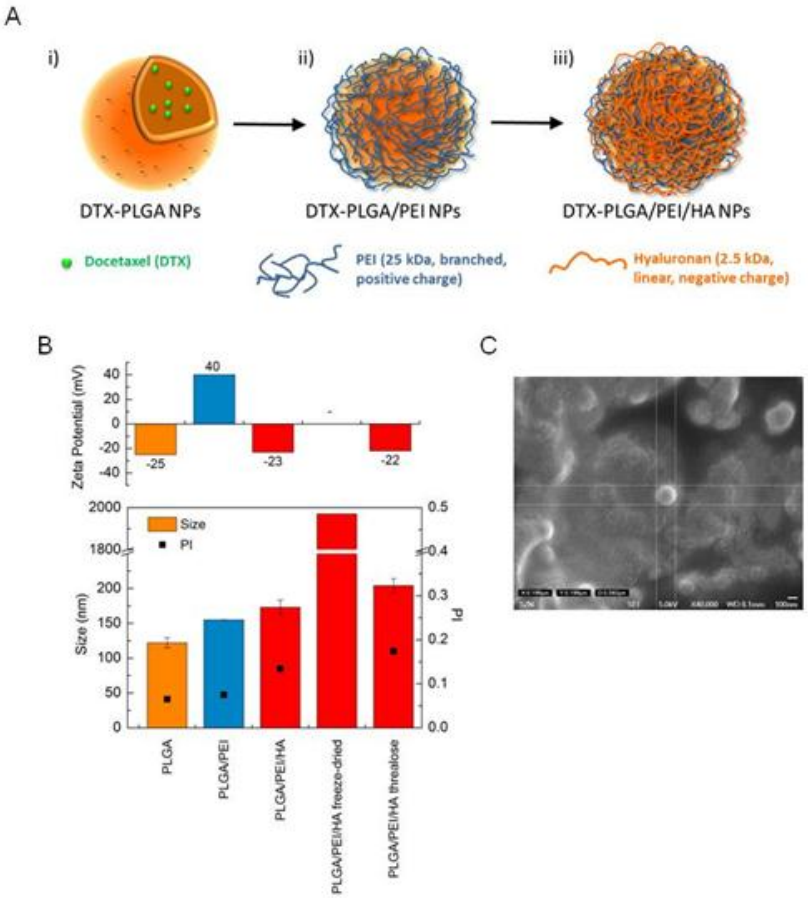

Fig. 1. Structure and properties of the NPs at different preparation steps. A) Schematic representation of the double coating process. B) Size, polydispersity (PI) and zeta potential of NPs during coating and after dispersion of final freeze-dried PLGA/PEI/HA NPs (without and with trehalose) in water. Results are the mean of three measurements obtained on three different NP batches ± SD. C) SEM micrographs of PLGA/PEI/HA NPs.

The process of polymer film growth onto NP surface can be severely altered by several experimental factors and mainly by salt concentration of the medium [27]. PEI layering was thereby carried out both in water and PBS 0.01 M at pH 7.4. However, only water allowed the prompt re-dispersion of PLGA/PEI NP pellet without aggregation. Thus, all the preparation steps were carried out in water. The addition of 125 μL of a PEI water solution at increasing concentration (0.5, 1.0 and 1.5 mg/mL) caused an inversion of zeta potential from negative to positive values (Fig. 2B). Optimal conditions for layering were found at 1 mg/mL since only a slight increase of size and polydispersity index (PI) was observed (Fig. 1B). PLGA/PEI NPs were further collected to eliminate un-adsorbed PEI and dispersed in water again. In the following step, PLGA/PEI NPs were finished with a HA layer giving PLGA/PEI/HA NPs, which displayed a slightly increased size and negative zeta potential.

Quantitative adsorption of HA on NP surface was confirmed by evaluating the amount of HA in the solution after collecting NPs (no free HA was detected in the medium). In developing translational NPs for intravenous route, it is of key importance to produce a lyophilized NP powder with a suitable shelf-life and with effective dispersion in the diluting vehicles usually employed for administration. While PLGA/PEI/HA NPs freeze-dried as such underwent extensive aggregation and could not be dispersed in water (Fig. 1B), the addition of a cryoprotectant such as trehalose gave a powder that, after dispersion in water, restored the original NP size, PI and zeta potential.

A

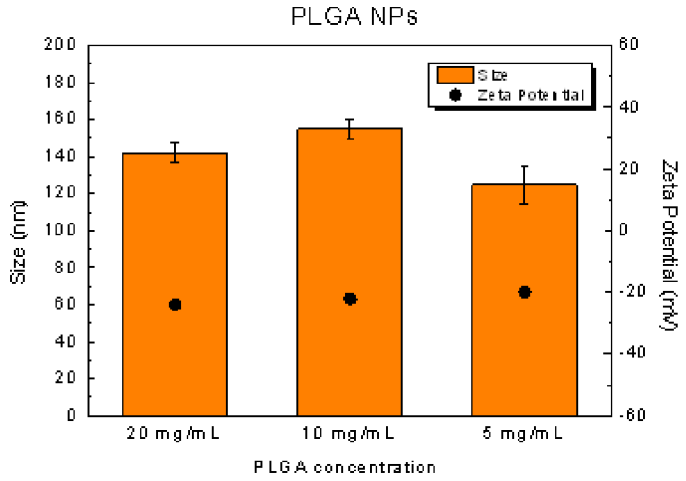

B

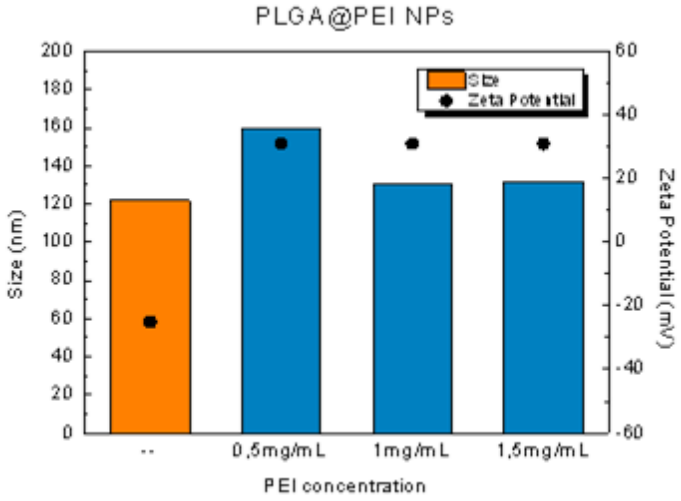

Fig. 2. Effect of formulation conditions on the properties of PLGA core template. A) Effect of PLGA concentration. B) Effect of PEI concentration.

.

3.2 Properties of DTX-loaded NPs

Overall properties of DTX-loaded PLGA/PEI/HA NPs are reported in Table 1. DTX entrapment in the PLGA core did not alter size, PI and zeta potential also after the freeze-drying step. Around 50% of the initial PEI amount was retained on NP surface whereas the absorption of HA was complete. The yield of the production process was found to be around 20% (Table 1), which is in line with values reported for layered NPs.

Table 1. Properties of DTX-loaded PLGA/PEI/HANPs. SD were calculated on five different batches.

	DTX-PLGA/PEI/HA	**DTX-PLGA/PEI/HA freeze-dried powder**
Trehalose/NP weight ratio	-	60
Yield (%± SD)	21.2 ± 0.8 [a]	-
Mean D_H (nm ± SD)	173 ± 10 [b]	203 ± 10 [c]
Polydispersity index	0.13 [b]	0.17 [c]
Zeta Potential (mV)	-23.2 [b]	-22.3 [c]
DTX actual loading (mg *per* 100 mg)	0.95 ± 0.5	0.013 ± 0.001
PEI actual loading (mg *per* 100 mg)	7.94 ± 2.1	0.132 ± 0.010
HA actual loading (mg *per* 100 mg)	12.2 ± 0.8	0.20 ± 0.03

[a] calculated as ratio between total component weight and NP weight
[b] as prepared NPsbefore freeze-drying
[c] after dispersion of freeze-dried powder in water

It is worth of note that final NPs can be loaded with amount of DTX in the PLGA core up to 15% without altering its size and zeta potential (Table 2). SEM analysis confirmed the spherical morphology and size of the final formulation (Fig. 1C). A drawback with a layering procedure

carried out in water could be the occurrence of weaker interactions between negative and positive polymer chains and, as a consequence, the formation of a loose and less stable coating. On these bases, we tested the stability of DTX-PLGA/PEI and DTX-PLGA/PEI/HA NPs in different media by measuring size and zeta potential (Fig. 3A). Both types of NPs were stable in NaCl 0.9% or glucose 5% solution giving size and zeta potential values comparable to those found in water. To mimic more closely NP behavior in cell culture experiments, stability was also assessed in DMEM without or with FBS (FBS- and FBS+, respectively).

Table 2. Entrapment efficiency of DTX at different loading into PLGA nanoparticles.

DTXtherorical loading (% w/w)	Hydrodynamic diameter (nm ± SD)	Zeta potential (mV)	Actual loading (mg/100 mg) [a]	Entrapment efficacy (% w/w) [b]
5	123 ± 10	-22	1.3 ± 0.5	26.5
10	124 ± 2.5	-21	2.7 ±1	27.2
15	127.5 ±3	-38	4 ±2.4	26.6

[a] Actual loading is expressed as the amount (mg) of drug encapsulated per 100 mg of NPs;
[b] Ratio between actual and theoretical loading×100.

The results suggested that DTX-PLGA/PEI greatly increase their size presumably due to extensive protein adsorption while size increase of DTX-PLGA/PEI/HA was limited. Size growth in the presence of proteins did not give macroscopic NP aggregation over time. Release profile of DTX from different NP type was evaluated by dialysis using DMEM FBS+ as dispersing medium and PBS at pH 7.4 and 37°C as external medium (sink conditions were realized). DTX release from DTX-PLGA/PEI and DTX-PLGA/PEI/HA NPs was monitored for 72 h and compared with that of free DTX (Fig. 3B). The transport of free DTX toward the external medium was found to be incomplete in this experimental set-up due to strong DTX-protein interaction inside the dyalisis bag hampering DTX transport in the external medium. This behavior is in agreement with previous data collected on DTX solubilized in human plasma [28]. However, a slower sustained release

A

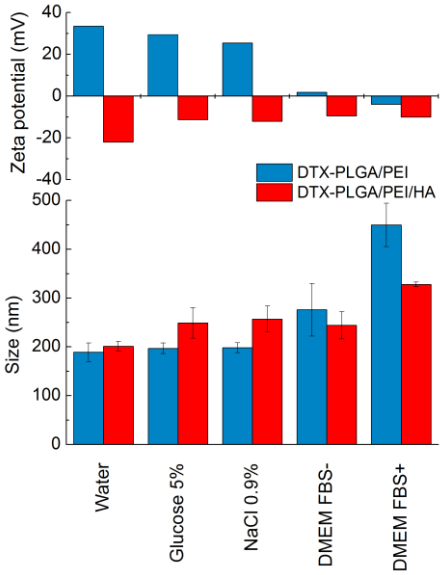

B

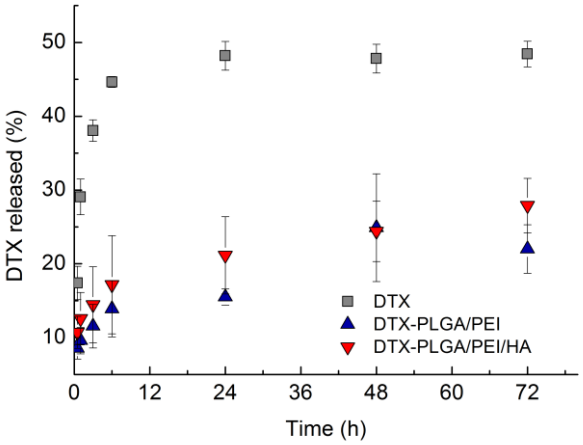

Fig. 3. Properties of DTX-PLGA/PEI and DTX-PLGA/PEI/HA NPs freeze-dried with trehalose. A) Size and zeta potential in different media. B) Release profile of DTX from NPs dispersed in DMEM FBS+. External dialysis medium was a PBS solution at pH 7.4. Free DTX is reported as control. Results are the mean of three experiments ± SD.

of DTX from DTX-PLGA/PEI and DTX-PLGA/PEI/HA NPs as compared with free DTX was found. the release rate observed for coated NPs was similar thus suggesting that for an unionized drug such as DTX,

the presence of the polyelectrolyte layer does not represent a further barrier to drug transport from the PLGA core.

3.3 Cytotoxicity of unloaded NPs

The cytotoxicity of PLGA/PEI/HA and PLGA/PEI NPs was evaluated since in biological environments NP shedding due to HA degradation can occur. Indeed, several cancers produce elevated levels of hyaluronidasess (hyals). A higher expression level of Hyal was also found in metastatic tumors as compared to non-metastatic [23]. In principle, cationic NPs can beformed by dissociation of the surface HA because of the excess hyals in tumor interstitium. The cytotoxicity was assessed by the 3-(4,5-dimethylthiazol-2-yl)-2,5-diphenyltetrazolium bromide (MTT) and lactate dehydrogenase (LDH) release assays. The experiments were performed in A549 and Calu-3 cells selected as CD44(+) and CD44(-) cell line, respectively[29]. Cells were incubated with a wide range of NP concentrations (from 0.1 mg to 2 mg) and tested upon 24 and 72 h of treatments. Data obtained from MTT and LDH assays after 72 h of treatments with PLGA/PEI/HA and PLGA/PEI NPs are shown in Fig. 4.

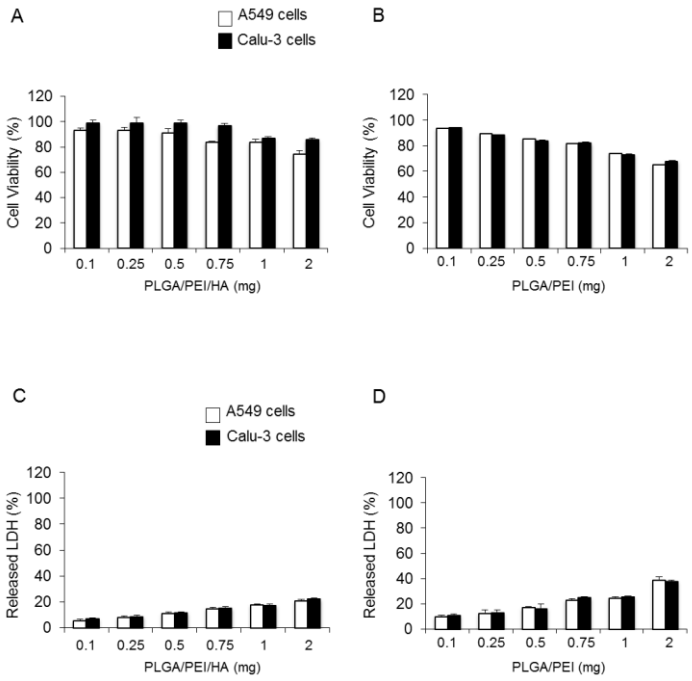

Fig. 4. A549 and Calu-3 cells were exposed to increasing concentrations (0.1-2 mg) of PLGA/PEI/HA NPs (A, C) and PLGA/PEI NPs (B, D) for 72 h. After incubation, cell viability and released of LDH % were evaluated using the MTT (A, B) and LDH (C, D) assay.

The cell viability and LDH release from untreated control were set to 100% and 0%, respectively. Cytotoxicity of PLGA NP and free PEI was also tested (Fig.5).

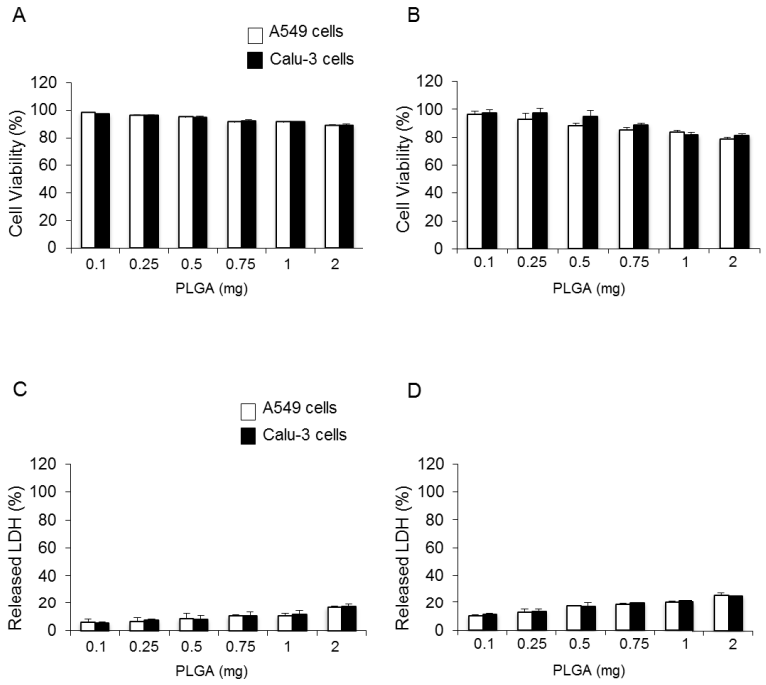

Fig. 5.A549 and Calu-3 cells were exposed to increasing concentrations (0.1-2 mg) of PLGA NPs for 24 h (A, C) and 72 (B, D) h. After incubation, cell viability and released of LDH % were evaluated using the MTT (A, B) and LDH (C, D) assay. The cell viability and LDH release from untreated control were set to 100% and 0%, respectively.

Results from MTT assay in Fig. 6A show that 24 h after the treatment, A549 and Calu-3 cells retained about 90% viability when treated with various concentrations of PLGA/PEI/HA NPs as compared with control (untreated cells set to 100%). At 24 h, the cytotoxicity curve for PLGA/PEI NPs followed almost similar pattern (Fig. 6B).The observed results were confirmed by the values of cell mortality from LDH assay. A549 and Calu-3 cells were incubated with the same concentrations of PLGA/PEI/HA and PLGA/PEI NPs. 24 h and 72 h later, cell membrane damage was assessed. Fig. 6 shows the dose-response histograms after 24h of treatment with PLGA/PEI/HA (Fig. 6C) and PLGA/PEI (Fig. 6D).

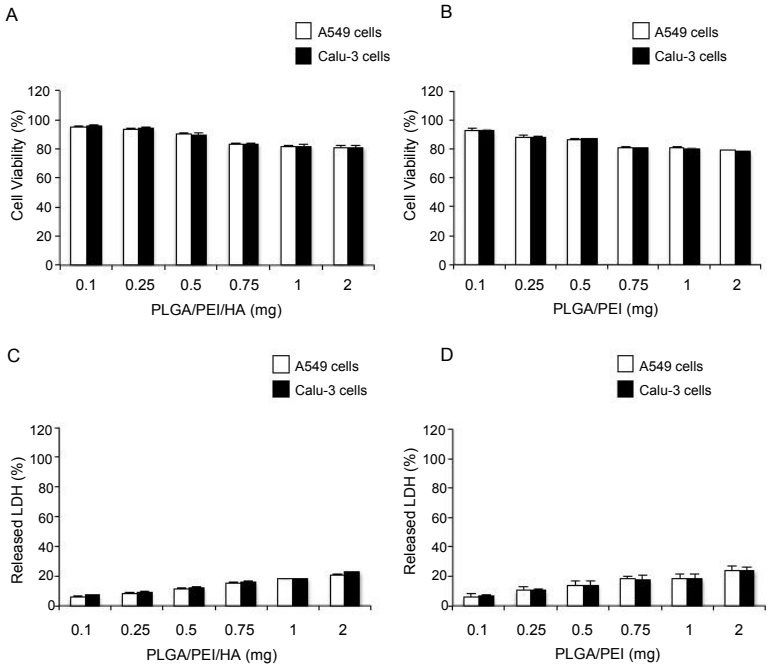

Fig. 6. A549 and Calu-3 cells were exposed to increasing concentrations (0.1-2 mg) of PLGA/PEI/HA and PLGA/PEI NPs for 24 h. After incubation, cell viability and released of LDH % were evaluated using the MTT (A, B) and LDH (C, D) assay. The cell viability and LDH release from untreated control were set to 100% and 0%, respectively. Results are presented as percentage (mean ± SEM) (n = 3) of the control cells.

Figure 3

As shown, the results obtained from the LDH assay were in line with those obtained with the MTT assay. All these results clearly showed that there was no statistically significant cytotoxic effect of PLGA/PEI/HA and PLGA/PEINPs in either A549 or Calu-3 cell lines.

3.4 Uptake of NPs

The natural turnover of free HA is predominantly based on its CD44 receptor-mediated internalization in cells[30]. Starting from this knowledge, we became interested to study the intracellular uptake of PLGA/PEI/HA and PLGA/PEI NPs in A549 (CD44(+)) and Calu-3 (CD44(-)) cells. To this aim, fluorescently labeled RHO-PLGA/PEI/HA and RHO-PLGA/PEI NPs were prepared from a core NP containing RHO-PLGA covalent derivative (Fig. 7). Properties of fluorescent RHO-NPs were comparable to those of untagged NPs (Table 3).

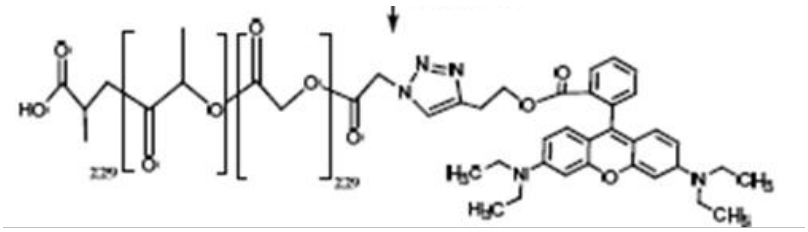

Fig. 7. Structure of fluorescent PLGA-RHO polymer. Synthesis is reported in Maiolino S et al., Nanoscale. 2015 Mar 19;7(13):5643-53.

Table 3. Properties of fluorescent NPs.

NP formulation	Hydrodynamic diameter (nm)	PI	Zeta potential (mV)
RHO-PLGA	138 ± 0.11	0.081	-24.7
RHO-PLGA/PEI	157 ± 0.19	0.083	+32.0
RHO-PLGA/PEI/HA	184.3 ± 2.6	0.100	-22.7

Next, A549 and Calu-3 cells were incubated with RHO-PLGA/PEI/HA and RHO-PLGA/PEI for 4 h and 24 h. The fluorescence intensity of the internalized RHO-NPs was measured by fluorimetry. As shown in Fig. 8 A, in A549 cells the treatment with RHO-PLGA/PEI/HA NPs was associated to an increasing time-dependent cellular uptake (30% and 80% after 4 h and 24 h, respectively). The observation that the lack of CD44 receptor did not provoke any significant uptake of RHO-PLGA/PEI/HA NPs in Calu-3 cells confirmed that the uptake of HA-decorated NPs was CD44 receptor-dependent. These results suggest that the endocytosis mechanism of PLGA/PEI/HA NPs internalization depends on the presence of HA onto the surface. As expected, RHO-PLGA/PEI NP uptake in A549 cells was comparable to that observed in Calu-3 cells (Fig. 8B). This finding highlighted the importance of CD44 receptor in the NPs cellular internalization process. However, it is important to note that RHO-PLGA/PEI NPs were still able to penetrate into cancer cells, giving about 10% and 35% NP uptake after 4 h and 24 h of treatment, respectively (Fig. 8B). This finding is very intriguing in the light of recent data demonstrating that in tumor microenvironment HA-coated NPs could be converted to uncoated NPs as results of hyaluronidases-mediated degradation (Yim et al., 2013).In perspective, loss of HA coating can allow in situ generation of cationic NPs, which are still able to effectively enter inside cancer cells. Next, to investigate the subcellular distribution of internalized NPs, we carried out confocal laser scanner microscopy (CLSM) analysis into A549 cells.

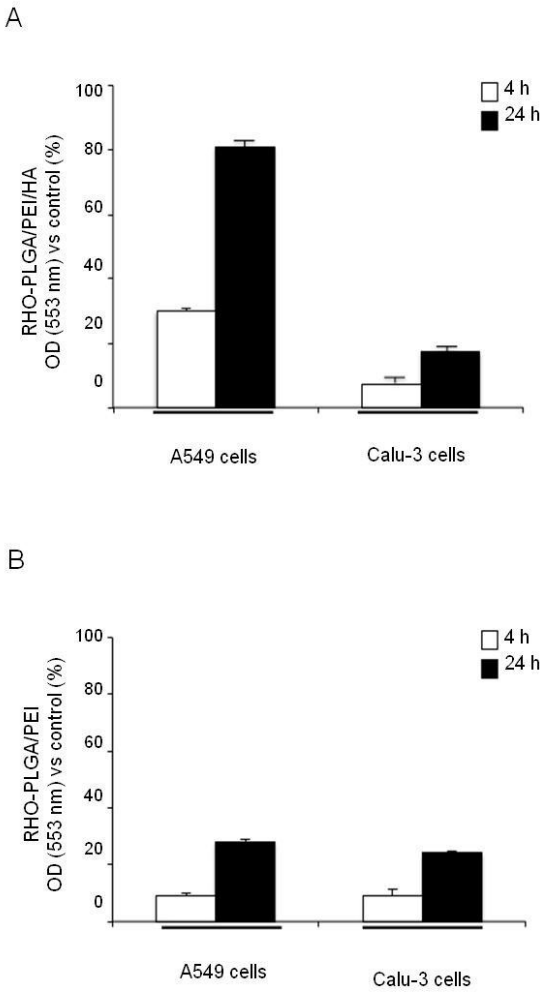

Fig. 8. Fluorescent RHO-PLGA/PEI and RHO-PLGA/PEI/HA NPs were used to detect the intracellular NPs levels. A549 and Calu-3 cells were incubated with 0.5 mg/ml of RHO-PLGA/PEI/HA (A) and RHO-PLGA/PEI (B) for 4 h and 24 h. All measurements were normalized to the fluorescence of RHO labeled NPs in cell medium set as 100%. Results are presented as percentage (mean ± SEM) (n = 3) of the control cells.

After incubation with RHO-PLGA/PEI/HA NPs (Fig. 9A) and RHO-PLGA/PEI NPs (Fig. 9E), the cells were stained with DAPI (Fig. 9B and 9F) and observed under the microscope. A large majority of the RHO-PLGA/PEI/HANPs-associated fluorescence appeared to be distributed in the vicinity, and surrounding, of the cells nuclei, confirming the internalization of NPs (Fig. 9C). The x-axis projections are shown in Fig. 9D. Analysis of z-sections taken through the cell nucleus showed the absence of any signal in the nucleus (Fig. 10). It may be noticed that the perinuclear accumulation of NPs after internalization in cells provides sustained drug delivery in the proximity of the nucleus. This feature might be interesting for the development of tumor suppressor gene-loaded NPs as apoptosis-induction adjuvant, aimed at improving the outcome of common anticancer therapies as 5-FU and L-OHP [31]. The localization of internalized RHO-PLGA/PEI NPs is shown in Fig. 9G and H. The quantification of fluorescence demonstrated the efficacy of HA to mediate RHO-PLGA/PEI/HANP internalization (about 80%) as compared to non-targeted RHO-PLGA/PEI NPs (about 30%). In addition to internalization mechanisms, the intracellular trafficking of NPs within the cell are critical elements to study when a new drug carrier is proposed. Among these issues, the degradation pathway of the NPs represents an important aspect of intracellular NP dynamics. Lysosomes are a common terminal degradative compartment of certain endocytotic pathways. Thus, understanding whether NPs are delivered to the lysosomes following their internalization is a key point [32].

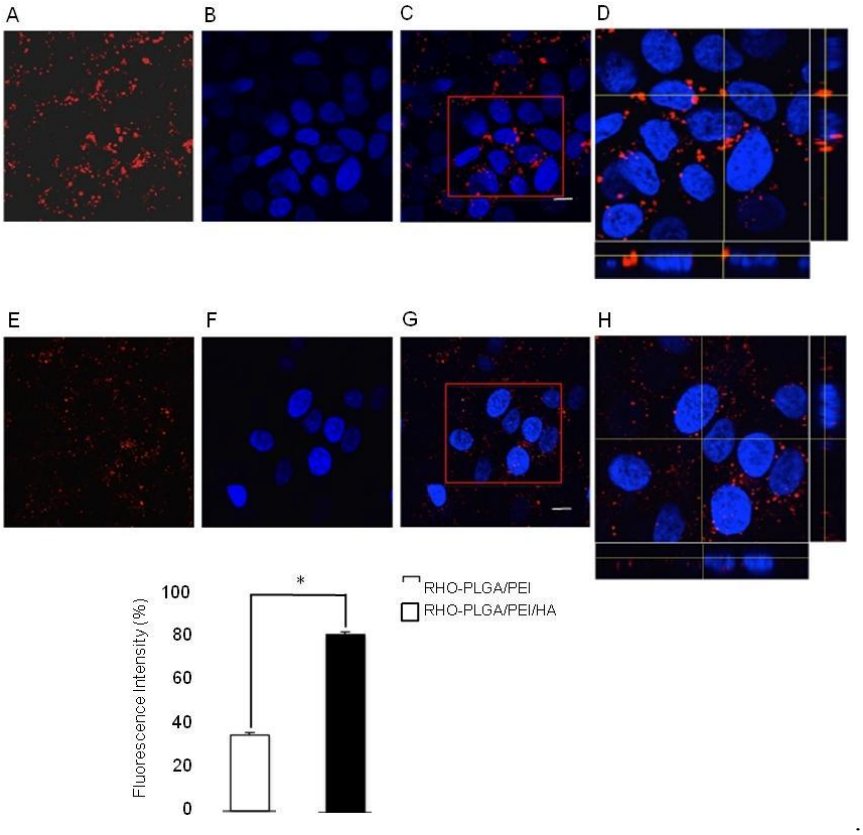

Fig. 9. A549 cells were incubated with RHO-PLGA/PEI/HA NPs (A) and RHO-PLGA/PEI NPs (E) for 24 h. Confocal microscope images 100X: A549 cell nuclei stained with DAPI (B, F).Merge of the same field for composite images (C, G), scale bar = 10 μm. Pictures were processed using ImageJ Software to reconstruct the x-axis projection using stack images (D, H). Quantification of intensity fluorescence is shown. Bars represent mean values ± SEM of experiments done in triplicate. $^{*}p < 0.005$

To determine whether the internalized RHO-PLGA/PEI/HA NPs were addressed to the lysosomal compartments, A549 cells were incubated with fluorescent RHO-PLGA/PEI/HANPs for 24 h (Fig. 10A) and then stained with LysoTracker Green (Fig.10B) and DAPI (Fig. 10C). As shown in Fig. 10D, a partial colocalization of RHO-PLGA/PEI/HA NPs with lysosome, as evident from the appearance of orange to yellow fluorescence, was observed.The x-axis projection is also shown (Fig. 10E).

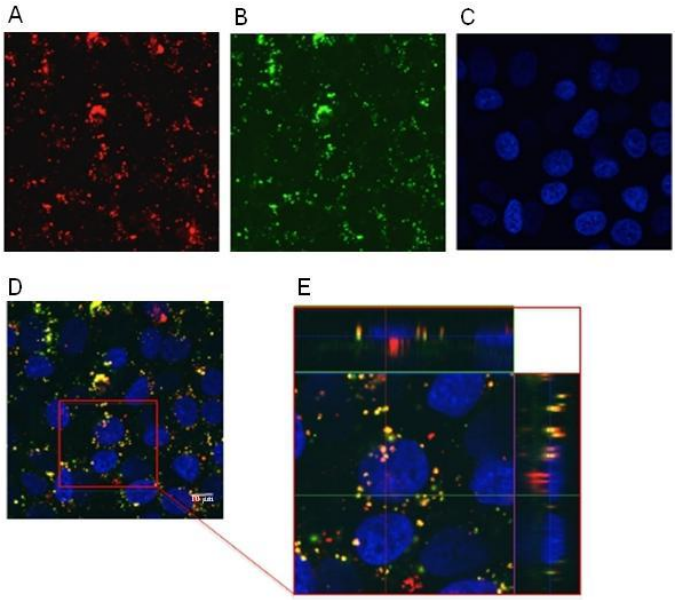

Fig. 10. A549 cells were incubated with RHO-PLGA/PEI/HA NPs for 24 h. Confocal microscope images 100X: RHO-PLGA/PEI/HA NPs (A), lysosomes of A549 cells stained with LysoTracker Green (B), A549 cell nuclei stained with DAPI (C),Merge of the same field for composite images (D), scale bar = 10 μm. Pictures were processed using ImageJ Software to reconstruct the x-axis projection using stack images (E). Composite image demonstrated colocalization of RHO-PLGA/PEI/HA NPs with lysosomes

3.5 Cytotoxicity of DTX-loaded NPs

Once the biological behavior of NPs was characterized, we tested their ability to improve the activity of DTX. *In vitro* cytotoxicity of DTX-PLGA/PEI/HA and DTX-PLGA/PEI NPs was evaluated in A549 cells after 24 h and 72 h exposure by using MTT and LDH assays and compared to that of free DTX. Extrapolation from the dose-response curve demonstrated that the dose causing 50% cell death (IC_{50}) in cells treated with free DTX was 0.1 μg/mL at 72 h while DTX loaded on PLGA/PEI/HA NPs gave the same effect at 0.05 μg/ml (Fig. 12A). These data suggest that the delivery of DTX through PLGA/PEI/HA NPs allowed a much more potent antiproliferative activity than free DTX. The observed results were confirmed by the values from LDH assay (Fig. 12C). Results from MTT and LDH assays of DTX-PLGA/PEINPs at 72 h (Fig. 12B and D) showed that the cytotoxicity induced by DTX-PLGA/PEINPs was increased of about 15% as compared with free DTX. This finding indicated that DTX-PLGA/PEI NPs, as hypothetical result of hyaluronidases-mediated degradation in tumor, are still able to improve the cytotoxic activity of free DTX contributing in this way to further increase the therapeutical potential of original DTX-PLGA/PEI/HA NPs. Data from MTT and LDH assays at 24 h are shown in Fig. 11.Taken together, results lead us to hypothesize that once the DTX-PLGA/PEI/HA NPs reach the CD44-overexpressed tumor site, they could be uptaken through CD44 receptor, be driven to lysosomes where drug release in a critical compartment more efficiently as compared with the free form is achieved.

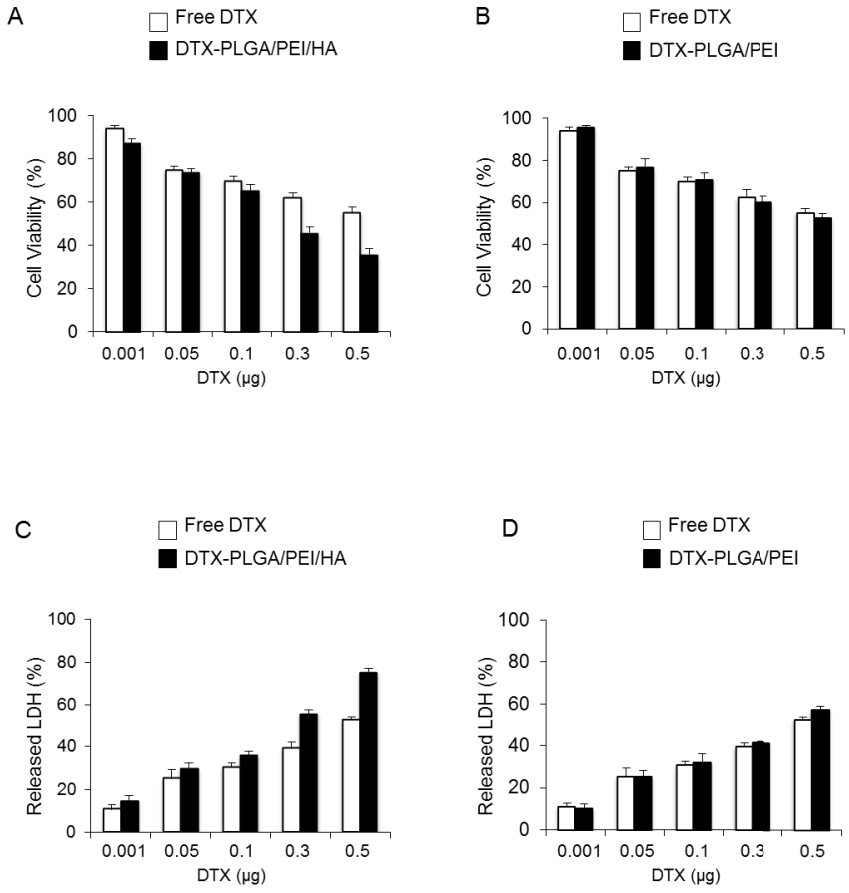

Fig. 11. A549 cells were exposed to increasing concentrations (0.001-0.5 μg) of free DTX, DTX- PLGA/PEI/HA or DTX-PLGA/PEI for 24 h. After incubation, cell viability and released of LDH % were evaluated using the MTT (A, B) and LDH (C, D) assay. The cell viability and LDH release from untreated cells were set to 100% and 0%, respectively. Results are presented as percentage (mean ± SEM) (n = 3) of the control cells. $^{*}P < 0.005$, $^{\#}P < 0.0001$.

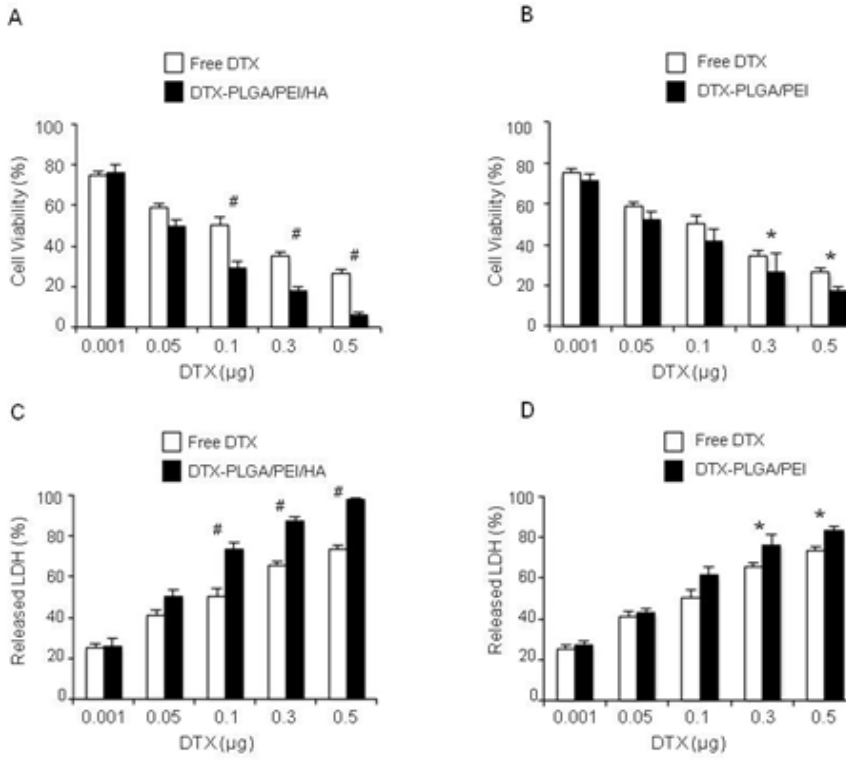

Fig. 12. A549 cells were exposed to increasing concentrations (0.001-0.5 μg) of free DTX, DTX- PLGA/PEI/HA NPs (A, C) or DTX-PLGA-PEI NPs (B, D) for 72 h. After incubation, cell viability and released of LDH % were evaluated using the MTT (A, B) and LDH (C, D) assay. The cell viability and LDH release from untreated cells were set to 100% and 0%, respectively. Results are presented as percentage (mean ± SEM) (n = 3) of the control cells

4 Conclusion

This study has demonstrated that it is possible to build CD44-targeted NPs with sustained drug delivery by electrostatic assembly of proper polymer building blocks. Bioresponsive NPs with excellent stability in complex media and demonstrating unprecedented uptake and activity in CD44-overepressing lung cancer cells as compared with free drug were obtained. Cationic NPs generated after possible HA shedding in tumor interstium were still more cytotoxic than free drug, further highlighting the therapeutic potential of the whole nanocarrier. Taken together, results lead us to hypothesize that biodegradable NPs developed here represent a very promising system to treat CD44 overexpressing lung cancer. In principle, this system can be extended to different single drugs and drug combinations taking advantage of the shell and core properties.

References

1. Jain KK: Advances in the field of nanooncology. *BMC Med* 2010, 8:83.
2. Jain RK, Stylianopoulos T: Delivering nanomedicine to solid tumors. *Nat Rev Clin Oncol* 2010, 7:653-664.
3. Wang AZ, Langer R, Farokhzad OC: Nanoparticle delivery of cancer drugs. *Annu Rev Med* 2012, 63:185-198.
4. Duncan R, Gaspar R: Nanomedicine(s) under the microscope. *Mol Pharm* 2011, 8:2101-2141.
5. Schroeder A, Heller DA, Winslow MM, Dahlman JE, Pratt GW, Langer R, Jacks T, Anderson DG: Treating metastatic cancer with nanotechnology. *Nature Reviews Cancer* 2012, 12:39-50.
6. Markman JL, Rekechenetskiy A, Holler E, Ljubimova JY: Nanomedicine therapeutic approaches to overcome cancer drug resistance. *Adv Drug Deliv Rev* 2013, 65:1866-1879.
7. Palakurthi S, Yellepeddi VK, Vangara KK: Recent trends in cancer drug resistance reversal strategies using nanoparticles. *Expert Opinion on Drug Delivery* 2012, 9:287-301.
8. Iyer AK, Singh A, Ganta S, Amiji MM: Role of integrated cancer nanomedicine in overcoming drug resistance. *Advanced Drug Delivery Reviews* 2013, 65:1784-1802.
9. Couvreur P: Nanoparticles in drug delivery: Past, present and future. *Advanced Drug Delivery Reviews* 2013, 65:21-23.
10. Hu CM, Fang RH, Luk BT, Zhang L: Polymeric nanotherapeutics: clinical development and advances in stealth functionalization strategies. *Nanoscale* 2014, 6:65-75.
11. Kamaly N, Xiao ZY, Valencia PM, Radovic-Moreno AF, Farokhzad OC: Targeted polymeric therapeutic nanoparticles: design, development and clinical translation. *Chem Soc Rev* 2012, 41:2971-3010.
12. Danhier F, Ansorena E, Silva JM, Coco R+, Le Breton A, Pr+®at V+: PLGA-based nanoparticles: An overview of biomedical applications. *Journal of Controlled Release* 2012, 161:505-522.
13. Gref R, Domb A, Quellec P, Blunk T, Muller RH, Verbavatz JM, Langer R: The controlled intravenous delivery of drugs using PEG-coated sterically stabilized nanospheres. *Advanced Drug Delivery Reviews* 2012, 64:316-326.

14. Ediriwickrema A, Zhou J, Deng Y, Saltzman WM: Multi-layered nanoparticles for combination gene and drug delivery to tumors. *Biomaterials* 2014, 35:9343-9354.
15. Xia T, Kovochich M, Liong M, Zink JI, Nel AE: Cationic polystyrene nanosphere toxicity depends on cell-specific endocytic and mitochondrial injury pathways. 2008, 2:85-96.
16. Leroueil PR, Berry SA, Duthie K, Han G, Rotello VM, McNerny DQ, Baker J, Orr BG, Holl MMB: Wide varieties of cationic nanoparticles induce defects in supported lipid bilayers. 2008, 8:420-424.
17. Huang Z, Yang Y, Jiang Y, Shao J, Sun X, Chen J, Dong L, Zhang J: Anti-tumor immune responses of tumor-associated macrophages via toll-like receptor 4 triggered by cationic polymers. *Biomaterials* 2013, 34:746-755.
18. Cubillos-Ruiz JR, Engle X, Scarlett UK, Martinez D, Barber A, Elgueta R, Wang L, Nesbeth Y, Durant Y, Gewirtz AT etal.: Polyethylenimine-based siRNA nanocomplexes reprogram tumor-associated dendritic cells via TLR5 to elicit therapeutic antitumor immunity. 2009, 119:2231-2244.
19. Stylianopoulos T, Soteriou K, Fukumura D, Jain RK: Cationic nanoparticles have superior transvascular flux into solid tumors: Insights from a mathematical model. *Annals of Biomedical Engineering* 2013, 41:68-77.
20. Yim H, Park SJ, Bae YH, Na K: Biodegradable cationic nanoparticles loaded with an anticancer drug for deep penetration of heterogeneous tumours. *Biomaterials* 2013, 34:7674-7682.
21. Lv H, Zhang S, Wang B, Cui S, Yan J: Toxicity of cationic lipids and cationic polymers in gene delivery. *Journal of Controlled Release* 2006, 114:100-109.
22. Toole BP: Hyaluronan: from extracellular glue to pericellular cue. *Nat Rev Cancer* 2004, 4:528-539.
23. Choi KY, Saravanakumar G, Park JH, Park K: Hyaluronic acid-based nanocarriers for intracellular targeting: interfacial interactions with proteins in cancer. *Colloids Surf B Biointerfaces* 2012, 99:82-94.

24. Qhattal HSS, Liu X: Characterization of CD44-Mediated Cancer Cell Uptake and Intracellular Distribution of Hyaluronan-Grafted Liposomes. *Molecular Pharmaceutics* 2011, 8:1233-1246.
25. Morton SW, Poon ZY, Hammond PT: The architecture and biological performance of drug-loaded LbL nanoparticles. *Biomaterials* 2013, 34:5328-5335.
26. Deng ZJ, Morton SW, Ben-Akiva E, Dreaden EC, Shopsowitz KE, Hammond PT: Layer-by-Layer Nanoparticles for Systemic Codelivery of an Anticancer Drug and siRNA for Potential Triple-Negative Breast Cancer Treatment. *Acs Nano* 2013, 7:9571-9584.
27. Iost RM, Crespilho FN: Layer-by-layer self-assembly and electrochemistry: Applications in biosensing and bioelectronics. *Biosensors & Bioelectronics* 2012, 31:1-10.
28. Palma G, Conte C, Barbieri A, Bimonte S, Luciano A, Rea D, Ungaro F, Tirino P, Quaglia F, Arra C: Antitumor activity of PEGylated biodegradable nanoparticles for sustained release of docetaxel in triple-negative breast cancer. *International Journal of Pharmaceutics* 2014, 473:55-63.
29. Taetz S, Bochot A, Surace C, Arpicco S, Renoir JM, Schaefer UF, Marsaud V, Kerdine-Roemer S, Lehr CM, Fattal E: Hyaluronic Acid-Modified DOTAP/DOPE Liposomes for the Targeted Delivery of Anti-Telomerase siRNA to CD44-Expressing Lung Cancer Cells. *Oligonucleotides* 2009, 19:103-115.
30. Sherman L, Sleeman J, Herrlich P, Ponta H: Hyaluronate Receptors - Key Players in Growth, Differentiation, Migration and Tumor Progression. *Current Opinion in Cell Biology* 1994, 6:726-733.
31. Esposito D, Crescenzi E, Sagar V, Loreni F, Russo A, Russo G: Human rpL3 plays a crucial role in cell response to nucleolar stress induced by 5-FU and L-OHP. *Oncotarget* 2014, 5:11737-11751.
32. Panyam J, Zhou WZ, Prabha S, Sahoo SK, Labhasetwar V: Rapid endo-lysosomal escape of poly(DL-lactide-co-glycolide) nanoparticles: implications for drug and gene delivery. *Faseb Journal* 2002, 16.
33. Ungaro F, De Rosa G, Miro A, Quaglia F: Spectrophotometric determination of polyethylenimine in the presence of an oligonucleotide for the characterization of controlled release

formulations. *Journal of Pharmaceutical and Biomedical Analysis* 2003, 31:143-149.

34. Fiorito F, Irace C, Di PA, Colonna A, Iovane G, Pagnini U, Santamaria R, De ML: 2,3,7,8-Tetrachlorodibenzo-p-dioxin promotes BHV-1 infection in mammalian cells by interfering with iron homeostasis regulation. *PLoS One* 2013, 8:e58845.
35. Russo A, Cirulli C, Amoresano A, Pucci P, Pietropaolo C, Russo G: cis-acting sequences and trans-acting factors in the localization of mRNA for mitochondrial ribosomal proteins. *Biochim Biophys Acta* 2008, 1779:820-829.

Chapter 3
Hyaluronan-decorated polymer nanoparticles targeting CD44 receptor for the combined photo/chemo-therapy of cancer

Published as:

Sara Maiolino, Francesca Moret, Claudia Conte, Aurore Fraix, Pasquale Tirino, Francesca Ungaro, Salvatore Sortino, Elena Reddi and Fabiana Quaglia

Nanoscale 7 (2015) 5643-53

Chapter 3

Backcover

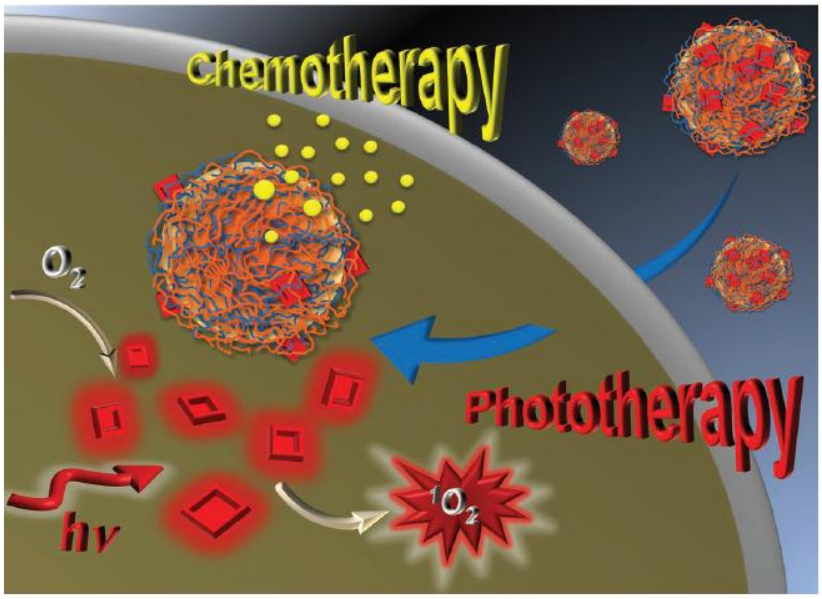

Showcasing Italian collaborative research from the Departments of Pharmacy and Chemistry, University of Napoli Federico II, the Department of Biology, University of Padova and the Department of Drug Science, University of Catania.

Hyaluronan-decorated polymer nanoparticles targeting the CD44 receptor for the combined photo/chemo-therapy of cancer

We propose a novel type of double-coated biodegradable nanoparticle based on electrostatic interactions and co-encapsulating a taxane chemotherapeutic and a porphyrine photosensitizer, which demonstrate a tremendous improvement in free drug activity and specificity. These findings provide a solid rational basis for future extension of the system to other drug combinations also in an *in vivo* setting.

As featured in:

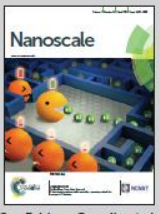

See Fabiana Quaglia *et al.* *Nanoscale*, 2015, 7, 5643.

ROYAL SOCIETY OF CHEMISTRY

www.rsc.org/nanoscale

Registered charity number: 207890

Chapter 3

Abstract

In the attempt to develop novel concepts in the design of targeted nanoparticles for combination therapy of cancer, here we proposeCD44-targeted hyaluronan-decorated double-coated nanoparticles(dcNPs) delivering the lipophilic chemotherapeutic Docetaxel (DTX) and the photosensitizerTetrasodium-Meso-tetra(4-sufonatophenyl)porphyrine ($TPPS_4$).dcNPs were fabricated through electrostatic interactions between a negative DTX-loaded nano scaffold of poly(lactide-co-glycolide), a polycationic Polyethyleneimine (PEI) cationic shell entangling negatively-charged $TPPS_4$andfinallydecorated with hyaluronan (HA) to promote internalization through CD44 receptor-mediated endocytosis. DTX/$TPPS_4$-dcNPs, prepared through layer-by-layer deposition, showed a hydrodynamic diameter around 170 nm, negative zeta potential and efficient loading of both DTX and $TPPS_4$. DTX/$TPPS_4$-dcNPs were freeze-dried with trehalose giving a powder that could be easily redispersed in different media. Excellent stability of dcNPs in specific salt- and protein-containing media was found. Spectroscopic behavior of DTX/$TPPS_4$-dcNPs demonstrated a face-to-face arrangement of the $TPPS_4$units in non-photoresponsive H-type aggregates accounting for a massive aggregation of the porphyrin embedded in the shell. Experiments in MDA-MB231 cells overexpressing CD44 receptor demonstrated a 9.4-fold increase of intracellular level of $TPPS_4$delivered from dcNPs as compared to free$TPPS_4$.Light-induced death was increased tremendously in cells that had been treated with the combination of $TPPS_4$ and DTX delivered through dons as compared with free drugs, presumably due to efficient uptake and co-localization inside cells. In perspective, the strategy proposed here to target synergistic drug combinations through HA-decorated NPs seems very attractive to improve specificity and efficacy of a cancer treatment.

1 Introduction

Combination chemotherapy has long been adopted as the standard of care against many cancer types. It is generally recognized that through the proper drug combination, the treatment can promote synergistic actions, improve target selectivity, and prevent the development of cancer drug resistance.[1-3]This approach has been found promising when Photodynamic Therapy (PDT) has been combined to conventional chemotherapy in the management of several cancer types.[4-7] In PDT a photosensitizer (PS), after irradiation at specific wavelength, causes mainly the formation of the cytotoxic species singlet oxygen ($^1O_2$) which reacts with tissue components, leading to cell death through the initiation of apoptosis and necrosis.[8]Indeed acting by different mechanisms, cytotoxic drugs can act in concert with PS for tumor killing, achieving potentiated therapeutic outcome through an anticancer synergistic effect.

Entrapment of multiple therapeutic agents in a nanocarrier offers an unprecedented opportunity to devise a better scheme for precise and controlled delivery of multiple therapeutic agents in the same area of the body and at predefined extra/intracellular level.[9-14] As compared to other nanocarriers, polymer-based nanoparticles (NPs) offer a great prospect in this area since they can be designed to target a solid tumor, to incorporate drugs with different solubility and to deliver them at finely tuned rates.[15]By exploiting the presence of dysfunctional endothelium of tumor capillary wall and the absence of effective lymphatic drainage in solid tumors, biomimetic and long –circulating NPs can extravasate from the blood circulation and reach solid tumor interstitium.[16,17] This mechanism referred as Enhanced Permeability and Retention (EPR) effect is the main determinant in passive targeting while surface modification with structural motifs able to specifically recognize peculiar elements of tumors have been explored to further ameliorate drug specificity and effective drug accumulation in tumors/cancer cells.[18-20] Furthermore, timing of drug release (temporal control of drug availability at target site) can be finely tuned. From a therapeutic standpoint, timing of drug release is of key importance to drive administration scheme (number of administrations, frequency) as well as to optimize cell response. In particular, sustained release of some chemotherapeutic from NPs is gaining overwhelming interest since it is expected to amplify cell response and extend activity to hypoxic zones of

certain tumors but also to improve drug activity resembling a metronomic therapy (subactive doses for longer time frames).[21]

Despite of the great potential, there have been very few attempts to developing tumor-targeted nanosystems for the co-delivery of PS and anticancer drugs.[22-26]A challenging task in the design of polymeric NPs for combination therapy resides in the design of systems carrying drugs with a different solubility. Core-shell architecture represents an effective way to serve this purpose and to attain multiple functionalities on a nanoscopic length scale. In one of the possible configurations, a polymeric hydrophobic core (template),generally carrying a lipophilic chemotherapeutic agent, is surrounded by one or more than on a polymeric hydrophilic layers that entraps an interacting drug and provides a functional interface with biological environment. As core-forming polymers, poly(lactide-co-glycolide)s are excellent candidates to form NPs with sustained delivery features. By varying polymer molecular weight and crystallinity, facile control on both encapsulation efficiency and biodegradation rate, and in turn on drug delivery rate, are attained.[27]Amid shell-forming hydrophilic polymers, hyaluronan (HA) is emerging for its activity as biological response modifiers in cancer.[28,29]HA is widely employed in cancer to direct a drug or a NP to tumor tissues due to its ability to recognize HA receptors (CD44, RHAMN) which are overexpressed in different cancer cell lines.[28,30] Receptor-mediated endocytosis facilitates drug transport inside the cells and contributes to improve cytotoxicity.[31] It has been recently demonstrated that targeting a receptor such as CD44, which can undergo recycling between cell surface and endosomes/lysosomes and mediate transcytosis, can also promote tumor penetration of NPs.[32]

Here, we develop CD44-targeted double-coated NPs(dcNPs) for the combined conventional and photodynamic therapy of cancer delivering the lipophilic taxane Docetaxel (DTX) and the negatively-charged PS Tetrasodium-Meso-tetra(4-sufonatophenyl)porphyrine ($TPPS_4$). dons based on a DTX-PLGA core template and decorated with HA via electrostatic interactions with PEI as positively-charged $TPPS_4$-containing bridging polymer were produced and fully characterized for colloidal properties, photochemical behavior and phototoxicity in cancer cell lines overexpressing the CD44 receptor.

2 Material and Methods

Docetaxel (DTX, MW=807.88) was purchased from LC laboratories (USA). Poly (D,L-lactide-*co*-glycolide) (PLGA) (50:50 Resomer RG 502H inherent viscosity 0.16-0.24 dl/g) was purchased from BoehringerIngelheim (Ingelheim, Germany). Tetrasodium-Meso-tetra(4-sufonatophenyl)porphyrine($TPPS_4$, MW=1239.1) was purchased from Frontier Scentific. Trehalose, Polyethyleneimine (PEI, MW= 10-25 kDa branched), Poloxamer 188 (Pluronic® F68) and Trifluoracetic acid (TFA) were purchased from Sigma-Aldrich. Acetonitrile and acetone were purchased from Carlo ErbaReagenti (Milan, Italy). DMEM and Fetal Bovine Serum (FBS) were purchased from Gibco life technologies. Hyaluronan (HA, MW <10 kDa) was a kind gift of Magaldi Life S.r.l. Ultrapure water was used throughout the study.N-(4,4-difluoro-5,7-dimethyl-4-bora-3a,4a-diazas-indacene-3-pentanoyl)sphingosine (BODIPY® FL C5-ceramide) and LysoTracker® Green DND-26were from Molecular Probes (Life Technologies, Milan, Italy). The CellTiter96®Aqueous One Solution Cell proliferation Assay (MTS) was from Promega Co (Madison, USA).

2.1 Preparation of double-coated nanoparticles (dcNPs)

dcNPs loaded with DTX,$TPPS_4$or DTX/$TPPS_4$ (DTX-dcNPs, $TPPS_4$-dcNPs,DTX/$TPPS_4$-dcNPs) were prepared by a layer-by-layer deposition method. Briefly, DTX-loaded PLGA NPs were prepared by solvent diffusion of an organic phase (10 mg of PLGA and 0.5 mg of DTX in 2 mL of acetone) in an aqueous phase (4 mL of water with Pluronic F68 0,1%). After solvent evaporation and washing, NPs were coated first with 125 µL of a PEI water solution (1mg/mL), centrifuged and then addedwith25µL of a $TPPS_4$water solution (0.2 mg/mL). Thereafter, 100 µL of a HA water solution(1 mg/mL) were added. The interval between each addition was kept constant at 15 min. dons were freeze-dried for 24 h with trehalose(60 mg) as cryoprotectant and kept at 4 °C. Recovery yield of production process was evaluated on an aliquot of DTX/$TPPS_4$-dcNPs(without cryoprotectant) by weighting the solid residue after freeze-drying. Results are expressed as the ratio of the actual NP weight to the theoretical polymer weight×100.

2.2 Characterization of dcNPs

2.2.1 Size, surface charge and morphology

Hydrodynamic diameter,polydispersity index (PI) and zeta potential of NPs after each preparation step were determined on a ZetasizerNano Z(Malvern Instruments Ltd., UK). Results are reported as mean of three separate measurements of three different batches (n=9)±SD. Particle morphology was analyzed by scanning electron microscopy (SEM) (Leica S440, Germany) after gold sputtering.

2.2.2 DTX and $TPPS_4$ actual loading

DTX loading inside DTX/$TPPS_4$-dcNPs was assessed by placing 0.5 mg of freeze-dried NPs (without cryoprotectant) in 500 µL of DCM and overnight stirring until a film was formed at bottom of the vial. Thereafter, 500 µL of water and 500 µL of acetonitrile were added and the sample was filtered through a 0.45 µm filter (RC, Chemtek, Italy). DTX was analyzed by HPLC on a Shimadzu apparatus equipped with a LC-10ADvp pump, a SIL-10ADvp autoinjector, a SPD-10Avp UV–Vis detector and a C-R6 integrator. The analysis was performed on a Supelco 5 µm, C18 column (250×4.6 mm, Å). The mobile phase was a 40:60 (v/v) mixture of water with TFA 0.1 % and acetonitrile pumped at a flow rate of 1 mL/min. The UV detector was set at 227 nm. A calibration curve for DTX in ethanol was constructed in the concentration range 0.980–19.6 µg/mL. The limits of quantification (LOQ) and detection (LOD) were 1.29 and 0.39 µg/mL, respectively.$TPPS_4$ loading inside DTX/$TPPS_4$-loaded dcNPs was evaluated in the supernatant by UV after NP centrifugation at 13000 x*g* for 15 min. A calibration curve was constructed at 413 nm (Shimadzu, UV 1800)in the $TPPS_4$ concentration range 0.05-5 µg/mL.

2.2.3 PEI and HA dosage

PEI amount in DTX/$TPPS_4$-dcNPswas quantified by a colorimetric method developed previously.[33]Freeze-dried NPs (0.5 mg, without cryoprotectant)were treated with 0.5 mL of 1 M NaOH and stirred overnight. The sample (0.5 mL) was diluted with 0.5 mL of 1 M acetic acid. The resulting solution (0.5 mL) was added to 1 mL of 0.1 M acetate buffer at pH 4.5, and complexed with 0.25 mL of a copper (II) sulphate

water solution. The absorbance value of each solution was recorded at 281 nm. A calibration curve was constructed in the same condition in the PEI concentration range 15–380 μg/mL. To evaluate the extent of HA adsorption onto NPs, DTX/$TPPS_4$-dcNPs(0.5 mg) were centrifuged at 13000 x*g* for 15 min and the supernatant was freeze-dried. The solid residue was then dissolved in 1mL of acetate buffer (0.2 M) at pH 6. Thereafter, 2mL of cetyltrimethylammonium bromide reagent was added and the sample was analyzed at 350 nm. A calibration curve was constructed in same condition in HA concentration range 10–200 μg/mL.

2.2.4 DTX and $TPPS_4$ release

In vitro release of DTX and $TPPS_4$ was performed on 30.5 mg of freeze-dried powder (corresponding to 0,5 mg of NPs)dispersed in 1 mL DMEM FBS+ 10% at 37°C. At predetermined time interval, the sample was centrifuged 13000 x g (15 min). $TPPS_4$ release as assessed in the supernatant by spectrophotometry at wavelength of 422 nm. A $TPPS_4$ calibration curve in the range 0.2-4 μg/mL was constructed in the release medium. DTX release was assessed by HPLC as reported in 2.2.2 after treating 1 mL of medium with acetonitrile (1 mL) to precipitate proteins and final centrifugation at 13000 x g (15 min).Results are expressed as % release overtime ± SD of three experiments.

2.3 Spectroscopic and photochemical experiments

2.3.1 Absorption and emission

UV/Vis absorption and fluorescence spectra were recorded with a thermostated HP-8452 diode array spectrophotometer and Fluorolog-2 (Model, F-111) spectrofluorimeter respectively. All measurements were performed in a thermostated quartz cell (1 cm path length, 3 mL capacity). Fluorescence spectra were corrected for the different fraction of the absorbed photons by the different samples at the excitation wavelength.

2.3.2 Laser flash photolysis

All samples were excited with the second harmonic of Nd–YAG Continuum Surelite II–10 laser (532 nm, 6 ns FWHM), using quartz cells with a path length of 1.0 cm. The excited solutions were analyzed with a

Luzchem Research mLFP–111 apparatus with an orthogonal pump/probe configuration. The probe source was a ceramic xenon lamp coupled to quartz fiber-optic cables. The laser pulse and the mLFP–111 system were synchronized by a Tektronix TDS 3032 digitizer, operating in pre-trigger mode. The signals from a compact Hamamatsu photomultiplier were initially captured by the digitizer and then transferred to a personal computer, controlled by Luzchem Research software operating in the National Instruments LabView 5.1 environment. The solutions were deoxygenated by bubbling with a vigorous and constant flux of pure nitrogen (previously saturated with solvent). In all of these experiments, the solutions were renewed after each laser shot (in a flow cell of 1 cm optical path), to prevent probable photodegradation processes. The sample temperature was 295 ± 2 K. The energy of the laser pulse, measured at each shot with a SPHD25 Scientechpyroelectric meter, was ca. 10 mJ/pulse.

2.4 Cell studies

2.4.1 Cells

Human breast cancer cell lines MDA-MB231 and MCF-7 were purchased from American Type Tissue Culture Collection (ATCC, Rockville, Maryland). The cells were grown in DMEM with Glutamax™ supplemented with 10% heat-inactivated foetal bovine serum (FBS), 1 mM sodium pyruvate, 100 U/mL streptomycin and 100 µg/mL penicillin G (Life Technologies, Milan, Italy), and maintained at 37 °C in a humidified atmosphere containing 5% CO_2.

2.4.2 Uptake studies

Flow cytometry experiments were carried out to investigate the expression level of CD44 receptor and its involvement in the internalization of fluorescent dcNPs labeled with rhodamine B (RHO-dcNPs) in MDA-MB231 and MCF-7 and to measure the uptake of $TPPS_4$ and $TPPS_4$-dcNPs in MDA-MB231 cells. RHO-dcNPs were used in place of $TPPS_4$-dcNPs to avoid any misleading result generated by $TPPS_4$ release in the cell external medium. Rho-dcNPs were prepared as described in 2.1 by incorporating a 20% w/w of PLGA covalently linked to rhodamine B in the PLGA core.

The preparation of PLGA-RHO conjugate was performed under inert nitrogen or argon atmosphere and dry conditions according to scheme 1.

*c-PLGA502H-N_3.*The terminal hydroxyl group of PLGA502H was changed into azide by two-step azidation with mesyl chloride activation. After 24 hours reaction mixture was concentrated and precipitated in diethyl ether methanol solution 1/1 v/v obtaining a sponge like solid. Thereafter, nucleophilic substitution with sodium azide was carried out in DMF and water solution (20/1 v/v) as described above, but temperature was set at 38°C. Reaction mixture was dried, redissolved in $CHCl_3$ and precipitated as described above.The conversion degree is higher than 95% as evaluated by ^{1}H-NMR analysis.

Rhodamine-alkyne. Rhodamine B was reacted with 3-Butynol in presence of DCC and DMAP to give alkyne ester. After 48 h reaction mixture was filtered from dicyclohexylurea, concentrated and purified by silica gel chromatography with $CHCl_3$/Methanol 9/1 v/v as eluent.

PLGA-RHO. Thereafter, the Huysgen cycloaddition between Rhodamine-alkyne and c-PLGA502H-N3 was carried out at 30% Rhodamine-alkyne molar excess. After 48 h, reaction mixture was concentrated, purified by Cu(I) catalyst by neutral alumina column and precipitated in diethyl ether methanol solution 1/1 v/v according to developed protocol.^{1}H-NMR analysis was used to confirm product chemical structure and conversion degree which is higher than 95%.

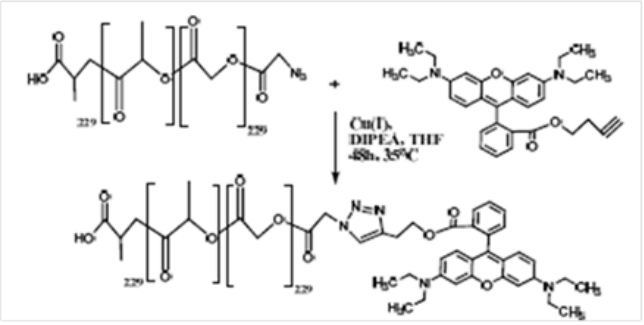

Scheme 1. Huysgen cycloaddition between Rhodamine-alkyne Rhodamine-alkyne and c-PLGA502H-N3.

The level of CD44 expression in MDA-MB231 and MCF-7 cells was measured by staining the cells with a FITC-conjugated anti-CD44 antibody (Abcam, Cambridge, UK). To study the role of CD44 in the uptake of RHO-dcNPs, 4 x 10^4 cells were grown in 24-well plates for 24 h and incubated for 2 h with 50 µg/mL of NPs diluted in medium added with 3% FBS. Some samples were pre-incubated for 1 h with 10 mg/mL free HA (Sigma-Aldrich, St. Louis, USA) before NP addition in order to saturate CD44 receptors (competition experiments). At the end of the incubation time, the cells were washed twice with Versene™, detached from the plates with trypsin, that was neutralized by the addition of FBS. Cells were centrifuged and resuspendedin Versene™before measuring RHO fluorescence using a BD FACSCanto™ II flow cytometer (Becton Dickinson, San Jose, USA). The blue laser at 488 nm was used for excitation and wavelengths longer than 560 nm were selected for the detection of RHOfluorescence. For each sample 10^5events were acquired and analyzed with the FACSDiva software. For $TPPS_4$ and $TPPS_4$-dcNPs uptake, cells were seeded and handled as described above and incubated for 24 h with increasing concentrations of PS in medium added with 3% FBS. For the detection of $TPPS_4$ fluorescence wavelengths longer than 670 nm were selected.

2.4.3 Intracellular localization of NPs

The intracellular localization of $TPPS_4$, free and in NPs ($TPPS_4$-dcNPs) was determined by confocal microscopy. MDA-MB231 cells (6 x 10^4), seeded in special tissue culture dishes for fluorescence

microscopy (μ-Dish $^{35mm,\ high}$, Ibidi GmbH, Planneg, Germany), were allowed to growth for 24 h and then incubated for 24 h with 1 μg/mL PS diluted in medium added with 3% FBS. Fifteen min before the end of the incubation with the PS, the cells were stained with BODIPY® FL C_5-Ceramide (15 μM) or LysoTracker® Green DND-26 (75 nM) used as markers for Golgi apparatus and lysosomes, respectively. Cells were then washed twice with PBS with Ca^{2+} and Mg^{2+}andimmediately analyzed with a Leica SP5 confocal laser-scanning microscope (Leica Microsystems Srl, Milan, Italy); the images were elaborated with the ImageJ software.

2.4.4 Cytotoxicity assay

Viability of MDA-MB231 cells incubated with free $TPPS_4$, free DTX, $TPPS_4$-dcNPs, DTX-dcNPs, DTX/$TPPS_4$-dcNPs and empty dcNPs in the absence of light was measured with the MTS assay. Cells (5 x 10^3) were seeded in 96-well plates (24 h of growth) and then incubated with the various formulations diluted in medium added with 3% FBS. Cell viability was measured at the end of incubation time (24, 48, 72 h) as well as after additional 24 h in which the cells were kept in drug-free medium (24 + 24 h). For MTS assay the culture medium was replaced with 100 μL of serum-free medium and 20 μL of CellTiter 96® Reagent and the wells were incubated for 1 h at 37 °C. The absorbance at 492 nm was measured with a Multiskan Go (Thermo Fischer Scientific, Waltham, USA) plate reader and the viability of treated cells was expressed as percentage of the absorbance of control cells that was taken as 100% viability.

2.4.5 In vitro photo-toxicity

MDA-MB231 cells (5 x 10^3) were grown for 24 h and incubated for further 24 h with free $TPPS_4$, combination of free $TPPS_4$and free DTX, $TPPS_4$-dcNPs, DTX/$TPPS_4$-dcNPs and empty dcNPs in the dark. After incubation with the drugs, the cells were washed twice with PBS with Ca^{2+} andMg^{2+}, and irradiated in PBS with 8 J $cm^{-2}$of blue light (390-460 nm, fluence rate 11 $mWcm^{-2}$) from a UV 236 lamp (WaldmannEclairage SA, Germany). Immediately after irradiation the cells were brought back to the incubator after replacement of PBS with fresh medium. Cell viability was measured with the MTS test after additional 24 h.

2.4.6 Cell cycle analysis

MDA-MB231 cells (1×10^6) were seeded in 100 mm culture dishes and incubated with free DTX or DTX NPs for 24 h. Treated and control cells were harvested, fixed in 70% cold ethanol and stored at 4 °C overnight. Before analysis, cells were washed in distilled water, centrifuged and resuspended in 1 mL PBS containing 50 µg/mL propidium iodide (Sigma-Aldrich) and 100 µg/mL RNAse, for DNA staining. Samples were incubated for 1 h at 37 °C and then analyzed by flow cytometry. Data from 2×10^4 cells/sample were acquired with the FACSDiva software and analyzed with the ModFit LT 3.0 software (BD Biosciences) to determine alterations in cell cycle distribution.

2.4.7 Statistical analysis

The Primer software for biostatistics (McGraw-Hill, Columbus, USA) was used for statistical analysis of the data. The data are expressed as means ± standard deviations (SD) of at least 3 independent experiments. The difference between groups were evaluated with the Student‘s t-test and considered significant for $p < 0.05$.

3 Results

3.1 Preparation and characterization of double-coated nanoparticles (dcNPs)

dcNPs made of a negatively-charged PLGA core loaded with the lipophilic drug DTX, a positively-charged bridging layer of PEI embedding the water-soluble$TPPS_4$and a negatively-charged HA coating were produced through electrostatically-driven layer-by-layer assembly (Fig 1A). Layering was followed through size and zeta potential measurements. DTXPLGA NPs have a negative charge and adsorb firstly the positively charged PEI and then the negatively charged $TPPS_4$through electrostatic interactions. Amount of PEI added strongly affects dispersibility of NPs after the washing step (data not shown). During layering, the size of NPs progressively increases up to around 50 nm and zeta potential is reversed after each polymer layer deposition step (Fig. 1B). $TPPS_4$ adsorption onto PEI layer covering DTX-PLGA core does not alter size and zeta potential of NPs up to a $TPPS_4$amount of 5 µg (Fig. 1C). At this concentration, $TPPS_4$is quantitatively adsorbed onto NPs as demonstrated by the fact that the supernatant does not give any appreciable ABS at maximum wavelength of $TPPS_4$adsorption. Final dcNPs show a hydrodynamic diameter below 180 nm and a net negative zeta potential. Actual loading of DTX and $TPPS_4$in the final formulation was 0.95 ± 0.5 and 0.97 ± 0.2 mg *per*100 mg of dcNPs, respectively. Amount of PEI and HA adsorbed onto final formulation was 7.94 ± 2.1 and12.2 ± 0.8mg*per*100 mg of dcNPs, respectively. DTX/$TPPS_4$-dcNPs can be freeze-dried with trehalose to produce a powder that can be easily redispersed in water giving the original NP properties (Table 1). SEM analysis confirms the morphology of the final dcNPs (Fig. 1D).

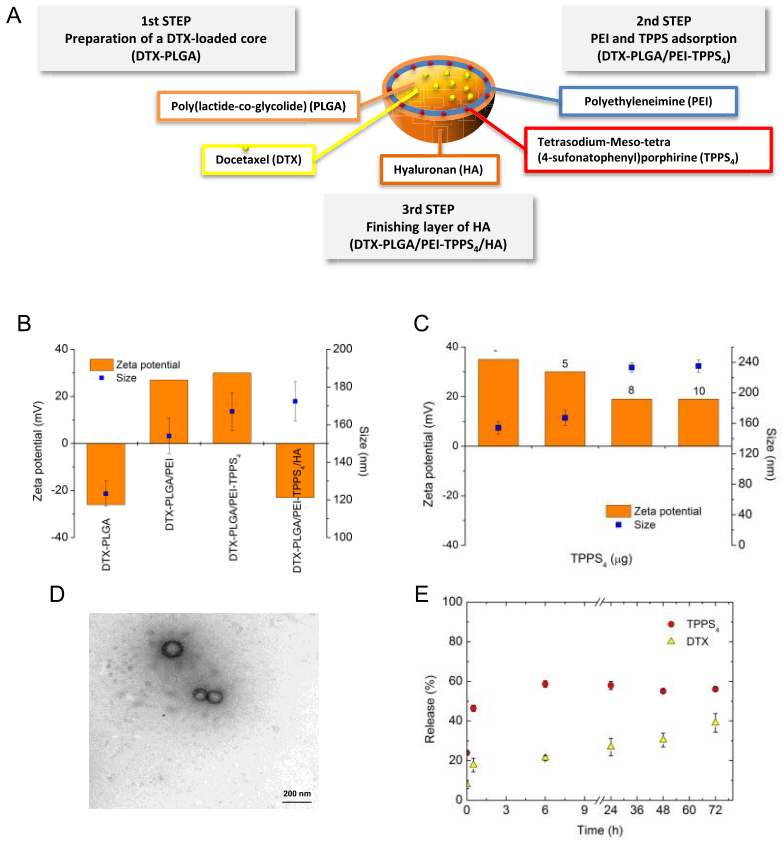

Fig. 1. Structure and properties of dcNPs. A) Schematic representation of the structure of DTX/$TPPS_4$-dcNPs and steps for their preparation; B) evolution of zeta potential and size during NP layering; C) effect of different concentration of $TPPS_4$ on zeta potential and size;C) SEM image of DTX/$TPPS_4$dcNPs;D) Release profile of $TPPS_4$

Table 1 Stability of dc NPs after freeze-drying.

	Mean D_H (nm ± SD)	**PI**	**Zeta potential (mV)**
Before freeze-drying	170 ± 10.4	0.13	-23.2
After freeze-drying	200 ± 10.1	0.17	-22.6

Effect of medium on DTX/$TPPS_4$-dcNPs colloidal properties were assessed (Table 2). Size of dcNPs in 5% glucose and 0.9% NaCl, commonly employed to disperse NPs before injection, does not greatly change. A slight size growth is observed in DMEM FBS- which becomes more marked in DMEM FBS+. In the case of PBS a significant three-fold increase of dcNP size occurred. In all the cases, no macroscopic aggregation of DTX/$TPPS_4$-dcNPs is observed. Nevertheless, zeta potential is decreased in the media tested and remains unaltered independently of the salt composition and presence of proteins.

Table 2. Properties of DTX/$TPPS_4$-dcNPs in different media.

	Size nm	**PI**	**Zeta potential mV**
Water	203 ± 10	0.15	-22
5% Glucose	221 ± 9	0.18	-11.3
0.9% NaCl	257 ± 27	0.2	-12.1
PBS	615 ± 58	0.25	-12.3
DMEM FBS-	244 ± 28	0.26	-9.5
DMEM FBS+	328 ± 10	0.27	-10.0

Release profile of DTX and $TPPS_4$ from DTX/$TPPS_4$-dcNPs was assessed in DMEM FBS+ at 37 °C and evaluated up to 72 h to simulate conditions occurring in cell studies. dcNPs display slow DTX release while60% of $TPPS_4$is immediately released probably due to its high solubility in the medium (Fig. 1E). DTX release is much slower than that of $TPPS_4$ as expected from their different lipophilicity.

3.2 Spectroscopic and photochemical experiments

Fig. 2 shows the absorption and fluorescence emission spectra of DTX/$TPPS_4$-dcNPs and, for comparison, those of free $TPPS_4$in water and in DMEM FBS+. In water solution, the free $TPPS_4$ shows a sharp Soret band with a maximum centered at 413 nm (a, left) and a double band fluorescence emission with maxima at 640 and 700 nm (a, right),

respectively. These spectral features are typical for the monomeric form of $TPPS_4$.[34] In the presence of DMEM medium the Soret absorption is always narrow but undergoes a slight hypochromism and significant red-shift (b, left). Besides, a red-shift was also observed in the fluorescence emission but the fluorescence quantum yield was only slightly affected by DMEM (b, right). This spectroscopic scenario excellently reflects that reported for the same porphyrin in the presence of micellar systems[34]and is consistent with the presence of $TPPS_4$ mainly as a monomer in DMEM FBS+.

The spectroscopic properties of $TPPS_4$ are profoundly affected when it is loaded within the dcNPs in the presence of DTX. In particular, a broadening of the Soret band accompanied by a dramatic hypocromic effects and blue-shift of ca. 6 nm was observed (c, left).Besides, the

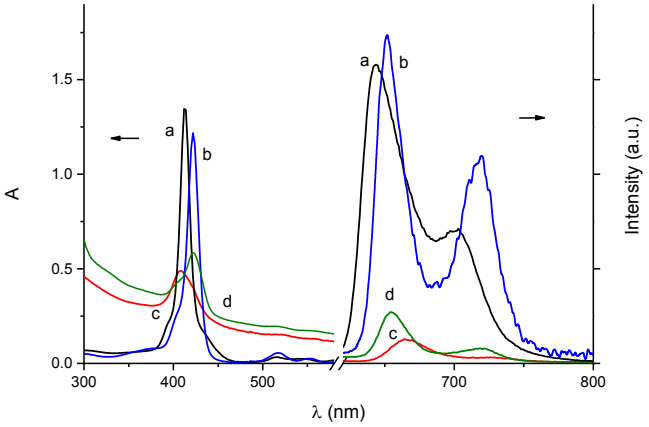

Fig. 2. Absorption (left) and fluorescence emission (right) spectra of $TPPS_4$ and DTX/$TPPS_4$-dcNPs in water (a,c) and in DMEM FBS+ (b,d). λ_{ex}= 530 nm are shown.

fluorescence was significantly suppressed and the emission bands were both red-shifted of ca. 16 nm (c, right). This spectroscopic behavior is typical for a face-to-face arrangement of the $TPPS_4$ units in non-photoresponsive H-type aggregates[34,35]and thus accounts for a massive aggregation of the porphyrin in the dcNPs. However, the low but not negligible fluorescence emission observed, suggests a slight deviation from the strict parallel arrangement of the dipole moments of $TPPS_4$

units.[36]The whole DTX/$TPPS_4$-dcNPs are quite stable in the presence of DMEM FBS+. In fact, the absorption spectrum (d, left) shows the Soret band shifted in two components with maxima at ca. 408 and 420 nm, respectively. While the former component is related to the H-types aggregates of $TPPS_4$ in the dcNPs, the latter indicates that a small fraction of $TPPS_4$ (ca. 20 %) undergoes displacement and is released in its monomeric form in DMEM medium. Accordingly the fluorescence spectrum (d, right) shows a slight revival with the emission maxima corresponding well to those observed for the free $TPPS_4$ in the same medium (see spectrum b, right). This scenario was well confirmed by the behavior of the lowest triplet state of $TPPS_4$. This excited state is the key transient intermediate for the photosensitization of $^1O_2$ and its effective generation is thus crucial for the photodynamic action.[37,38]

Laser flash photolysis with nanosecond time-resolution is a powerful tool for obtaining spectroscopic and kinetic features of excited triplets of porphyrins since these transient species exhibit very intense absorptions in the visible region and possess lifetimes falling in the microsecond time scale.[39] Figure 3 shows that the transient spectra observed 0.1 μs after laser excitation of $TPPS_4$ free and DTX/$TPPS_4$-dcNPs dispersed in water and in DMEM FBS+, respectively. Excitation of aqueous solutions of free $TPPS_4$ results in the formation of a transient absorption with a maximum at ca. 440 nm and a bleaching due to the Soret ground-state absorption (Figure 3, spectrum a). This species decays mono-exponentially with a lifetime of ca. 20 μs (Figure 4A), and can be safely attributed to the lowest excited triplet state of the $TPPS_4$.

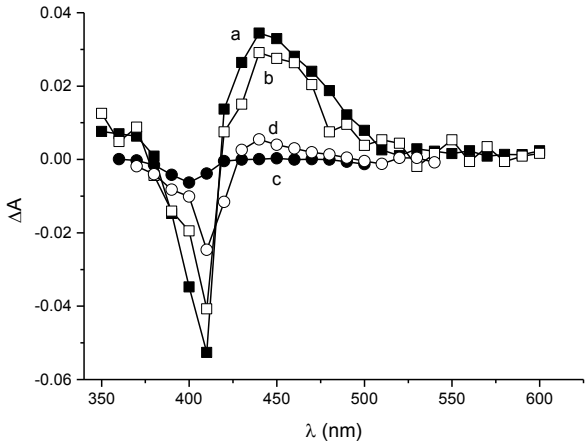

Fig.3. Transient absorption spectra observed 0.1 μs after 532 nm laser excitation (E_{532} ~ 10 mJ/ pulse) of N_2-saturated solutions of $TPPS_4$ in water (a) and DMEM FBS+ (b) and DTX/$TPPS_4$-dcNPs in water (c) and DMEM FBS+ (d).

The triplet state of $TPPS_4$ was also effectively populated in the presence of DMEM FBS+ (Fig. 3, spectrum b) but its lifetime was much longer being ca. 1.5 ms (Fig. 4B). In contrast no significant transient signal was observed for DTX/$TPPS_4$-dcNPs in water (Fig.3, spectrum c) according to the assembling of the porphyrin in the form of non-photoresponsive H-type aggregates within dcNPs. In the presence of DMEM FBS+, DTX/$TPPS_4$-dcNPs exhibited a weak revival of the triplet signal. The appearance of this signal can be due to the displacement of the $TPPS_4$ from the NPs and its release in DMEM medium under as photoactive monomeric form. The triplet decay observed in these conditions (Fig. 4C) was in fact virtually the same to that observed for the free $TPPS_4$ under the very same experimental conditions (Fig. 4B)

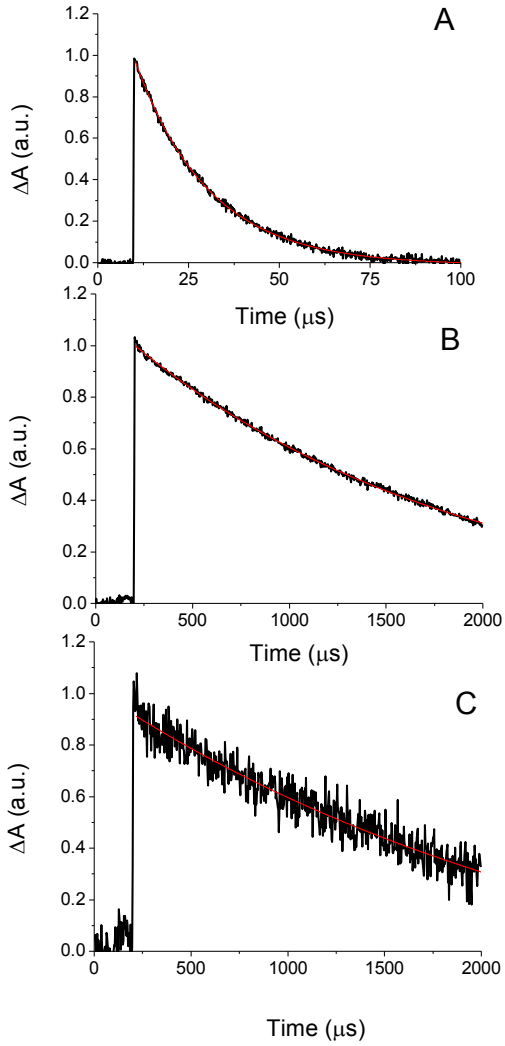

Fig. 4. Normalized decay traces monitored at 440 nm and the related first-order fittings, observed upon 532 nm laser excitation (E_{532} ~ 10 mJ/ pulse) of N_2-saturated of$TPPS_4$in water (A) and DMEM FBS+ (B) and DTX/TPPS-dcNPs in DMEM FBS+ (C).

3.3 CD44-mediated cell uptake of dcNPs

The involvement ofCD44 receptor in the uptake of HA-coated NPs was studied measuring the uptake of RHO-dcNPs in MDA-MB-231 and MCF-7 cells exhibiting high and low CD44 expression, respectively. As shown in Fig. 5 A, RHO-dcNPs were taken up by both cells lines but as expected, the uptake was significantly higher in MDA-MB-231 with respect to MCF-7cells. The active role of CD44 in mediating the uptake of dcNPs was further confirmed with the competition experiments in which the cells were pre-incubated with an excess of free HA in order to saturate the receptors.

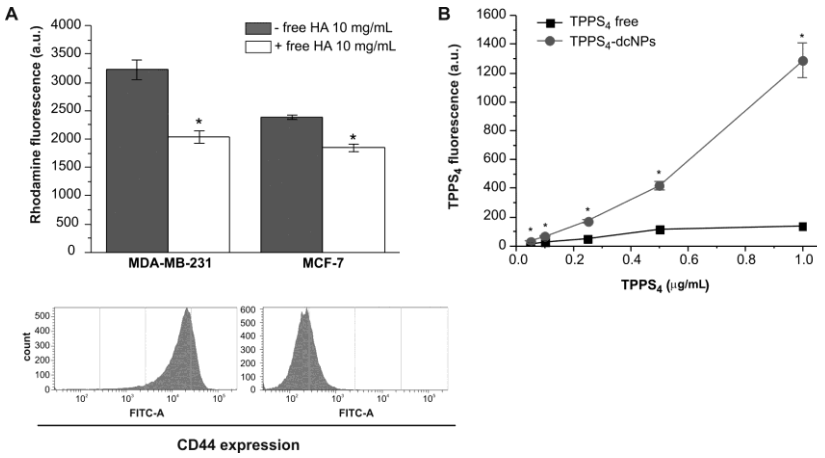

Fig.5. Uptake of RHO-dcNPs and $TPPS_4$-dcNPs. A) Uptake of RHO-dcNPs (50 μg/mL) in MDA-MB-231 (high CD44 expression) and MCF-7 (low CD44 expression) cells after 2 h incubation at 37 °C in medium with or without 10 mg/mL free HA.* $p<0.001$, with respect to the sample not incubated with free HA (Student's t test). B) Concentration-dependent uptake of free $TPPS_4$ and $TPPS_4$-dcNPs in MDA-MB-231 cells after 24 h incubation at 37 °C. * $p<0.001$, with respect to $TPPS_4$ free (Student's t test).

The reduction of NP uptake caused by free HA was significant in both cell lines but it was more important in MDA-MB-231 than MCF-7 cells (37% vs 23%) showing a clear dependence on the expression levels of CD44. Given the more important role of CD44 in MDA-MB-231, with respect to

MCF-7 cells, the first were selected for our uptake and cytotoxicity studies on $TPPS_4$ and DTX delivered by dcNPs.

The uptake of $TPPS_4$, delivered to the cells in the free form or incorporated in $TPPS_4$-dcNPs was measured by flow cytometry after 24 h of cell incubation (Fig. 5 B).Delivery through dcNPs significantly increased the uptake of the PS at all tested concentrations and, at the highest concentration of 1 μg/mL, the uptake of $TPPS_4$-dcNPs was about 9.4-folds that of free $TPPS_4$.Confocal microscopy analysis revealed that while free $TPPS_4$ was localized both in lysosomes and Golgi apparatus, $TPPS_4$-dcNPs localized exclusively in lysosomes (Fig. 6).

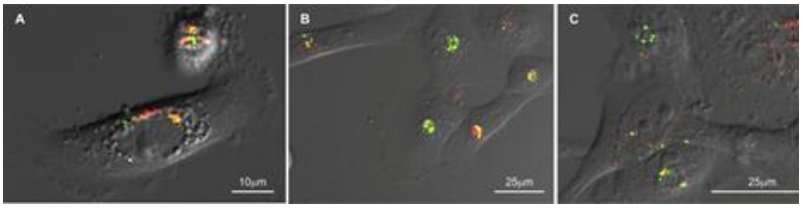

Fig. 6. Confocal microscopy images showing the intracellular localization of $TPPS_4$-dcNPs (A) and free $TPPS_4$ (B, C) in MDA-MB-231 cells incubated for 24 h. A and C: merged images of $TPPS_4$and LysoTracker green; B: merged images of $TPPS_4$andBODIPY® FL C5-ceramide.

3.4 Cytotoxicity of dcNPs

The cytotoxicity of DTX toward MDA-MB-231 cells was determined for the free and DTX-dcNP formulation by incubating the cells up to 72 h. The cell viability was reduced at low drug concentrations but reached a plateau at approx. 0.1 μg/mL DTX(Fig. 7).

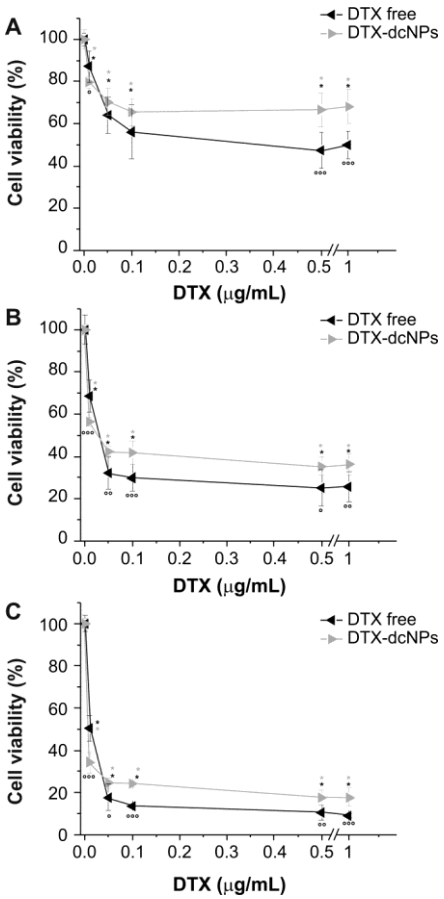

Fig. 7. Cell viability of MDA-MB-231 cells exposed to increasing concentrations of free DTX or DTX-dcNPs for 24 (A), 48 (B), 72 h (C). * $p<0.001$, with respect to control(Student's t test). ° $p<0.05$, °° $p<0.01$, °°°$p<0.001$, with respect to DTX-dcNPs (Student's t test).

The residual cell viability in the plateau region decreased prolonging the time of treatment for both formulations. DTX delivered by dcNPs was significantly more cytotoxic at very low concentrations (e.g. 0.01 μg/mL) while, increasing the dose, free DTX resulted more effective in inducing cell death. DTX induced cell death by causing an arrest in the phase G_2M of the cell cycle as already shown for taxanes (Fig. 8). However, our cell cycle analyses carried out after 24 h of treatment with DTX showed that DTX-dons were significantly more efficient in

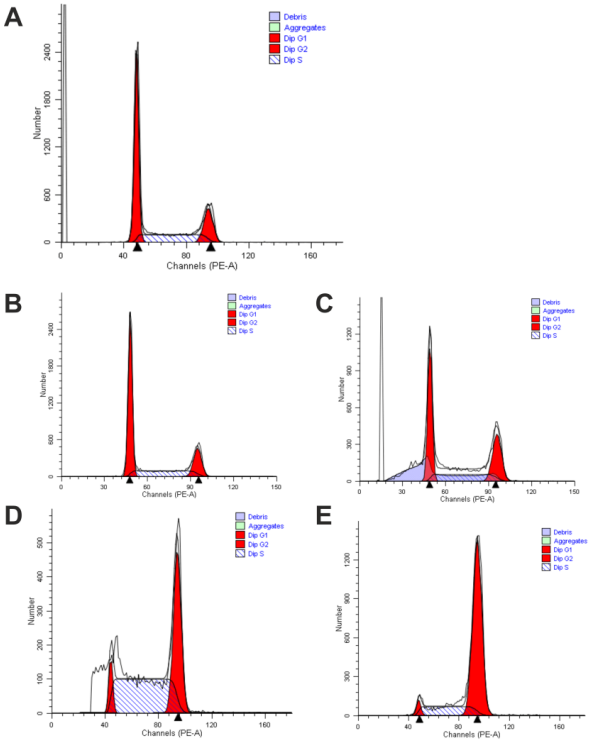

F

Phase (%)	[DTX] 0.01 µg/mL		[DTX] 0.1 µg/mL		
	free	dcNPs	free	dcNPs	Control
G1	55.70	6.49	43.76	3.44	54.14
S	25.27	55	26.11	20.22	27.34
G2-M	19.03	38.51	30.13	76.28	18.51
Viability	12.89	20.4	43.82	34.61	100

..

Fig. 8: Analysis of cell cycle of MDA-MB-231 cells exposed to free DTX or DTX-dcNPs for 24 h. Control cellsA); cells exposed to free DTX at 0.01 µg/mLB) or 0.1 µg/mL D); cells exposed to DTX-dcNPs at 0.01 µg/mLC) or 0.1 µg/mL E). Percentages of cells the various phases are shown in F).

inducing the block in G_2M, especially at doses as low as 0.01 µg/mL. At this concentration, free DTX did not cause appreciable alterations of cell distribution in the various phases of the cycle while DTX-dcNPs increased the percentage of cells in S and G_2M phases. This result is

consistent with higher loss of cell viability measured at low concentrations of DTX-dcNPs with respect to free DXT.

The toxicity of free $TPPS_4$and$TPPS_4$-dcNPswas measured in the absence of light after 24 h or 24 + 24 h of cell incubation for concentrations up to 1 µg/mL. Both PS formulations were scarcely cytotoxic toward MDA-MB-231 cells, with no more than 20% of cell mortality at 1 µg/mL $TPPS_4$(Fig. 9 A, B). Prolonging the incubation up to 72 h did not increase cytotoxicity (data not shown). MDA-MB-231 cells treated for 24 h with DTX/$TPPS_4$-dcNPs showed a decrease of viability similar to that induced by DTX-dcNPs ($p>0.05$, Bonferroni test) (Fig. 7 A), indicating that in the dark cytotoxicity is mainly due to DTX. The combination of the two drugs in their free form caused a decrease of cell viability similar to that of DTX/$TPPS_4$-dcNPs at concentrations higher than 0.25 µg/mL while at lower concentrations the combination of the free drugs was significantly less cytotoxic than DTX/$TPPS_4$-dcNPs (Fig. 9 A, B).

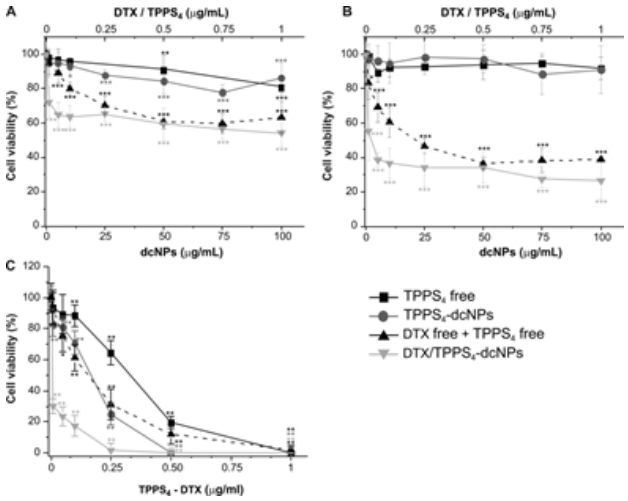

Fig. 9. Viability of MDA-MB-231 cells exposed in the dark to drugs free or loaded in dcNPs for 24 h (A) or 24 + 24 h (B). *p<0.05, **p<0.01, ***p<0.001, with respect to control (Student's t test). In C) the cells were irradiated with 8 J/$cm^2$of blue light after 24 h of exposure to the drugs and viability was measured 24 h post-irradiation. *p<0.01, **p<0.001, with respect to control (Student's t test).

No effects on cell viability was observed incubating the cells with empty dcNPs up to 72 h (Fig. 10) with NP concentrations up to 100 μg/mL.

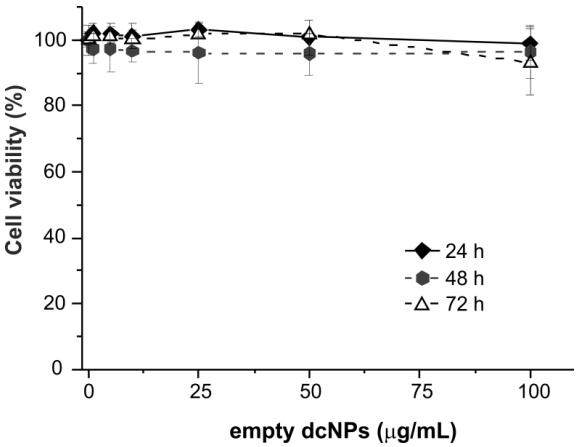

Fig. 10. Cell viability of MDA-MB-231 cells exposed up to 72 h to increasing concentrations of empty dcNPs.

Cytotoxicity was also measured in cells incubated for 24 h with the various $TPPS_4$formulations and then exposed to 8 J $cm^{-2}$of blue light. As shown in fig. 9 C, $TPPS_4$ delivered through dcNPs was significantly more phototoxic than the free form, with an IC_{50} of 0.17 and 0.33 μg/mL PS, respectively. As expected, light-induced death was increased in cells that had been treated with the combination of $TPPS_4$ and DTX in dcNPs (IC_{50} 0.008 μg/mL PS). Interestingly, the decrease of cell viability after irradiation induced by DTX/$TPPS_4$-dcNPs was significantly higher than that induced by the combination of the free drugs (IC_{50} 0.16 μg/mL PS).

4 Discussion

The main goal of this work was to develop biodegradable core-shell dcNPs for combined delivery of photo- and chemo-therapeutic sin cancer cells overexpressing CD44 receptor. To this end, we exploited the strong electrostatic interactions between different and *ad-hoc* chosen, functional blocks. A biodegradable PLGA nanoscaffold, carrying the hydrophobic

chemotherapeutic DTX, was surrounded by a HA/PEI shell, entangling the hydrophilic PDT agent$TPPS_4$ to give the complete nanoassembly. The rationale behind this logical design is summarized in the following: (1) HA is expected to be exposed at the dcNPs periphery, ensuring the active targeting to cancer cells; (2) the hydrophobic DTX and the hydrophilic $TPPS_4$ are located in different compartments of the dcNPs (*i.e.,* the core and the shell); such a large separation distance rules out any intermolecular communication between the photoexcited PDT agent and DTX(*i.e.*photoinduced electron transfer); (3) the cationic PEI is expected to encourage the massive aggregation of the PDT agent at the dcNPs shell; as a consequence, $TPPS_4$is expected to be non-fluorescent and unable to photosensitize $^1O_2$ until it is released from the dcNPs in its monomeric form. From a formulation standpoint, the amount of $TPPS_4$loaded on PEI-coated NPs had an impact on size, which suggests that upon $TPPS_4$adsorption some rearrangement of PEI chains due to altered negative to positive charge ratio could occur. Freeze-drying of dcNPs was feasible by using trehalose as cryoprotectant. After dispersion of the powder in water, spherical, non-aggregated DTX/$TPPS_4$-dcNPs with unaltered hydrodynamic diameter and zeta potential were obtained. Size below 200 nm and negative surface perfectly fit the biological requirements for injectable NPs.[40] As generally found for polyelectrolyte systems, the size of DTX/$TPPS_4$-dcNPs was very dependent on the presence of salts and proteins. As a general trend, dcNPs were prone to size and zeta potential (less negative) increase in the presence of salts. For polyelectrolyte NPs where HA is adsorbed onto chitosan cross-linked NPs, a tendency to NP shrunk is observed due to an increased osmotic pressure of the medium which decreases NP swelling.[31]Indeed, we observed an opposite trend for DTX/$TPPS_4$-dcNPs which could be contributed by formation of weaker electrostatic interactions between PEI and HA and formation of a looser PEI/HA network. The different arrangement of PEI/HA chains can explain also the burst release of monomeric $TPPS_4$(around 20%). Finally, a further increase of dcNP size in DMEM FBS+ could be attributed by protein adsorption onto NP structure possibly due to higher extent of exposition of positively-charged PEI to the medium. It is expected that PEI positive amino groups are prone to protein interaction as demonstrated for PEI or different types of NPs.[41,42] Concerning

release kinetics, $TPPS_4$release in DMEM FBS+ was incomplete in the time-frame of cell experiment while DTX release was slower due to both its low water solubility and longer distance to cover in order to reach the medium. Targeting ability of HA-coated NPs is strongly related to the morphology of the surface HA and in turn its mode of exposition to CD44 receptor.[43,44]. We have evidence that dcNPs bind CD44 receptor and are internalized by the cells with an efficiency that depends on the level of CD44 expression (Fig. 5 A); as a matter of fact the uptake of Rho-dcNPs was significantly higher in MDA-MB-231 cells that exhibit a high CD44 expression than MCF-7 cells. The active role of CD44 was confirmed by the higher inhibition of dcNP uptake in MDA-MB-231 with respect to MCF-7 cells when an excess of free HA was added to the cell medium before incubation with NPs. Both $TPPS_4$ and DTX entrapped in dcNPs could benefit of the CD44-mediated internalization of their carrier by increasing selective uptake and cytotoxicity in CD44 over-expressing cancer cells. $TPPS_4$is an efficient hydrophilic photosensitizer of $^1O_2$ in solutions.[45]Nevertheless it remains a poor photosensiting agent *in vitro* and *in vivo* due to its inability to enter and to be retained inside the cells[46,47] at adequate concentrations able to produce efficient cell photoinactivation. Its incorporation into dcNPs greatly enhances its uptake in MDA-MB-231 cells and consequently increases the efficiency of light-induced cell mortality. $TPPS_4$ loaded in dons at 1μg/mL was clearly detected in the lysosomes of the cells while intracellular fluorescence of free $TPPS_4$was much less intense and was localized both in lysosomes and Golgi apparatus. It is worth mentioning that previous studies on cellular localization of free $TPPS_4$ were carried out at a concentration of 75 μg/mL for gaining a fluorescence signal sufficient to detect a precise lysosomal localization of the porphyrin in the cells.[48] In line with our observations, Varchi et al.[49]reported undetectable fluorescence in HepG2 cells incubated with free $TPPS_4$ (20 μg/mL) while $TPPS_4$ delivered to cells in poly(methylmethacrylate) NPs showed a high intracellular fluorescence. Consistent with these observations our flow cytometry measurements showed higher uptake of $TPPS_4$ in dcNPs with respect to the free form; at 1 μg/mL the uptake in NPs was increased by approximately 10-fold. The increased uptake led to increased phototoxicity to MDA-MB-231 cells which well correlated with the increased cellular fluorescence signals. Both the remarkable

fluorescence of $TPPS_4$observed in cells as well as the extent of cell photoinactivation, cannot be ascribed to an internalization of the dcNPs without disassembling of the PDT agent. In fact, spectroscopic and photochemical results obtained in both aqueous solution and DMEM FBS+ showed negligible red fluorescence and barely detectable signal of the excited triplet state precursor of the $^1O_2$ as a result of the massive aggregation of the PDT agent in the dcNPs, mainly as H-type aggregates, which are well known to be photochemically unactive.[35] As a consequence, we believe that $TPPS_4$is most likely released as photoactive monomer, characterized by good fluorescence and excellent photodynamic properties, after cellular internalization. The enhancement of DTX toxicity after incorporation into dcNPs was evident at the lowest tested concentration of 10 ng/mL. Percentages of death in MDA-MB-231 cells exposed to DTX for 24 h were about 13 and 20%, respectively, for free and DTX-dcNP. The higher cytotoxicity is very likely the consequence of a faster and more efficient block in the S and G2/M phases of the cell cycle. In fact after 24 h of exposure, free DTX did not cause significant perturbations of the cell cycle while DXT-dcNPs caused an increase of the percentage of cells in S phase (55% vs 27% of the control) as well as G2/M phases (38% vs 18% of the control). Slightly different are the effects described by Huang et al.[50] on the same cell line with 10 ng/mL DXT and this is very likely explained by the fact that cell cycle perturbations were analyzed after 48 h of treatment; in any case, in agreement with our observations, the arrest in G2/M phases was more evident with DTX-dcNPs rather than with free DTX. At concentrations higher than 10 ng/mL DXT-dcNPs caused an arrest of the cells in the G2/M phases stronger than that of free DTX but this effect did not translate into increased cell death also after prolonged treatment (48 and 72 h). The dark cytotoxicity of DTX-dcNPs toward MDA-MB231 cells was not affected significantly by the incorporation of $TPPS_4$. On the contrary following light activation of DTX/$TPPS_4$-dcNPs, cell death was increased tremendously and reached 100% at drug concentrations less than 0.2 μg/mL. Extremely important is the observation that the combination of the two drugs in their free form, especially at concentrations below 0.2 μg/mL, was much less powerful in inducing cell death than the combination delivered through dcNPs. Whether the enhancement of cytotoxicity is the result of a synergistic

interaction of the two treatments will be determined with properly planned experiments and analyses of the data. In any case the results reported here strongly indicate that dcNPs are a very useful tool to potentiate the cytotoxic effects of the combination $TPPS_4$ plus light and DTX. Very likely NPs favor the perfect timing and location of delivery of the two drugs to cell targets, namely microtubules. DTX is a well-known microtubule-stabilizing agent that interferes with mitosis and cell division and cause death of breast cancer cells through mitotic catastrophe.[51] Also light activated $TPPS_4$ exerts its cytotoxic effects by perturbing the assembling of the mitotic spindle and arresting the cells in mitosis.[52] It can therefore be hypothesized that the high efficiency of DTX/$TPPS_4$-dcNPs in inducing cell death is related to a concerted action of the co-delivered drugs on reorganization of microtubules that leads to arrest in mitosis followed by death for excessive damage to mitotic apparatus.

5 Conclusions

We have proposed a novel type of targeted dcNPs nanoparticles for the combined chemotherapy and photodynamic therapy of cancers overexpressing CD44 receptor. These dcNPs are achieved by taking advantage of electrostatic interactions between different building blocks, contain HA as a targeting moiety, co-encapsulate the chemotherapeutic DTX and the PDT agent $TPPS_4$ in the core and the shell, respectively. dcNPs have the PDT agent completely aggregated and photochemically unactive at their surface and release it as active monomer after cell internalization. This feature is of relevance in view of further in vivo studies. Indeed, the dcNPs are expected to be non-fluorescent and non-photoactive while in the circulatory system. Targeting mechanisms localize the dcNPs in tumor tissue, where the PDT component is disassembled from the dcNPS surface and becomes highly fluorescent and phototoxic. The concerted release of the chemotherapeutic results in a tremendous improvement of single drug activity. This strategy turns to be very attractive to selectively co-localize different drugs in the same cell compartment and to find out possible synergic effects.

References

1. Hu CMJ, Zhang L. Nanoparticle-based combination therapy toward overcoming drug resistance in cancer. 2012;83:1104-11.
2. Zuluaga MF, Lange N. Combination of photodynamic therapy with anti-cancer agents. Curr Med Chem 2008;15:1655-73.
3. Lehar J, Krueger AS, Avery W, Heilbut AM, Johansen LM, Price ER, Rickles RJ, Short GF, III, Staunton JE, Jin X, Lee MS, Zimmermann GR, Borisy AA. Synergistic drug combinations tend to improve therapeutically relevant selectivity. Nat Biotechnol 2009;27:659-66.
4. Khdair A, Chen D, Patil Y, Ma L, Dou QP, Shekhar MP, Panyam J. Nanoparticle-mediated combination chemotherapy and photodynamic therapy overcomes tumor drug resistance. J Control Release 2010;141:137-44.
5. Zuluaga MF, Lange N. Combination of photodynamic therapy with anti-cancer agents. Curr Med Chem 2008;15:1655-73.
6. Parhi P, Mohanty C, Sahoo SK. Nanotechnology-based combinational drug delivery: an emerging approach for cancer therapy. Drug Discov Today 2012;17:1044-52.
7. Conte C, Ungaro F, Mazzaglia A, Quaglia F: Photodynamic Therapy for Cancer: Principles, Clinical Applications, and Nanotechnological Approaches; in Alonso MJ, Garcia-Fuentes M, (eds): Nano-Oncologicals.Advances in Delivery Science and Technology. Springer International Publishing, 2014, pp 123-160.
8. Agostinis P, Berg K, Cengel KA, Foster TH, Girotti AW, Gollnick SO, Hahn SM, Hamblin MR, Juzeniene A, Kessel D, Korbelik M, Moan J, Mroz P, Nowis D, Piette J, Wilson BC, Golab J. Photodynamic therapy of cancer: an update. CA Cancer J Clin 2011;61:250-81.
9. Couvreur P. Nanoparticles in drug delivery: Past, present and future. Advanced Drug Delivery Reviews 2013;65:21-23.
10. Egusquiaguirre SP, Igartua M, Hernandez RM, Pedraz JL. Nanoparticle delivery systems for cancer therapy: advances in clinical and preclinical research. Clinical & Translational Oncology 2012;14:83-93.

11. Hu CM, Fang RH, Luk BT, Zhang L. Polymeric nanotherapeutics: clinical development and advances in stealth functionalization strategies. Nanoscale 2014;6:65-75.
12. Jain KK. Advances in the field of nanooncology. BMC Med 2010;8:83.
13. Jain RK, Stylianopoulos T. Delivering nanomedicine to solid tumors. Nat Rev Clin Oncol 2010;7:653-64.
14. Nazir S, Hussain T, Ayub A, Rashid U, MacRobert AJ. Nanomaterials in combating cancer: Therapeutic applications and developments. Nanomedicine-Nanotechnology Biology and Medicine 2014;10:19-34.
15. Kamaly N, Xiao ZY, Valencia PM, Radovic-Moreno AF, Farokhzad OC. Targeted polymeric therapeutic nanoparticles: design, development and clinical translation. Chem Soc Rev 2012;41:2971-3010.
16. Fang J, Nakamura H, Maeda H. The EPR effect: Unique features of tumor blood vessels for drug delivery, factors involved, and limitations and augmentation of the effect. Advanced Drug Delivery Reviews 2011;63:136-51.
17. Maeda H. Macromolecular therapeutics in cancer treatment: The EPR effect and beyond. Journal of Controlled Release 2012;164:138-44.
18. Huynh NT, Roger E, Lautram N, Benoit JP, Passirani C. The rise and rise of stealth nanocarriers for cancer therapy: passive versus active targeting. Nanomedicine (Lond) 2010;5:1415-33.
19. Bertrand N, Wu J, Xu X, Kamaly N, Farokhzad OC. Cancer nanotechnology: The impact of passive and active targeting in the era of modern cancer biology. Adv Drug Deliv Rev 2013.
20. Mahon E, Salvati A, Baldelli Bombelli F, Lynch I, Dawson KA. Designing the nanoparticle-biomolecule interface for targeting and therapeutic delivery. Journal of Controlled Release 2012;161:164-74.
21. Pasquier E, Kavallaris M, Andre N. Metronomic chemotherapy: new rationale for new directions. Nat Rev Clin Oncol 2010;7:455-65.
22. Fan W, Shen B, Bu W, Chen F, He Q, Zhao K, Zhang S, Zhou L, Peng W, Xiao Q, Ni D, Liu J, Shi J. A smart upconversion-based

mesoporous silica nanotheranostic system for synergetic chemo-/radio-/photodynamic therapy and simultaneous MR/UCL imaging. Biomaterials 2014;35:8992-9002.

23. Xiang GH, Hong GB, Wang Y, Cheng D, Zhou JX, Shuai XT. Effect of PEG-PDLLA polymeric nanovesicles loaded with doxorubicin and hematoporphyrin monomethyl ether on human hepatocellular carcinoma HepG2 cells in vitro. Int J Nanomedicine 2013;8:4613-22.
24. Miao W, Shim G, Lee S, Lee S, Choe YS, Oh YK. Safety and tumor tissue accumulation of pegylated graphene oxide nanosheets for co-delivery of anticancer drug and photosensitizer. Biomaterials 2013;34:3402-10.
25. Conte C, Ungaro F, Maglio G, Tirino P, Siracusano G, Sciortino MT, Leone N, Palma G, Barbieri A, Arra C, Mazzaglia A, Quaglia F. Biodegradable core-shell nanoassemblies for the delivery of docetaxel and Zn(II)-phthalocyanine inspired by combination therapy for cancer. Journal of Controlled Release 2013;167:40-52.
26. Separovic D, Breen P, Boppana NB, Van BE, Joseph N, Kraveka JM, Rahmaniyan M, Li L, Gudz TI, Bielawska A, Bai A, Bielawski J, Pierce JS, Korbelik M. Increased killing of SCCVII squamous cell carcinoma cells after the combination of Pc 4 photodynamic therapy and dasatinib is associated with enhanced caspase-3 activity and ceramide synthase 1 upregulation. Int J Oncol 2013;43:2064-72.
27. Danhier F, Ansorena E, Silva JM, Coco R+, Le Breton A, Pr+®at V+. PLGA-based nanoparticles: An overview of biomedical applications. Journal of Controlled Release 2012;161:505-22.
28. Ossipov DA. Nanostructured hyaluronic acid-based materials for active delivery to cancer. Expert Opin Drug Deliv 2010;7:681-703.
29. Choi KY, Saravanakumar G, Park JH, Park K. Hyaluronic acid-based nanocarriers for intracellular targeting: Interfacial interactions with proteins in cancer. Colloids and Surfaces B-Biointerfaces 2012;99:82-94.
30. Misra S, Heldin P, Hascall VC, Karamanos NK, Skandalis SS, Markwald RR, Ghatak S. Hyaluronan-CD44 interactions as potential targets for cancer therapy. FEBS J 2011;278:1429-43.
31. Almalik A, Karimi S, Ouasti S, Donno R, Wandrey C, Day PJ, Tirelli N. Hyaluronic acid (HA) presentation as a tool to modulate

and control the receptor-mediated uptake of HA-coated nanoparticles. Biomaterials 2013;34:5369-80.
32. El-Dakdouki MH, Pure E FAU - Huang X, Huang X. Development of drug loaded nanoparticles for tumor targeting. Part 2: Enhancement of tumor penetration through receptor mediated transcytosis in 3D tumor models. Nanoscale 2013.
33. Ungaro F, De Rosa G, Miro A, Quaglia F. Spectrophotometric determination of polyethylenimine in the presence of an oligonucleotide for the characterization of controlled release formulations. Journal of Pharmaceutical and Biomedical Analysis 2003;31:143-49.
34. Maiti NC, Mazumdar S, Periasamy N. J- and H-aggregates of porphyrin-surfactant complexes: Time-resolved fluorescence and other spectroscopic studies. Journal of Physical Chemistry B 1998;102:1528-38.
35. Gandini SCM, Yushmanov VE, Borissevitch IE, Tabak M. Interaction of the tetra(4-sulfonatophenyl)porphyrin with ionic surfactants: Aggregation and location in micelles. Langmuir 1999;15:6233-43.
36. McRae EG, Kasha M. Enhancement of Phosphorescence Ability upon Aggregation of Dye Molecules. The Journal of Chemical Physics 1958;28:721-22.
37. Pandey R, Zheng G: The Porphyrine Handbook. San Diego, Academic Press, 2000.
38. Chatterjee DK, Fong LS, Zhang Y. Nanoparticles in photodynamic therapy: an emerging paradigm. Adv Drug Deliv Rev 2008;60:1627-37.
39. Kalyanasundaram K, Neumann-Spallart M. Photophysical and redox properties of water-soluble porphyrins in aqueous media. J Phys Chem 1982;86:5163-69.
40. D'Angelo I, Conte C, Miro A, Quaglia F, Ungaro F. Core-shell nanocarriers for cancer therapy. Part I: Biologically oriented design rules. Expert Opinion on Drug Delivery 2014;11:283-97.
41. Mazzaferro L, Breccia JD, Andersson MM, Hitzmann B, Hatti-Kaul R. Polyethyleneimine-protein interactions and implications on protein stability. International Journal of Biological Macromolecules 2010;47:15-20.

42. Walkey CD, Chan WC. Understanding and controlling the interaction of nanomaterials with proteins in a physiological environment. Chem Soc Rev 2012;41:2780-99.
43. Almalik A, Donno R, Cadman CJ, Cellesi F, Day PJ, Tirelli N. Hyaluronic acid-coated chitosan nanoparticles: Molecular weight-dependent effects on morphology and hyaluronic acid presentation. Journal of Controlled Release 2013;172:1142-50.
44. Mizrahy S, Raz SR, Hasgaard M, Liu H, Soffer-Tsur N, Cohen K, Dvash R, Landsman-Milo D, Bremer MG, Moghimi SM, Peer D. Hyaluronan-coated nanoparticles: the influence of the molecular weight on CD44-hyaluronan interactions and on the immune response. J Control Release 2011;156:231-38.
45. Wilkinson F, Helman WP, Ross AB. Quantum Yields for the Photosensitized Formation of the Lowest Electronically Excited Singlet-State of Molecular-Oxygen in Solution. Journal of Physical and Chemical Reference Data 1993;22:113-262.
46. Moan J, Peng Q, Evensen JF, Berg K, Western A, Rimington C. Photosensitizing Efficiencies, Tumor-Uptake and Cellular-Uptake of Different Photosensitizing Drugs Relevant for Photodynamic Therapy of Cancer. Photochemistry and Photobiology 1987;46:713-21.
47. Evensen JF, Moan J. A Test of Different Photosensitizers for Photodynamic Treatment of Cancer in A Murine Tumor-Model. Photochemistry and Photobiology 1987;46:859-65.
48. Berg K, Bommer JC, Winkelman JW, Moan J. Cellular Uptake and Relative Efficiency in Cell Inactivation by Photoactivated Sulfonated Meso-Tetraphenylporphines. Photochemistry and Photobiology 1990;52:775-81.
49. Varchi G, Benfenati V, Pistone A, Ballestri M, Sotgiu G, Guerrini A, Dambruoso P, Liscio A, Ventura B. Core-shell poly-methylmethacrylate nanoparticles as effective carriers of electrostatically loaded anionic porphyrin. Photochemical & Photobiological Sciences 2013;12:760-69.
50. Huang J, Zhang H, Yu Y, Chen Y, Wang D, Zhang G, Zhou G, Liu J, Sun Z, Sun D, Lu Y, Zhong Y. Biodegradable self-assembled nanoparticles of poly (d,l-lactide-co-glycolide)/hyaluronic acid

block copolymers for target delivery of docetaxel to breast cancer. Biomaterials 2014;35:550-66.
51. Morse DL, Gray H, Payne CM, Gillies RJ. Docetaxel induces cell death through mitotic catastrophe in human breast cancer cells. Molecular Cancer Therapeutics 2005;4:1495-504.
52. Berg K, Moan J, Bommer JC, Winkelman JW. Cellular-Inhibition of Microtubule Assembly by Photoactivated Sulfonated Meso-Tetraphenylporphines. International Journal of Radiation Biology 1990;58:475-87.

Chapter 4
PLGA nanoparticles for the delivery of a doxorubicin-nitric oxide photodonor molecular hybrid

Chapter 4

Abstract

Chemotherapy results in severe side effects due to drug accumulation at non-target sites and the necessity of high drug doses to eradicate tumor. Furthermore, multidrug resistance (MDR) is believed to compromise treatment and to be the reason for tumor recurrence despite intensive chemotherapy. In view of its multifaceted role in cancer biology, nitric oxide (NO) delivery with a very precise control of site, time and dosage, presents high potential and opens fascinating prospects for innovative/combined treatment modalities.

In this work, we intend to develop a novel strategy based on the light-regulated release of NO from tailored NO photodonors (NOPD) to overcome the above drawbacks, amplifying doxorubicin(DOX) anticancer efficacy in both resistant and non-resistant cancer cells.

A covalent DOX-NOPD molecular hybrid was entrapped in biodegradable polymer nanoparticles (NPs) made of poly(lactic-co-glycolic) acid. NPs were below 200 nm and had a negative zeta potential. Fluorescence of DOX-NOPD was preserved inside NPs which displayed, under light, a faster NO photorelease as compared to a methanol solution. It is anticipated that NO photorelease from NPs can amplify DOX anticancer efficacy allowing not only to maximize the overall therapeutic efficacy but also to reduce the massive dosage of DOX with consequent reduction of its cardiotoxicity.

1. Introduction

Combination chemotherapy is becoming increasingly relevant to attain long-term prognosis and better quality of life in cancer patients. The basic concept in this strategy is to attack tumor on different sides by acting on a single oncogenic pathway through different mechanisms or across parallel pathways without intensification of side effects [1].Hence, there is a critical need of novel therapeutic strategies that can enhance response to chemotherapeutics and reverse resistance.

In recent years, nitric oxide (NO) has stimulated an explosion of interest not only due to its pivotal role in the maintenance and bioregulation of vital functions, but also for its promising anticancer activity.[2] NO radical is able to attack biological substrates of different nature like the plasma membrane [3],the mitochondria [4]and the cell nucleus [5],representing a multitarget cytotoxic agent, which does not suffer MDR problems[6] encountered with target-specific "conventional" anticancer drugs. Evidence of NO-induced death in various cell types, both by apoptosis and necrosis, is discussed in relevant reviews [7,8]. Further, the short half-life in blood (< 1s), the lack of charge, the good lipophilicity and the small size, allow NO to easily diffuse in the cellular environment over short distances (< 200 μm) [9]confining the region of action without inflicting systemic side effects common to several chemotherapeutics. An additional, peculiar advantage of NO is a low toxicity towards healthy cells, especially at concentrations toxic to cancer cells [2]. Furthermore, NO delivery to hypoxic regions, which are typical for solid tumors, increases significantly the local blood flow and enhances the susceptibility to chemotherapy and radiotherapy [10]. However, concentration, location and dose of NO strictly dictate its biologic effects[7]. Many classes of NO donors have been developed in recent years. However, they suffer important limitations since they are cleared rapidly in the body, release NO with limited control and need to be tailored to reach the specific target.

Light represents a powerful and minimally invasive trigger for the release of NO in biological systems with a superb spatiotemporal accuracy by using suitable NO photodonors (NOPD)[11]. These compounds allow to confine the site of action of NO at the illuminated

area with high spatial precision and to control its dosage with great accuracy by tuning the light intensity and/or duration. These unique features make the NOPD, especially those activated with Visible (Vis) and Near Infrared (NIR) light, a therapeutic arsenal much more appealing than that based on NO donors activated by thermal, enzymatic or pH stimuli [12]. In addition, light triggering is biofriendly, provides fast reaction rates and offers the great benefit of not affecting physiological parameters such as temperature, pH and ionic strength, fundamental requisite for biomedical applications.

Doxorubicin (DOX) is one of the most widely employed chemotherapeutics in fighting a vast variety of cancers. Despite its large use, DOX suffers two main limitations for an effective cancer therapy: i) cardiotoxicity, which can occur at both acute and chronic dose-related forms, ii) development of resistance through different mechanisms, the main of which is the overexpression of ABC transporters. Under the action of these transporters, DOX is extruded from the cancer cells, its cellular accumulation is decreased and consequently its cytotoxicity impaired. Interestingly,NO is also able to inhibit both Pgp and MRPs pumps by nitration processes [8]. The consequent decrease of their activity leads to an increase of DOX accumulation in the cancer cells with a resulting increase in its cell toxicity. Also in this case, NO concentration released remains a key issue to be addressed and therefore the use of NO precursors with controllable NO release is highly desirable.

Inspired by the above background, we propose a novel strategy to amplify the DOX anticancer efficacy in both resistant and non-resistant cancer cells based on the appropriate combination of NOPD with DOX. To this purpose a DOX-NOPD hybrid was entrapped inside biodegradable NPs of poly(lactic-co-glycolic) acid and its photochemical properties studied.

2. Material and methods

Poly(lactic-co-glycolic) acid (PLGA) (50:50 Resomer RG 502H inherent viscosity 0.16-0.24 dl/g) was purchased from BoehringerIngelheim (Ingelheim, Germany). Threalose, hyaluronidases 400-1000 units, Polyethyleneimine (PEI, MW= 10-25 kDa branched) and Poloxamer 188 (Pluronic® F68) were purchased from Sigma-Aldrich. Acetonitrile, ethanol and acetone were purchased from Carlo ErbaReagenti (Milan, Italy). DMEM and Fetal Bovine Serum (FBS) were purchased from Gibco life technologies. Hyaluronan (HA, MW <10 kDa) was a kind gift of Magaldi Life S.r.l. Ultrapure water was used throughout the study.

2.1 Preparation of nanoparticles (NPs)

DOX-NPs and DOX-NO NPs were prepared by a layer-by-layer deposition method as previously shown [13].Briefly PLGA NPs were prepared by solvent diffusion of an organic phase (10 mg of PLGA in acetone) in an aqueous phase (4 mL of water with Pluronic F68 0.1%). After solvent evaporation NPs were splitting in 4 eppendorf tube and washing, each eppendorf (0.5 mg NPs/mL) was coated first with a PEI and then with HA water solution (1mg/mL). The interval between each addition was kept constant at 15 min and, after each polymeric deposition, NPs are centrifugated and redisperded in water. NPs were freeze-dried for 24 h with threalose (60 mg) as cryoprotectant and kept at 4 °C.

2.2 NP characterization

Hydrodynamic diameter, polydispersity index (PI) and zeta potential of NPs after each preparation step were determined on a ZetasizerNano Z (Malvern Instruments Ltd., UK). Results are reported as mean of three separate measurements of three different batches (n=9)±SD.

For actual loading, NPs were centrifuged at 13000 rpm for 5 min and the amount of DOX and DOX-NOPD in water phase was analyzed by UV. Release profile of DOX from NPs (2mg) was evaluated by dialysis using DMEM FBS+ as dispersing medium and PBS (0.01 M) at pH 7.4

and 37°C as external medium (sink conditions were realized). DOX release was monitored for 72 h and compared with free DOX.

2.3 Photochemical properties

Photobleaching experiments were carried out by irradiating the samples with a 405 nm CW laser 200 mW cm^{-2}. Absorption and emission spectra were recorded with a HP 2452 diode array spectrophotometer and a Fluorolog Mod 111 spectrofluorimeter equipped with a double monocromator.NO release was measured with a World Precision Instrument, ISO-NO 1000 meter, equipped with a data-acquisition system and based on direct amperometric detection of NO with short-response time.

3. Results and discussion

A conjugate between DOX and a NO photodonor (DOX-NOPD) was synthesized by the group of Prof. Fruttero at the University of Torino. The chemical structure is reported in Fig. 1.

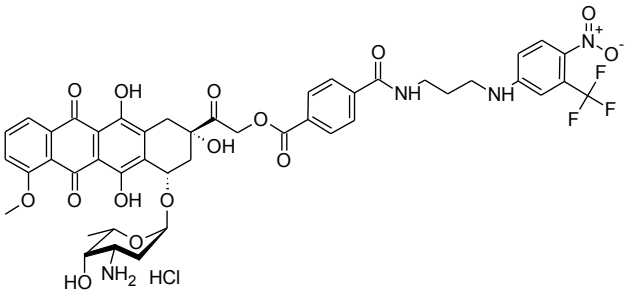

Fig. 1. Chemical structure of DOX-NOPD.

DOX-NOPD was entrapped inside PLGA core by nanoprecipitation. DOX alone was also entrapped and employed as control formulation. All NPs present a hydrodynamic diameter below 200 nm and entrapped around 50% of drug initially added. (Table 1).

Table.1 Properties of NPs loaded with DOX or DOX-NOPD.

NPs	Mean D_H (nm ± SD)	PI	Zeta potential (mV)	Actual loading
DOX NPs	170 ± 10	0.13	-23.2	1.9 ± 0.2
DOX-NOPD NPs	200 ± 10	0.17	-22.6	1.7 ± 0.1

The release of DOX from DOX-loaded NPs dispersed in DMEM with FBS 10% was slower as compared with free DOX that was released in 72h(Fig.2).

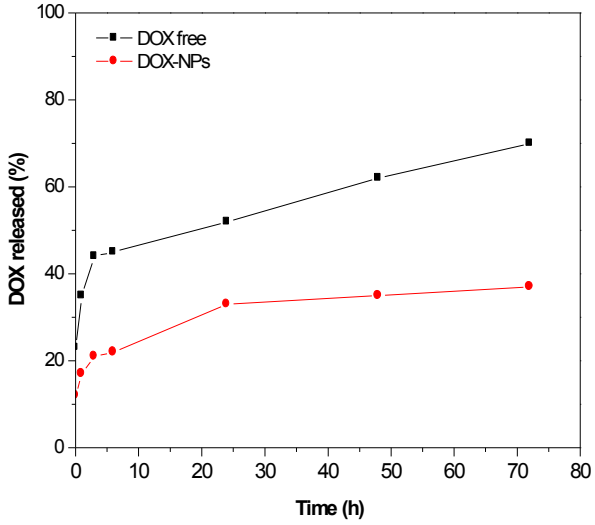

Fig. 2. Release of DOX from NPs compared to free DOX.

UV spectra of DOX-NOPD encapsulated in the NPs show a band with a maximum at 390 nm corresponding to the NO photoreleasing chromophore and around 500 nm corresponding to DOX absorption (Fig.3).The spectroscopic behavior observed under laser excitation at 405 nm was compared to that of free DOX-NOPD dissolved in methanol. (meOH)UV spectra of DOX-NOPD in the NPs collected after 5, 10, 15 and 20 min of irradiation show a bleaching of the 400 nm absorption band, according to the release of NO(Fig.3). The behavior was investigated also whit DOX-NOPD in meOH (Fig. 3) and kinetic of NO release reported as difference of absorbance at 390 nm after each single time interval (5, 10 and 15 min) and time 0 (A-A0) (Fig. 4). This release is clearly faster when DOX-NOPD is loaded into NPs as compared to DOX-NOPD in meOH (Fig. 3).

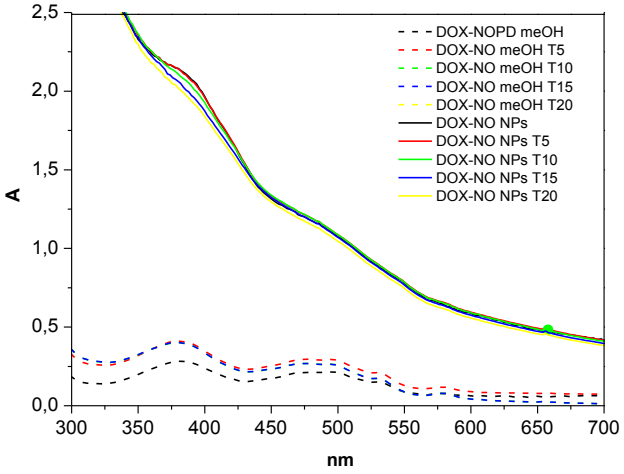

Fig. 3. Uv spectra of DOX-NOPD upon irradiation at 405 nm up to 20 min.

This behavior is the result of the presence of a large number of abstractable H-atoms present in the core of the polymer, which better favor the formation of the phenol derivative after NO photorelease through a radical mediated decomposition pathway. In order to verify if the photorelease of NO affected the integrity of the DOX component, fluorescence emission spectra were simultaneously recorded after each irradiation step.

The results reported in Fig. 5show that no significant change occurs upon light irradiation of the sample, according with the preservation of the DOX chromogenic unit in the molecular hybrid.

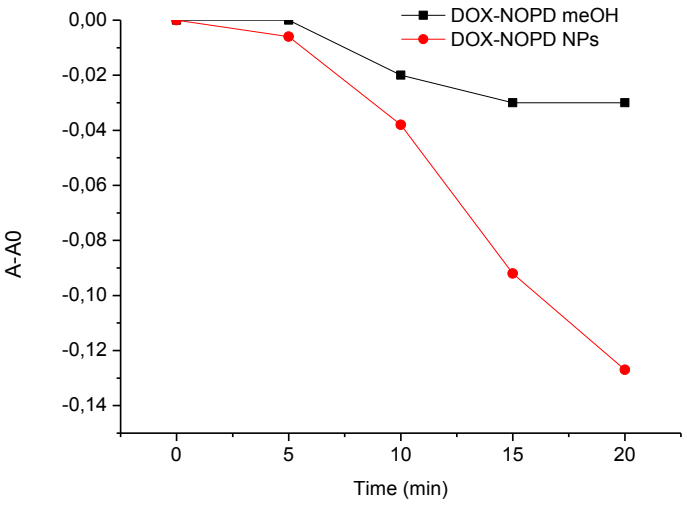

Fig. 4. Kinetic profile of photobleaching of DOX-NOPD NPs in water and DOX-NOPD free in meOH.

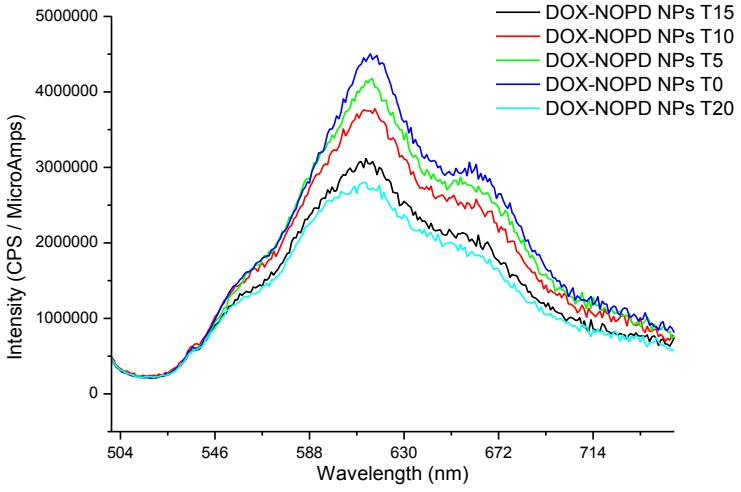

Fig. 5. Emission spectra of DOX-NOPD NPs upon irradiation at 405 nm up to 20 min.

We also performed time-resolved fluorescence experiments with the goal to gain insight into the dynamic behavior of the excited state of the DOX component. Normalized decay of DOX in NPs is bi-exponential with a lifetime of0.5 ns (64%) for DOX-NOPD loaded NPs as compared to DOX NPs showing a life time of 25 ps (59%) . The decay of DOX and DOX/-NO inside NPs was slower as compared to the corresponding free drugs respectively DOX/-NO and DOX (Fig. 6).

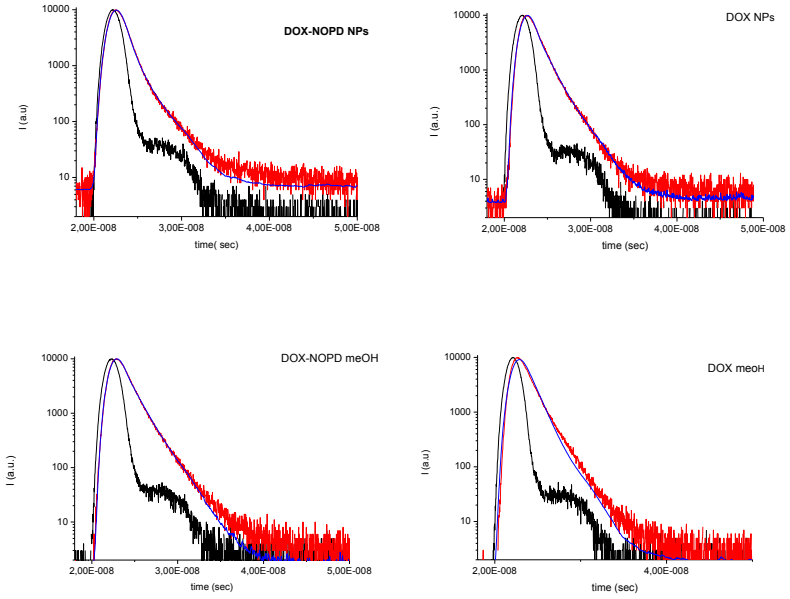

Fig. 6. Normalized decay traces observed upon 532 nm laser excitation (E_{532} ~ 10 mJ/ pulse) of DOX-NOPD NPs , DOX NPs, DOX-NO, DOX in meOH.

An ultrasensitive electrode which detects NO evolution amperometrically was used to evaluate NO release. The results illustrated in Fig. 7shows that the release process trictly depends on the external light input. In fact it promptly stops as the light turns off and restart again as the light is turned on.

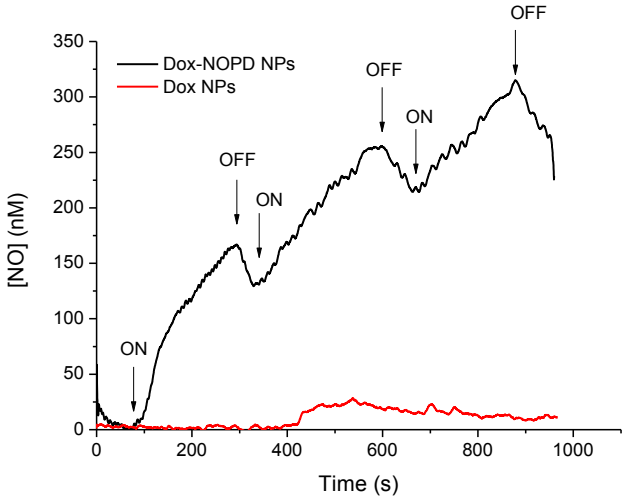

Fig. 7. Amperometric detection of NO release from DOX-NOPD NPs and DOX NPs under light irradiation.

4. Conclusions

DOX-NOPD can be encapsulated with high efficiency in PLGA NPs, according to our logical design. VIS light excitation of the loaded NPs leads to photoregulated release of NO from the nitroaniline moiety which converts to a phenyl derivate without inducing any photodecomposition of DOX, which well-retains its typical fluorescence in the red region. Preliminary cell results show that DOX-NOPD hybrid is much more accumulated in human M14 melanoma cells which express several ABC transporter and induced significant cytotoxicity compared to native DOX. Based on this preliminary data DOX-NOPD NPs can be tested onto different cancer cell lines in order to ameliorate DOX pharmacological profile.

References

1. Kemp JA, Shim MS, Heo CY, Kwon YJ: "Combo" nanomedicine: Co-delivery of multi-modal therapeutics for efficient, targeted, and safe cancer therapy.*Advanced Drug Delivery Reviews* 2015.

2. Fukumura D, Kashiwagi S, Jain RK: The role of nitric oxide in tumour progression.*Nature Reviews Cancer* 2006, 6: 521-534.

3. Gupta S, Mcarthur C, Grady C, Ruderman NB: Stimulation of Vascular Na+-K+-Atpase Activity by Nitric-Oxide - A Cgmp-Independent Effect.*American Journal of Physiology* 1994, 266: H2146-H2151.

4. Nishikawa M, Sato EF, Utsumi K, Inoue M: Oxygen-dependent regulation of energy metabolism in ascites tumor cells by nitric oxide.*Cancer Research* 1996, 56: 4535-4540.

5. Routledge MN, Wink DA, Keefer LK, Dipple A: Dna-Sequence Changes Induced by 2 Nitric-Oxide Donor Drugs in the Supf Assay.*Chemical Research in Toxicology* 1994, 7: 628-632.

6. Schroeder A, Heller DA, Winslow MM, Dahlman JE, Pratt GW, Langer R *et al*.: Treating metastatic cancer with nanotechnology.*Nature Reviews Cancer* 2012, 12: 39-50.

7. Carpenter AW, Schoenfisch MH: Nitric oxide release: Part II. Therapeutic applications. 2012, 41: 3742-3752.

8. Bonavida B, Baritaki S, Huerta-Yepez S, Vega MI, Chatterjee D, Yeung K: Novel therapeutic applications of nitric oxide donors in cancer: Roles in chemo- and immunosensitization to apoptosis and inhibition of metastases.*Nitric Oxide-Biology and Chemistry* 2008, 19: 152-157.

9. Ignarro LJ: *Nitric Oxide: Biology and Pathobiology*. Elsevier Inc; 2010.

10. Cook T, Wang Z, Alber S, Liu KH, Watkins SC, Vodovotz Y *et al*.: Nitric oxide and ionizing radiation synergistically promote apoptosis and growth inhibition of cancer by activating p53.*Cancer Research* 2004, 64: 8015-8021.

11. Vittorino E, Sciortino MT, Siracusano G, Sortino S: Light-Activated Release of Nitric Oxide with Fluorescence Reporting in Living Cells.*Chemmedchem* 2011, 6: 1551-1554.

12. Sortino S: Photoactivated nanomaterials for biomedical release applications.*J Mater Chem* 2012, 22: 301-318.

13. Maiolino S, Russo A, Pagliara V, Conte C, Ungaro F, Russo G *et al*.: Biodegradable nanoparticles sequentially decorated with Polyethyleneimine and Hyaluronan for the targeted delivery of docetaxel to airway cancer cells.*J Nanobiotechnology* 2015, 13: 29.

Chapter 5
Combining chemotherapy and gene therapy through nanoparticles decorated with a Polyethyleneimine -hyaluronan sequential layer

Abstract

The possibility to develop nanoparticles (NPs) combining different drugs which act on different biological pathways offers an unprecedented opportunity for finding novel treatment strategies for cancer. In this paper we designed double coated NPs based on a core of poly(lactic-co-glycolic) acid (PLGA) and a polymer shell of sequential layers of Polyethyleneimine (PEI) and Hyaluronan (HA) for the co-delivery of a conventional drug 5-Fluorouracil (5FU) and a plasmid encoding for the fusion proteinrpL3-GFP (pL3) in CD44+ HCT 116 $^{p53-/-}$colon cancer cells to find out if a combined effect could occur.

NPs showed a negative zeta potential and a hydrodynamic diameter below 200 nm, with a satisfactory actual loading of both 5FU and pL3. PEI adsorbed plasmid tightly onto NP surface as confirmed by gel retardation assay. Release profile of 5FU from NPs evaluated by dialysis using DMEM FBS+ as dispersing medium and PBS at pH 7.4 and 37°C as external medium showed a sustained release as compared with the free drug. Cytotoxicity of 5FU-loaded NPsHCT 116 $^{p53\ -/-}$colon cancer cells was higher as compared to free 5FU. Transfection studies in A549 lung cancer and HCT 116 $^{p53\ -/-}$colon cancer cells demonstrated that plasmid-loaded NPs are capable of a persistent GFP expression up to 96 h as compared to conventional lipofectamine. Results on the combination of5FU and pL3in HCT 116 $^{p53\ -/-}$cells indicate again a potentiated cytotoxic effect of the combination as compared to single plasmid and 5FU.

Chapter 5

1. Introduction

In cancer, the combination of various drugs acting on different biological targets has paved the way to a novel view of old chemotherapeutics in the attempt to enhance their therapeutic effect, thus decreasing the dose and side effects, and to limit multidrug resistance (MDR). The knowledge of molecular pathways involved in the cytotoxic effect of conventional chemotherapeutic drugs offers an infinite number of possibility to amplify a certain biological effect by modifying the expression of a single gene [1].

In cancer cell proliferation the rate of ribosome production plays a key role since an abundance of ribosomes is needed to sustain cell growth and proliferation suggesting that cancer cells are more sensitive to nucleolar stress than normal cells. Thus, chemotherapeutic agents that selectively target ribosome biogenesis could be less toxic to normal and differentiated cells. Many common anticancer drugs as 5FU[2] and Actinomycin D [3] interfere with rRNA synthesis and/or processing thereby inhibiting ribosome biogenesis. The resulting nucleolar stress activates signaling pathways including ribosomal protein-MDM2-p53 pathway to mediate cell cycle arrest, apoptosis, differentiation and/or senescence [4]. Although these pathways are well studied, most cancer cells contain mutant p53 or no p53 at all and p53-independent pathways mediating the nucleolar stress response are emerging. In fact, accumulating data revealed the existence of p53-independent but still ribosomal protein-dependent mechanisms that links nucleolar stress to cell cycle arrest. Recently, we demonstrated that ribosome-free rpL3 plays a crucial role in cell response to nucleolar stress induced by anticancer drugs known to interfere with RNA metabolism as 5FU, Actinomycin D and Oxaliplatin in colon and lung cancer cells devoid of p53 [5]. In particular, we demonstrated that upon drug-induced nucleolar stress free rpL3 is able to induce cell cycle arrest and apoptosis, and to inhibit cell proliferation and migration by controlling p21 expression both at post-transcriptional and post-translational levels independently from p53 [6]. It is noteworthy that the depletion of pL3 abolishes the cytotoxic effects of 5FU in colon cancer cells lacking functional p53 indicating that the loss of pL3 makes drug cytotoxic effects ineffective; consistently, pL3

overexpression associates to a strong increase of drug cytotoxicity. Taking together these results show that the efficacy of 5FU chemotherapy depends on pL3 status. Along this line, the knowledge of pL3 status in p53 null cancers may have a significant value in terms of the efficacy of chemotherapy based on 5FU. Hence, the development of treatments aimed at upregulating pL3 may be beneficial for the treatment of these cancers.

In recent years, non-viral carriers for plasmid DNA delivery have been introduced because viral carriers, although showing good transfection properties, induce immune response and possible recombination with wild-type virus [7]. The main class of cationic polymers for gene delivery include poly-L-lysine (PLL) and polyethyleneimmine (PEI) which are effective agents for transfection of short sequences of DNA, RNA and plasmids, but characterized by severe cytotoxicity due to ionic interaction with negatively-charged cell membranes resulting in collapse of membrane potential [8]. Cationic polymers with low molecular weight or linear structure show lower toxicity as compared to their high molecular weight counterpart but also a reduction of DNA condensation ability and reduced transfection.

Biodegradable polymers such as poly(lactic-co-glycolic) acid (PLGA) have been tested as gene nanovectors [9]. PLGA is a biodegradable polymer with a long history of safe use in pharmaceutical formulations and suitable for sustained delivery of small and large molecules [10]. Plasmid DNA can be either entrapped inside or adsorbed onto the surface of PLGA NPs. The encapsulation of plasmid DNA in PLGA is rather problematic since low encapsulation efficacy of DNA generally occurs [11]. Several attempts have been reported to enhance the loading of PLGA, comprising DNA condensation whit poly-L-lysine or PEI [12].

Over recent decades, nanotechnology has been found an interesting tool to combine different drugs with complementary mechanisms in one delivery system allowing their localization at the pharmacological target [13]. Some examples of NPs based on a PLGA core template including as cationic polymers PLL or PEI have been investigated for combined gene therapy and chemotherapy with the aim to overcome MDR. For example, co-delivery of camptothecin (CPT) and a plasmid

encoding TNF-related apoptosis genes loaded in multilayer NPs has shown a synergic effect in MDA-MB231 breast cancer cells [14]. Also the group of Paula Hammond attempted co-delivery of doxorubicin (DOX) and a siRNA for multidrug resistance protein (MRP1) to breast cancer cells through multilayer NPs based on PLGA and decorated with PLL layers [15]

We have also engineered double-coated NPs based on PLGA and decorated with a layer of Hyaluronic acid to deliver selectively drug cargo to cancer cells overexpressing CD44 receptor [16]. The ability of this system to co-deliver DTX in combination with photosensiting agents has been highlighted [17].

On this basis, we tried to investigate the possible combined cytotoxic effect of these NPs delivering 5FU and a plasmid of the proapoptoticL3 protein (pL3) in HCT 116C$^{p53\ -/-}$cells, a colon cancer cell line devoid of p53.

2 Material and methods

Poly(D,L-lactic-co-glycolic) acid (PLGA) (50:50 Resomer RG 502H inherent viscosity 0.16-0.24 dl/g) was purchased from Boehringer Ingelheim (Ingelheim, Germany). Threalose, Hyaluronidases 400-1000 units, 5-Fluorouracil (5FU), glucuronic acid, Carbazole reagent, Polyethyleneimine (PEI, MW= 10-25 kDa branched), Poloxamer 188 (Pluronic® F68), heparin, formic and solforic acid were purchased from Sigma-Aldrich. Acetonitrile, ethanol and acetone were purchased from Carlo ErbaReagenti (Milan, Italy). DMEM and Fetal Bovine Serum (FBS) were purchased from Gibco life technologies. Hyaluronan (HA, MW <10 kDa) was a kind gift of Magaldi Life S.r.l. Ultrapure water was used throughout the study.

2.1 Plasmid Construction

The cDNA of pL3 was obtained by RT–PCR from HCT 116 $^{p53\ -/-}$ cells using the primers 5′-ATGTCTCACAGAAAGTTC-3′ (forward) and 5′-TTAAGCTCCTTCTTCCTT-3′ (reverse) and subsequently inserted downstream from the reporter gene GFP (green fluorescence protein) in the pEGFP-C1 expression vector (Clontech, Palo Alto, CA, USA) using the *EcoR*I and *Xba*I cloning sites. The plasmid pEGFP-C1 and the fusion plasmid pL3 were purified using QIAGEN Plasmid Mega Kit (QiagenGmbH, Hilden, Germany). The pGFP- plasmid was sequenced to verify the accuracy of the construct.

2.2 Preparation and characterization of nanoparticles

NPs loaded with 5FU, pL3 or 5FU/pL3(5FU-NPs, pL3-NPs, 5FU/ pL3-NPs, respectively) were prepared by a layer-by-layer deposition method as previously shown [16]. Briefly 5FU-loaded PLGA NPs were prepared by solvent diffusion of an organic phase (2 mL) in an aqueous phase (4 mL of water with Pluronic F68 0.1%). Organic phase was prepared by dissolving 10 mg of PLGA in acetone and adding different amount of 5FU in ethanol in a acetone/ethanol ratio 5:1 v/v). After solvent removal at reduced pressure and room temperature, NP dispersion was splitted in 4 eppendorf tubes, centrifuged (8.000 rpm)

and redispersed in water (1 mL). Thereafter, 125 μL of a PEI solution (2.5 mg/mL) was added and the NPs centrifuged again (6.000 rpm)for washing. Each eppendorf (0.5 mg NPs/mL) was coated first with a PEI and then with HA water solution (1mg/mL). The interval between each addition was kept constant at 15 min and, after each polymeric deposition, NPs are centrifuged and redispersed in water. For NPs loaded with pL3, 25 μL of a pL3 water solution at different concentrations were added in each eppendorf tube before HA absorption. Thereafter, 100 μL of a HA water solution (2 mg/mL) were added. NPs were freeze-dried for 24 h with threalose (60 mg) as cryoprotectant and kept at 4 °C.

2.2.1 Size, surface charge and morphology of NPs

Hydrodynamic diameter, polydispersity index (PI) and zeta potential of NPs after each preparation step were determined on a ZetasizerNano Z (Malvern Instruments Ltd., UK). Results are reported as mean of three separate measurements on three different batches (n=9)±SD.

2.2.2 5FU and pL3 actual loading

5FU loading inside NPs was assessed by placing 0.5 mg of freeze-dried NPs (without cryoprotectant) in 500 μL of DCM and 500 μL of water. Thereafter, sample was mixed vigorously and centrifuged at 5000 rpm for 5 min. The amount of 5FU in the water phase was analyzed by HPLC on a Shimadzu apparatus equipped with a LC-10ADvp pump, a SIL-10ADvp autoinjector, a SPD-10Avp UV–Vis detector and a C-R6 integrator. The analysis was performed on a Synergy Hydro, C18 column (25x 4.6 mm). The mobile phase was a 100% (v/v) mixture of water with formic acid (99:1) pumped at a flow rate of 1 mL/min. The UV detector was set at 285 nm. A calibration curve of 5FU in water was constructed in the concentration range 1–100 μg/mL.

pL3 loading inside NPs was evaluated by a DNA KIT ASSAYPICOGREEN (life technologies) at Ex-Em 480-520 nm. After NP centrifugation at 13000 rpm for 5 min the pellet was treaty with DCM and water (1:1 ratio) then water phase was freeze dried and redisperded in 100μL of TE buffer 1X(10 mM Tris-HCl,1mM EDTA

pH 7.5) with heparin (5 mg/mL), in order to separate plasmid from complex with PEI. A calibration curve was constructed in a concentration range 0.026-1.3 μg/mL.

2.2.3 5FU and pL3 release

Release of 5FU from 5FU/ pL3-NPs(2mg) was evaluated by dialysis using DMEM FBS+ as dispersing medium and PBS at pH 7.4 and 37°C as external medium (sink conditions were realized). 5FU release was monitored for 72 h and compared with free 5FU.

In vitro release ofpL3 was performed on 30 mg of freeze-dried powder (corresponding to 0.5 mg of NPs) dispersed in 1 mL DMEM FBS+ 10% at 37°C.At predetermined time interval, the sample was centrifuged at 13000 rpm for 5 min. pL3 released was assessed indirectly in the pellet as reported above. A pL3 calibration curve in the range 0.02-1 μg/mL was constructed.

2.2.4 Stability of 5FU/ pL3-NPs

The stability of pL3 association to NPs was analyzed by the gel retardation assay. NPs (10 μL, 0.5 mg/mL) with theoretical amount of 10% of 5FU and 2.6 or 5.2 μg/mL of pL3, respectively, were mixed with a TE buffer and then loaded on a 0.8% agarose gel. After running the gel at 100 V for 30 min, staining with ethidium bromide in TBE buffer was carried out. NPs were compared to cationic NPs (without the external PEI layer) and free plasmid.

2.2.5 Enzymatic degradation of hyaluronic acid shell

Unloaded NPs (2 mg) were added to0.5mL of a hyaluronidases 1 FROM BOVINE testes (Sigma) solution in acetate buffer (0.1M) at pH6 (0.5 mg). The sample was placed into a dialysis bag (3500 kDa)at 37°C. External phase was the same buffer acetate at pH 6. At predetermined intervals 1 mL of external phase was collected and replaced with 1 mL of fresh medium. The quantity of glucuronic acid released was determined according to a reported method. 200 μL of sample was treated with concentrated sulfuric acid (3 mL)[18]. Carbazole reagent (0.1%, 100 μL) was added to the sample and mixed. The sample was then incubated at 60° in a water bath for 1 h and cooled at room temperature in another water bath. The absorbance of

the pink- to red-colored samples was read on a spectrophotometer at 530 nm against a water blank.

2.3 Cell cultures and treatments

The HCT $116^{-/-\ p53}$ cell line was cultured in Dulbecco's Modified Eagle's Medium (DMEM) supplemented with 10% heat-inactivated fetal bovine serum (FBS) (Invitrogen, Life Technologies, Italy), 1.5 mM l-glutamine, 100 units/ml penicillin, and 100 µg/ml streptomycin under humidified atmosphere of 5% CO_2 at 37 °C. Treatments of cells were performed replacing the culture medium with those containing increasing concentrations of 5FU-NPs or free 5FU (0.05-100 µM). Subsequently, treatments of cells were performed replacing the culture medium with those containing increasing concentrations of free 5FU (0.05-100 µM), 5FU-NPs, pL3-NPs or 5FU/ pL3-NPs (0.06-3,6-10 µM).

2.3.1 Transfection

For DNA transfection, HCT 116 $^{-/-\ p53}$ cells were seeded sub confluent on 60-mm plates; 24 h after plating, transfection was carried out using 2 µg of pL3 plasmid using Lipofectamine 3000 (Invitrogen). Untrasfected HCT 116 $^{-/-\ p53}$ cells were used as basal control.

2.3.2 MTT assay

HCT $116^{-/-\ p53}$ cells were seeded onto 96-well plates (2×10^4cells/well) and after the treatments with NPs, their viability was evaluated, after 72 and 96 h, as mitochondrial activity using the MTT assay. Briefly, the medium was removed and cells incubated with 100 µl MTT (0.5 mg/ml) for 1 h. After that, the solution was removed, formazan solubilized in 100 µl DMSO and the absorbance measured at 575 nm using a microplate reader (Labsystems Multiskan, MS).

2.3.3 Fluorescence microscopy

HCT $116^{-/-\ p53}$ cells were plated on coverslips at a density of 2×10^4cells per well in 6-well plates. At the end of the treatment (48, 72

and 96 h) with NPs, cells were washed three times with PBS and were fixed with 4% paraformaldehyde for 5 min. After washing, coverslips were mounted with PBS 1X-Glicerol (1:1) and stained with 4,6-diamidino-2-phenylindole (DAPI) (Vector Laboratories, CA, USA) to visualize the nuclei. Images have been acquired by using the Zeiss Cell Observer system composed by a motorized inverted microscope (Axiovert 200M) and a digital camera (Axiocam H/R). The fluorescence was measured with a Zeiss acquisition software (Axiovision 4.8.1).

2.3.4 Western Blotting

Whole protein extracts were prepared by lysing cells in 50 mM Tris–HCl pH 8.0, 150 mM NaCl, 0.5% sodium deoxycholate, 0.1% SDS, 1 mM EDTA, 1% Igepal, 1× protease inhibitor (Roche Applied Science, Italy) and phosphatase inhibitor cocktail (Calbiochem, Italy). Protein concentration was determined by the Bradford protein assay using bovine serum albuminas standard. Protein extracts (40 μg) were separated on 10% SDS-PAGE and transferred to a nitrocellulose membrane (Millipore) and then incubated with rabbit monoclonal antibody raised against GFP) (1:1000, Santa Cruz) and goat polyclonal antibody raised against β actin (1:2000, Santa Cruz), used as protein loading control.

2.3.5 Statistical analysis

Error bars represent mean ± SEM from n = 3 biological replicates. Statistical comparisons were made by one-way ANOVA followed by Bonferroni‘s test for multiple comparisons. $P<0.05$ was considered significant, $P<0.001$ was considered highly significant. $P>0.05$ was considered not statistically significant.

3 Results and discussion

In order to find an increased cytotoxicity of a conventional drug 5FU in association whit plasmid pL3, we developed biodegradable NPs endowed with facilitated entry in cells overexpressing CD44 receptor. We first assessed: i) the ability of NPs to entrap 5FU in the PLGA core and pL3 in the PEI shell; ii) the stability of pL3 association in biologically-relevant media and iii) release of drug and pL3 from NPs. Next, we assessed cytotoxicity of 5FU-NPs in CD44(+) colon cancer cells and combined activity of 5FU/pL3-NPs.

3.1 Preparation and characterization of NPs

Preparation of NPs is a multistep process comprising i) the preparation of a PLGA core template; ii) the absorption of a cationic PEI layer; iii) the absorption of a anionic layer of HA. Briefly, 5FU-NPs were prepared by nanoprecipitation of an organic mix composed by a PLGA acetone solution and a 5FU ethanol solution in ratio 5:1 v/v in a Pluronic F68 water solution. After NP collection, a positive layer of PEI was adsorbed through electrostatic interactions by incubating NPs with a PEI water solution followed by centrifugation and redispersion in water. In the following step, cationic NPs were decorated with a HA layer giving PLGA NPs with a double PI/HA coating.

The ability of PLGA core to entrap 5FU was investigated in the range 2-15% theoretical loading. NPs presents a slight increase of size, a negative zeta potential which confirms the absorption of anionic layer of HA and show a crescent actual loading up to a theoretical amount of 15% w/w. (Table.1).

Table 1. Properties of 5FU-NPs with 5FU theoretical loading from 2% w/w to 15 % w/w. SD were calculated on five different batches.

5FU theoretical loading (% w/w)	Hydrodynamic diameter (nm ± SD)	Zeta potential (mV)	P.I.	Actual loading (mg/100 mg)[a]
2	150 ± 10	-22	0.10	0.15 ± 0.1
5	160 ± 2	-18	0.18	0.63 ± 0.1
10	170 ± 7	-23	0.15	0.9 ± 0.4
15	185	-20	0.11	0.6± 0.1

[a] Actual loading is expressed as the amount (mg) of drug encapsulated per 100 mg of NPs.

PEI is a one of the most potent polymer for gene delivery and was first described by Behr et al. [19]. However it is toxic to cells because the high charge density of polyplexes contributes to membrane disruption[20]. Otherwise, dcNPs with PEI developed here exert no toxicity on different cell lines up to 1 mg/mL [16].

For pL3-NPs different amounts of plasmid in water were incubated with NPs (0.5mg/mL). All NPs show good loading of pL3 and the amount of plasmid did not influence the hydrodynamic diameter up to a concentration of 10.4 μg/mL where a macroscopic aggregation was found. Adorption of pL3 onto PEI-coated NPs is due to the formation a complex between the anionic charge of the phosphates along the DNA backbone and the cationic charge displayed by PEI. The formation of complex is spontaneous and entropically driven [21]. Zeta potential after pL3 adsorption was still positive since the adsorption of plasmid did not neutralize all the cationic charges onto the surface thus allowing the further adsorption of HA.

As expected, the amount of adsorbed pL3 onto final HA-coated NPs was related to the amount of plasmid initially added (Table 2).

Table 2. Characterization of pL3-loaded NPs. SD were calculated on five different batches.

pL3 (µg/mL NPs)	Hydrodynamic diameter (nm ± SD)	Zeta potential (mV)	P.I.	Actual loading (mg/100mg)[a]
2.6	166	+35	0.1	0.15 ± 0.1
5.2	158	+33	0.18	0.36 ± 0.1
10.4	260	+25	0.15	1.2 ± 0.7

[a] Actual loading is expressed as the amount (mg) of drug encapsulated per 100 mg of NPs

Final NPs were below 200 nm with a negative zeta potential. NPs could be freeze dried and redispersed in water or DMEM with FBS 10% giving stable colloidal dispersion with a limited increase of size and without any macroscopic aggregation over time (data not shown).

In table 3, properties of combined NPs prepared at constant loading of pL3and at increasing loading of 5FU core are also shown. As it can be seen, our strategy allows to tune the reciprocal amount of the delivered species with only simple adjustments of the experimental conditions.

Table 3. Properties of combined NPs.

5FU Th. Load. (% w/w)	pL3 Th. Load. (µg/mL)	Size (nm ± SD)	Zeta Potential (mV)	P.I.	pL3 Ac. Load. (mg/100 mg)	5FU Ac. Load. (mg/100 mg)
2	2.6	160 ± 5	-26	0.10	0.15±0.1	0.2±0.05
5	2.6	165 ± 10	-25	0.13	0.15±0.1	0.4±0.02
10	2.6	181 ± 8	-22	0.20	0.15±0.1	0.88±0.1

[a] Actual loading is expressed as the amount (mg) of drug encapsulated per 100 mg of NPs.

To evaluate the effective association of plasmid to NPs, a gel retardation assay was performed. We used two theoretical concentrations of plasmid (2.6 and 5.2 µg/mL) and compared cationic NPs (Fig. 1 E,G) to both HA-coated NPs (D,F) and free plasmid(B,C).The results show that the run of pL3 loaded in NPs are retarded thus confirming the formation of a strong complex. From the comparison with PEI-coated NPs, it is evident that the adsorption of HA does not alter the stability of complex. All formulation show that plasmid was effectively associated to the NPs.

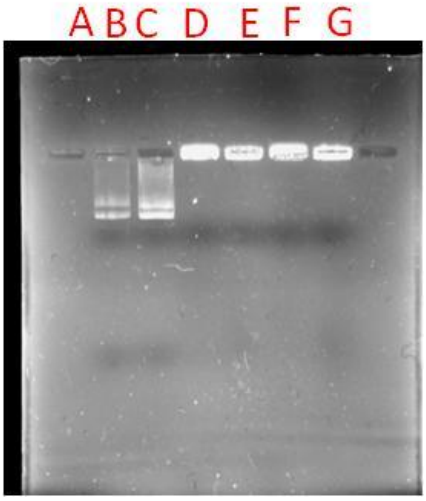

Fig. 1. Gel retardation assay. A)10 µl of NPs 0.5 mg/mL. B) 2.6 µg/mL and C) 5.2 µg /ml free plasmid; PEI-coated NPs loaded with plasmid D) 2.6 µg/mL and E) 5.2 µg /mL; NPs loaded with plasmid F) 2.6 µg/mL and G) 5.2 µg /mL.

Intracellular degradation of HA is predominantly mediated by Hyal-1 and occurs after incorporation of HA by CD44. Although Hyal-1 is active only in the intracellular compartment, a certain amount of the enzyme can be secreted to extracellular space. Hyal-2 is the enzyme involved in the extracellular degradation of HA and is overexpressed in several tumors [22]. To mimic more closely NP behavior in the presence of hyaluronidasess, quantitative release of glucuronic acid from NPs was assessed. Since the method can detect also HA oligomers, a control sample without hyaluronidases 1 was run. As observed in Fig. 2 a higher production of glucuronic acid is observed, which confirms the degradation of hyaluronic acid from NPs.

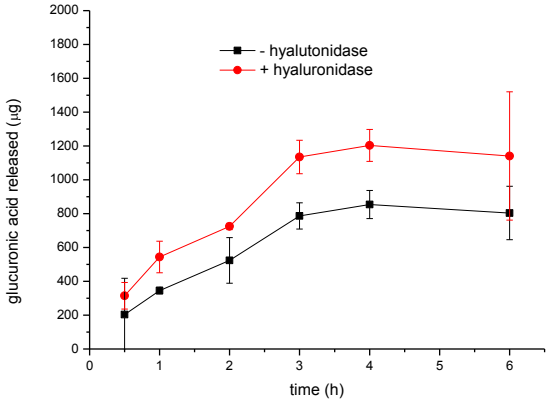

Fig. 2. Degradation of hyaluronic acid by hyaluronidases as followed by the amount of glucuronic acid released.

Release profile of 5FU from NPs was evaluated by dialysis using DMEM FBS+ as dispersing medium and PBS at pH 7.4 and 37°C as external medium (sink conditions were realized). 5FU release was monitored for 72 h and compared with that of free DTX (Fig. 3 A). A sustained release of 5FU from dc-NPs as compared with free 5FU was found. Free 5FU was completely released at 72 h while only a 40% of 5FU was released from NPs. This result is in agreement with previous studies [23].

The pL3 amount released was assessed indirectly from the pellet in a separate experiment. The results (Fig. 3 B) suggest that within the first 3 h the release was around 50% while it was around 80% after 24 h. The results are in agreement with Su et al. who showed a similar behavior for PLGA/PEI-NPs [24].

A

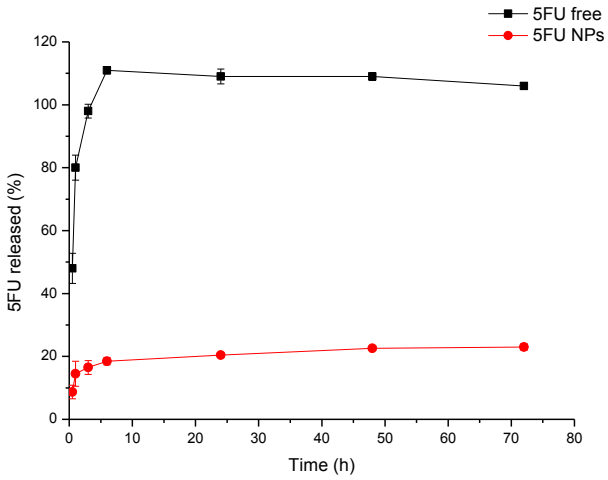

B

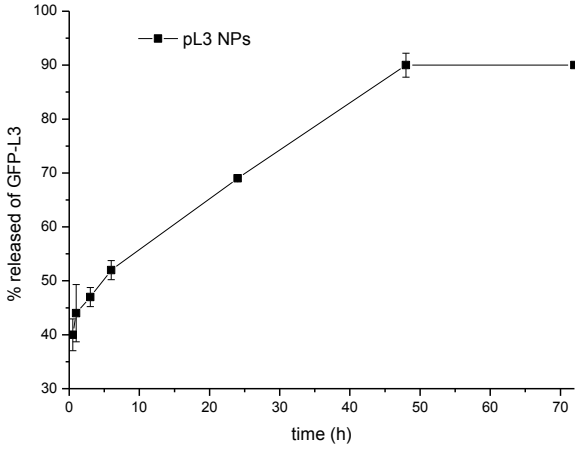

Fig. 3. Release of 5FU (A) and pL3 (B) from NPs at 72 h.

3.2 In vitro activity of 5FU-NPs in HCT 116 $^{p53-/-}$ cells

We have previously demonstrated that NPs represent a very promising system for the targeted delivery of drug in CD44 positive cancer cells taking advantage of the shell and core properties [17]. In fact, we have already tested the ability of this NPs to improve the cytotoxic activity of DTX in different cancer cells. Here, HCT116 $^{p53-/-}$ cells were treated with a wide range of 5FU-NPs concentrations (0.05-100 μM) and evaluated *in vitro* cytotoxicity after 72 and 96 h exposure by using MTT assay as compared to that of free 5FU. As shown in Fig. 4, a significant decrease in the $IC_{50}$was observed in cells treated with 5FU-NPsat both 72h and 96h (IC_{50}5 and1 μM,respectively) as compared to cells treated with free 5FU (IC_{50}10 and 5 μM,respectively). These results suggest that NPs enhanced antiproliferative activity of 5FU in CD44 positive colon cancer cells.

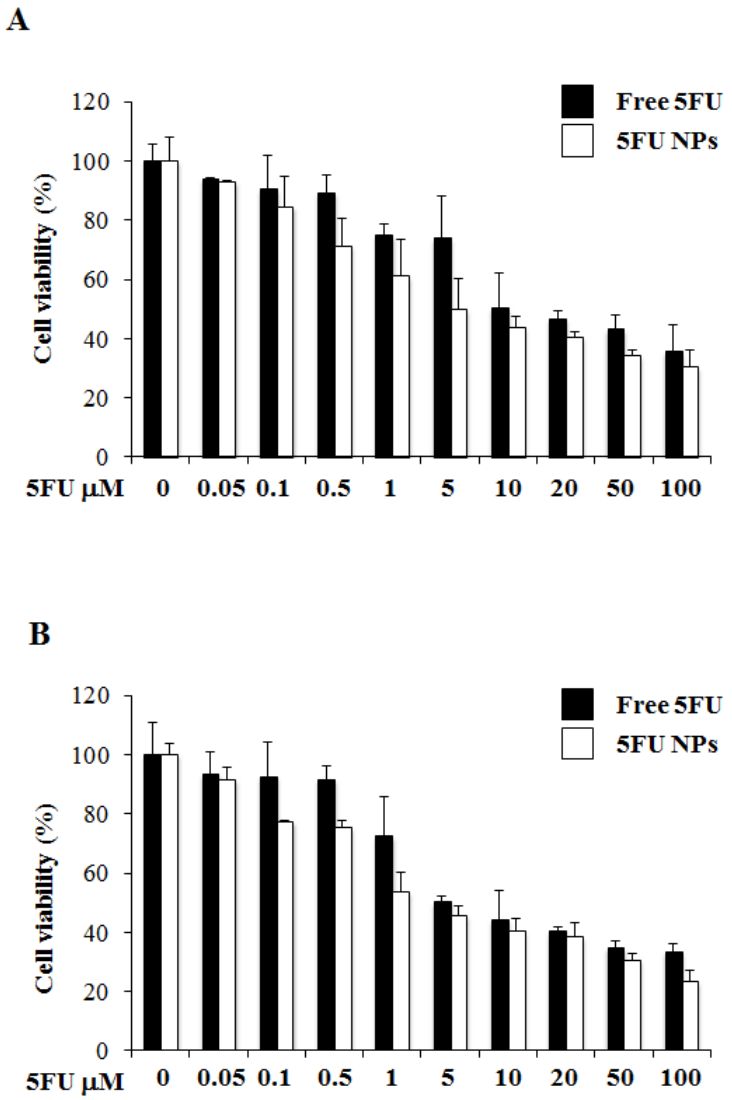

Fig. 4. In vitro cytotoxicity of free 5FU and 5FU NPs toward HCT 116 $^{-/-\ p53}$ cells. The cells were exposed to increasing concentrations of free 5FU and 5FU NPs for 72 h (A) and 96 h (B). After incubation, cell viability was evaluated using the MTT assay. The cell viability from untreated cells was set to 100%. Results are presented as percentage (mean ± SEM) (n = 3) of the control cells.

3.3 Determination of pL3 protein levels in HCT 116 $^{p53\ -/-}$ cells transfected with pL3-NPs

As the goal of this study is to assess the potential of pL3 to sensitize colon cancer cells devoid of p53 to c 5FU, we performed a study to demonstrate the ability of pL3-NPs to mediate a slow release and efficient expression of pL3 into tumor cells. To this aim, we monitored the time-dependent changes in the pL3 protein levels by transiently transfecting HCT 116$^{p53\ -/-}$ cells with rpL3 complexed with pL3-NPs 24, 48, 72 and 96 h later, cells were lysed and protein extracts were analyzed by western blotting using anti-pL3 antibodies. The obtained results illustrated in Fig. 5 demonstrate that pL3-NPs lead to an efficient and prolonged expression (96h) of the pL3 in tumor cells. Furthermore, different expression levels of pL3 protein were observed for different plasmid formulations.

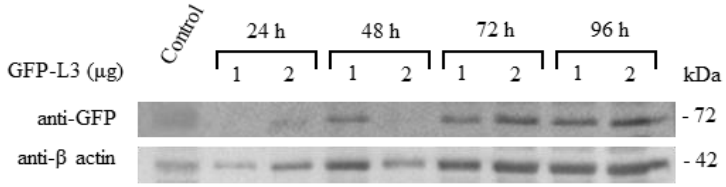

Fig. 5. Time-dependent changes in pL3-GFP protein expression in HCT 116 p53 -/- cells after treatment with the pL3-NPs. Western blot analysis of rpL3-GFP and actin protein levels at 24, 48, 72 and 96 h post-treatment of HCT 116 p53 -/- cells with pL3-NPs. Densitometric quantification of the Western blot is shown.

Next, to further characterize the ability of pL3-NPs to allow the delivery into the cells of rpL3, we compared their behavior with that of a commercially available DNA-transfecting agent such as Lipofectamine 3000. To this purpose HCT 116 $^{p53\ -/-}$ cells were transiently transfected with pL3-NPs or with Lipofectamine 3000 (pL3-Lipofectamine).

After 24, 48, 72 and 96 h, cells were analyzed by fluorencence microscopy. As shown in Fig 6 both NP and Lipofectamine mediated transfection lead to an efficient and prolonged expression of pL3 in tumor cells. In particular, cells transfected with pL3-NPs demonstrated a sustained and significantly higher pL3 protein level than those obtained by transfecting the cells with pL3-Lipofectamine likeky due to the slow release of pL3 from NPs localized inside the

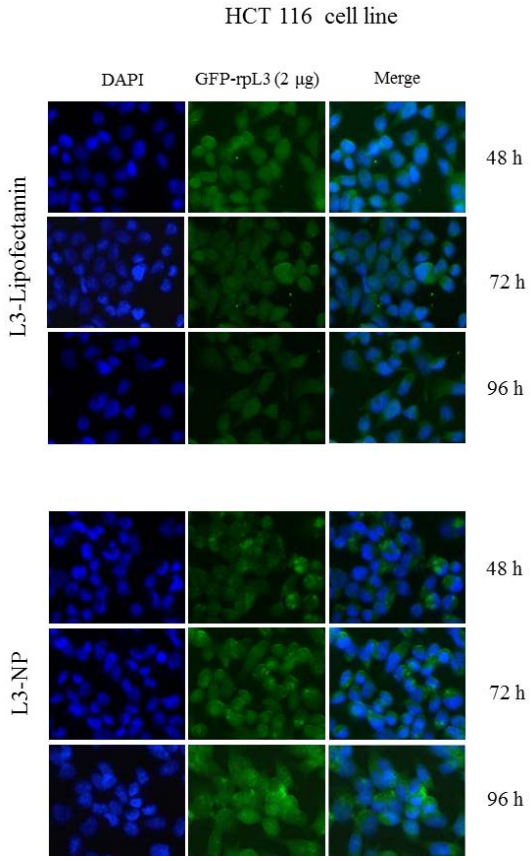

Fig. 6. Fluorescence images of HCT 116 $^{p53\ -/-}$ cells transiently transfected with pL3-Lipofectamine or pL3-NPs. Cells were transfected with 2µg of pL3 for different times (48,72 and 96 h) in cell culture medium. DAPI is used as a nuclear stain (shown in blue). pL3 dependent fluorescence of GFP is shown in green. In merged images (Merge), the two fluorescent emissions are overlapped. The images shown are representative of three independent experiments related to the indicated times.

cells.

3.4 Cytotoxicity studies of combined NPs on HCT-116 $^{p53\ -/-}$ colon cancer cells

Cytotoxicity results show that empty NPs are not cytotoxic to HCT116 $^{p53\ -/-}$colon cancer cells. This is very important because confirm that no cytotoxic effect of PEI is found when it is adsorbed onto NPs also in association whit plasmid. Lipofectamine/pL3 (Lipo/pL3) induced significant cytotoxicity at 72 h which was not found after 96 h. Analogously, pL3-NPs induced transient cytotoxicity only after 72 h. Cytotoxicity of combined 5FU/pL3 NPs in HCT-116$^{p53\ -/-}$cells indicate a potentiated cytotoxic effect at 5FU concentration of 10 μM as compared with corresponding 5FU-NPs after 96 h (Fig. 7).

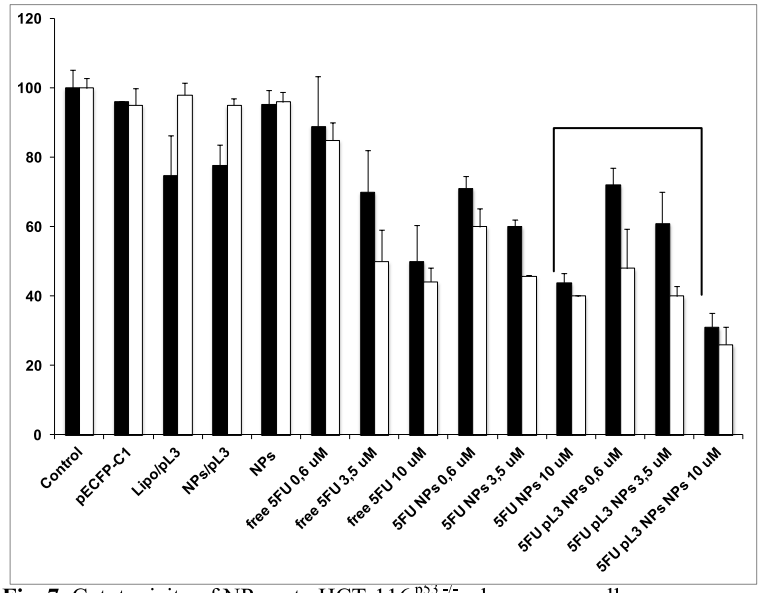

Fig. 7. Cytotoxicity of NPs onto HCT-116 $^{p53\ -/-}$colon cancer cells.

Studies are in progress to elucidate the effect of different amount of plasmid on 5FU cytotoxicity and possibly translate the results to mouse models of colon tumors.

4 Conclusions

In this paper we have demonstrated that hyaluronan-coated NPs are a robust system to deliver plasmid in cancer cells and demonstrate superior activity to lipofectamine. Furthermore, plasmid can be combined to conventional chemotherapeutics to potentiate their cytotoxicity. We validated this approach on 5FU co-delivered with a plasmid to pL3 protein in colon cancer cells thus paving the way to testing different nucleic acid/chemotherapeutic combinations and traslation of the NPs in an in vivo setting.

References

1. Kemp JA, Shim MS, Heo CY, Kwon YJ: **"Combo" nanomedicine: Co-delivery of multi-modal therapeutics for efficient, targeted, and safe cancer therapy.***Advanced Drug Delivery Reviews* 2015.

2. Sun XX, Dai MS, Lu H: **5-fluorouracil activation of p53 involves an MDM2-ribosomal protein interaction.***Journal of Biological Chemistry* 2007, **282:** 8052-8059.

3. Bhat KP, Itahana K, Jin AW, Zhang YP: **Essential role of ribosomal protein L11 in mediating growth inhibition-induced p53 activation.***Embo Journal* 2004, **23:** 2402-2412.

4. Jin A, Itahana K, O'Keefe K, Zhang Y: **Inhibition of HDM2 and activation of p53 by ribosomal protein L23.***Molecular and Cellular Biology* 2004, **24:** 7669-7680.

5. Esposito D, Crescenzi E, Sagar V, Loreni F, Russo A, Russo G: **Human rpL3 plays a crucial role in cell response to nucleolar stress induced by 5FU and L-OHP.***Oncotarget* 2014, **5:** 11737-11751.

6. Russo A, Pagliara V, Albano F, Esposito D, Sagar V, Loreni F *et al.*: **Regulatory role of rpL3 in cell response to nucleolar stress induced by Act D in tumor cells lacking functional p53.***Cell Cycle* 2016, **15:** 41-51.

7. Luten J, van Nostruin CF, De Smedt SC, Hennink WE: **Biodegradable polymers as non-viral carriers for plasmid DNA delivery.***J Controlled Release* 2008, **126:** 97-110.

8. Fischer D, Li YX, Ahlemeyer B, Krieglstein J, Kissel T: **In vitro cytotoxicity testing of polycations: influence of polymer structure on cell viability and hemolysis.***Biomaterials* 2003, **24:** 1121-1131.

9. Pietersz GA, Tang CK, Apostolopoulos V: **Structure and design of polycationic carriers for gene delivery.***Mini-Reviews in Medicinal Chemistry* 2006, **6:** 1285-1298.

10. Danhier F, Feron O, Preat V: **To exploit the tumor microenvironment: Passive and active tumor targeting of nanocarriers for anti-cancer drug delivery.***J Controlled Release* 2010, **148:** 135-146.

11. Jong YS, Jacob JS, Yip KP, Gardner G, Seitelman E, Whitney M *et al.*: **Controlled release of plasmid DNA.***J Controlled Release* 1997, **47:** 123-134.

12. Oster CG, Kim N, Grode L, Barbu-Tudoran L, Schaper AK, Kaufmann SHE *et al.*: **Cationic microparticles consisting of poly(lactide-co-glycolide) and polyethylenimine as carriers systems for parental DNA vaccination.**.*J Controlled Release* 2005, **104:** 359-377.

13. Egusquiaguirre SP, Igartua M, Hernandez RM, Pedraz JL: **Nanoparticle delivery systems for cancer therapy: advances in clinical and preclinical research.***Clinical & Translational Oncology* 2012, **14:** 83-93.

14. Ediriwickrema A, Zhou JB, Deng Y, Saltzman WM: **Multi-layered nanoparticles for combination gene and drug delivery to tumors.***Biomaterials* 2014, **35:** 9343-9354.

15. Deng ZJ, Morton SW, Ben-Akiva E, Dreaden EC, Shopsowitz KE, Hammond PT: **Layer-by-Layer Nanoparticles for Systemic Codelivery of an Anticancer Drug and siRNA for Potential Triple-Negative Breast Cancer Treatment.***Acs Nano* 2013, **7:** 9571-9584.

16. Maiolino S, Russo A, Pagliara V, Conte C, Ungaro F, Russo G *et al.*: **Biodegradable nanoparticles sequentially decorated with Polyethyleneimine and Hyaluronan for the targeted delivery of docetaxel to airway cancer cells.**.*J Nanobiotechnology* 2015, **13:** 29.

17. Maiolino S, Moret F, Conte C, Fraix A, Tirino P, Ungaro F *et al.*: **Hyaluronan-decorated polymer nanoparticles targeting the CD44 receptor for the combined photo/chemo-therapy of cancer.***Nanoscale* 2015, **7:** 5643-5653.

18. Taylor KA, Buchanan-Smith JG: **A colorimetric method for the quantitation of uronic acids and a specific assay for galacturonic acid.***Anal Biochem* 1992, **201:** 190-196.

19. Boussif O, Gaucheron J, Boulanger C, Santaella C, Kolbe HVJ, Vierling P: **Enhanced in vitro and in vivo cationic lipid-mediated gene delivery with a fluorinated glycerophosphoethanolamine helper lipid.**.*Journal of Gene Medicine* 2001, **3:** 109-114.

20. Stanic V, Arntz Y, Richard D, Affolter C, Nguyen I, Crucifix C *et al.*: **Filamentous condensation of DNA induced by pegylated poly-L-lysine and transfection efficiency.***Biomacromolecules* 2008, **9:** 2048-2055.

21. Pack DW, Hoffman AS, Pun S, Stayton PS: **Design and development of polymers for gene delivery.***Nature Reviews Drug Discovery* 2005, **4:** 581-593.

22. Harada H, Takahashi M: **CD44-dependent intracellular and extracellular catabolism of hyaluronic acid by hyaluronidase-1 and-2.***Journal of Biological Chemistry* 2007, **282:** 5597-5607.

23. Nair KL, Jagadeeshan S, Nair SA, Kumar GS: **Biological evaluation of 5-fluorouracil nanoparticles for cancer chemotherapy and its dependence on the carrier, PLGA.***Int J Nanomedicine* 2011, **6:1685-97. doi: 10.2147/IJN.S20165. Epub@2011 Aug 17.:** 1685-1697.

24. Su WP, Cheng FY, Shieh DB, Yeh CS, Su WC: **PLGA nanoparticles codeliver paclitaxel and Stat3 siRNA to overcome cellular resistance in lung cancer cells.***Int J Nanomedicine* 2012, **7:4269-83. doi: 10.2147/IJN.S33666. Epub@2012 Aug 3.:** 4269-4283.

General conclusions

The experimental work illustrated in this thesis was aimed to design novel double coated NPs for cancer therapy. We explain how to build NPs with a functional double coating through a layer-by-layer strategy, entrapping a chemotherapeutic in the core together with a photosensitizer and a plasmid in the shell. NPs present good entrapment efficacy and an excellent stability in different complexmedia.

Double-coated NPs with Hyaluronan on the top demonstrate specificity toward CD44+ cancer cells which results in increased cytotoxicity of chemotherapeutics alone or in combination as compared to free drugs. It is demonstrated that dcNPs are a versatile platform to deliver drug combinations in cancer cells which can be considered for further testing in mice models of tumor.

ANNEX-I
Pluronic P123/F127 mixed micelles delivering Sorafenib and its combination with Verteporfin in cancer cells

Published as:
Diogo Pellosi, Francesca Moret, Aurore Fraix, Nino Marino, Sara Maiolino, Elisa Gaio,Noboru Hioka, Elena Reddi, Salvatore Sortino and Fabiana Quaglia

International Journal of Nanomedicine(2016) in press

Abstract

Here, we develop Pluronic P123/F127 mixed micelles for the intravenous delivery of the anticancer drug sorafenib (SRB) or its combination with Verteporfin (VP), a photosensitizer for photodynamic therapy which should complement well cytoxicity profile of the chemotherapeutic. SRB loading inside the core of micelles was governed by drug: Pluronic weight ratio while in the case of SRB/VP combination a mutual interference between the two drugs occurred and only specific ratios could ensure maximum loading efficiency. Co-entrapment of SRB did not alter photophysical properties of VP, confirming that SRB does not participate in any bimolecular process with the photosensitizer. Fluorescence Resonance Energy Transfer (FRET) measurement of micelles in serum protein-containing cell culture medium demonstrated the excellent stability of the system in physiologically-relevant conditions. These results were in line with the results of the release study showing a release rate of both drugs in the presence of proteins slower than in phosphate buffer. SRB release was sustained while VP remained substantially entrapped in micelle core. Cytotoxicity studies in MDA-MB231 cells revealed that at 24 h SRB-loaded micelles were more active than free SRB only at very low SRB concentrations while at 24 + 24 h prolonged cytotoxic effect of SRB-loaded micelles was observed very likely mediated by the block in the S phase of the cell cycle. The combination of SRB with VP under light exposure was less cytotoxic than both the free combination and VP-loaded micelles + SRB-loaded micelles combination. This behaviour was clearly explained in term of micelle uptake and intracellular localization. Beside the clear advantage of delivering SRB in Pluronic micelles, our results provide a clear example that each photo-chemotherapeutic combination needs detailed investigations on their particular interaction and no generalization on enhanced cytotoxic effects should be derived a priori.

1. Introduction

Nanotechnologies promise to refine cancer treatments trying to overcome several issues associated to conventional chemotherapy by improving treatment efficacy, decreasing systemic side effects and overcoming multi drug resistance. In the wide scenario of nanoplatforms available for anticancer drug delivery, polymeric micelles based on biocompatible polymers have been attracting interest due to great versatility, small size, ease of functionalization and potential to transport a multidrug-cargo for combination therapies.[1-3] Representatives of such materials are Pluronic® copolymers that are surfactants molecules containing two hydrophilic poly(ethylene oxide) (PEO) and one hydrophobic poly(propylene oxide) (PPO) regions arranged in a PEO-PPO-PEO triblock structure. In water Pluronic self-assemble in core-shell nano-sized micelles and entrap poorly water-soluble drugs increasing their apparent solubility. Furthermore, drug-loaded Pluronic micelles can passively target tumor by the enhanced permeability and retention (EPR) effect after intravenous injection. Pluronic unimers have also shown ability to hypersensitize multiple drug resistant cells by inhibiting glycoprotein P mediated drug efflux.[4;5] Pluronic mixed micelles made of more than one type of Pluronic manifest properties superior to those made of the individual components. In fact, the correct selection of Pluronic type and unimer ratio induces a synergistic aggregation thus producing micelles with improved characteristics in term of colloidal stability and drug loading efficiency.[6] For example, in a very recent paper we demonstrated that Pluronic P123/F127 mixed micelles enhanced the solubility and photodynamic activity of very hydrophobic benzoporphyrin derivatives.[7]Sorafenib (SRB) is a drug approved for the treatment of advanced inoperable hepatocellular and advanced renal cancers after oral administration (Nexavar®).[8;9] Its possible use for systemic treatment of liver fibrosis[10] and hepatocellular carcinoma[11-13] has been recently highlighted. SRB is an inhibitor of different Raf serine/threonine kinases isoforms mediating cell proliferation and blocks upstream receptor tyrosine kinases, which play an important role in angiogenesis.[14] Angiogenesis and tumor revascularization due to VEGF expression is a major problem associated with photodynamic therapy (PDT) application in cancer.[15] Indeed, PDT

is a therapeutic procedure that uses a light-activated photosensitizer (PS) to produce reactive oxygen species, especially singlet oxygen ($^1O_2$), which trigger the destruction of tumor cells, damage to tumor vasculature and a severe inflammatory action.[16;17] Co-administration of PDT agents with antiangiogenic chemotherapeutics could be a promising strategy to potentiate photodynamic treatments. Verteporfin (VP) is a FDA clinically approved agent for PDT of age-related macular degeneration (Visudyne®) and is currently in phaseI/II clinical trials to treat locally advanced pancreatic cancer.[18] It was found that VP induced angiogenesis in the chicken chorioallantoic membrane model could be inhibited by SRB, giving prolonged vascular occlusion in the treated areas due to a synergistic effect.[19]Since the entrapment of multiple therapeutic agents in a single nanocarrier allows a precise and controlled delivery of the optimal drug-ratio in the same area of the body, enormous clinical advantages can be brought about.[3;20;21]Currently, this novel ‗two-in-one' approach is under clinical and preclinical investigation against several cancer types.[22;23] Furthermore, delivery in a nanocarrier can also alleviate poor water solubility, a drawback shared by several chemotherapeutics and PS. Although very promising in principle, there have been very few attempts in developing Pluronic micelles for the co-delivery of PS and other anticancer molecules.[24;25] In this contribution we aim to explore the potential of Pluronic P123/F127 mixed micelles as a suitable intravenous nanocarrier to deliver SRB while maintaining its activity and mechanism of action. Besides, we also focus on the combined delivery of SRB and VP, investigating how it can affect single drug cytotoxicity. To this end, Pluronic P123/F127 micelles were loaded with SRB alone or in combination with VP. Drug loading efficiency and release rate, spectroscopic and photodynamic properties of the micelles as well as stability in complex media were assessed. Finally, cytotoxicity of SRB and its combination with VP and trafficking of micelles in MDA MB-231 breast carcinoma cells were investigated.

2. Material and methods

2.1 Materials

SRB free base (MW = 464.8 g mol^{-1}) was purchased from LC Laboratories, Division of PKC Pharmaceuticals, Inc., Woburn, MA (U.S.A.). VP (benzoporphyrin derivative monoacid ring A, MW = 718.8 g mol^{-1}) was kindly supplied by Prof D. Dolphin (University of British Columbia, Vancouver, Canada). Pluronic P123 (EO_{20}–PO_{65}–EO_{20}, MW = 5750 g mol^{-1}), Pluronic F127 (EO_{100}–PO_{65}–EO_{100}, MW = 12600 g mol^{-1}), trehalose, polysorbate 80 and Nile Red were purchased from Sigma-Aldrich. Ethanol, dichloromethane, diethyl ether, acetone and acetonitrile were purchased from Carlo Erba Reagents. All the other chemicals were of analytical reagent grade and used without previous purification.

2.2 Preparation of drug-loaded micelles

Unloaded, SRB, and SRB/VP-loaded Pluronic P123/F127 micelles were prepared by the thin-film hydration method.[26] Briefly, 10 mg of Pluronic P123/F127 mixture (proportion 2:1 w/w, which correspond to 3.33 mg of F127 and 6.67 mg of P123) were dissolved in 1 mL of ethanol in a round-bottom flask. For drug-loaded micelles, different amounts of SRB (100-200 μg) and VP (4- 10 μg) were dissolved in 1 mL ethanol and added to the Pluronic solution. Then, the solvent was evaporated by rotary evaporation at 50 °C for about 20 minutes. Residual solvent in the film was removed under vacuum overnight. After that, the dried film was hydrated with 1 mL of filtered distilled water under sonication for 5 minutes to obtain a limpid solution and filtered through 0.22 μm filters (RC Chemtek, Italy) to remove the unloded drug or possible large cylindrical aggregates formed by P123. When necessary, the resulting solution was lyophilized for 24 h in the presence of trehalose (2:1 mass ratio with the copolymer).

2.3 Micelle characterization

Hydrodynamic diameter (D_H), polydispersity index (PI) and zeta potential of micelles were determined using a Zetasizer Nano ZS (Malvern Instruments Ltd, UK). The freeze-dried formulations were dispersed in Milli-Q water and measurements were performed at 37.0 °C on 90° angle. Results are reported as mean of three separated measurements on three different micelle batches ±SD.

2.4 SRB and VP entrapment efficiency

SRB and VP encapsulation efficiency was evaluated by dissolving a known amount of freeze-dried micelles (10 mg) in 1 mL of ethanol. Before the analysis, the sample was filtered through a 0.22 μm filter (RC, Chemtek, Italy). Results are reported as mean of three separated measurements of three different samples ±SD.

SRB was analyzed by HPLC on a Shimadzu apparatus equipped with a LC-10ADvp pump, a SPD-10Avp UV–Vis detector and a C-R6 integrator. The analysis was performed on a Sphereclone ODS-2 5 μm, C18 column (250×4.6 mm, 80 Å) (Phenomenex, USA). The mobile phase was a 35:65 (v/v) mixture of water and acetonitrile pumped at a flow rate of 1 mL/min. The water phase contained triethylamine (2% v/v) and was adjusted to pH 5.4 with phosphoric acid. The UV detector was set at 265 nm. A calibration curve for SRB in ethanol was constructed in the concentration range 0.002-0.2 mg/mL. To exclude a possible interference of VP on SRB quantitative analysis, an amount of VP-loaded micelles was dissolved in ethanol and analyzed in the same conditions reported above.

VP quantification was carried out by spectrophotometry on a Shimadzu UV-1800. The concentration of VP was calculated by means of a standard calibration curve derived for ethanol solutions of VP at known concentrations (20.0–0.1 ug/mL). Potential interference of SRB on absorption was preliminarily assessed spiking a VP solution in ethanol with different amounts of SRB.

2.5 Absorption, emission and transient spectroscopy

UV/Vis absorption and fluorescence spectra were recorded with a Jasco V-560 spectrophotometer and Fluorolog-2 (Model, F-111) spectrofluorimeter, respectively. All measurements were performed in a thermostated quartz cell (1 cm path length, 3 mL capacity).Steady-state emission of $^1O_2$ was recorded in D_2O solutions with a Fluorolog-2 Mod-111 spectrometer, equipped with a InGaAs detector maintained at –196 °C, by illuminating orthogonally the sample at 405 nm with a continuous-wave laser. Laser flash photolysis. All of the samples were excited with the second harmonic of Nd–YAG Continuum Surelite II–10 laser (532 nm, 6 ns FWHM), using quartz cells with a path length of 1.0 cm. The excited solutions were analyzed with a Luzchem Research mLFP–111 apparatus with an orthogonal pump/probe configuration. The probe source was a ceramic xenon lamp coupled to quartz fiber-optic cables. The laser pulse and the mLFP–111 system were synchronized by a Tektronix TDS 3032 digitizer, operating in pre-trigger mode. The signals from a compact Hamamatsu photomultiplier were initially captured by the digitizer and then transferred to a personal computer, controlled by Luzchem Research software operating in the National Instruments LabView 5.1 environment. The solutions were deoxygenated by bubbling with a vigorous and constant flux of pure argon (previously saturated with solvent). In all of these experiments, the solutions were renewed after each laser shot (in a flow cell of 1 cm optical path), to prevent probable auto-oxidation processes. The sample temperature was 295 ± 2 K. The energy of the laser pulse was measured at each shot with a SPHD25 Scientech pyroelectric meter.

2.6 Micelle behaviour in cell culture medium

Micelle stability in the medium employed for cell studies (DMEM enriched with 10% FBS) was evaluated. Briefly, 20 mg of micelles were added to 2 mL of cell culture medium and incubated at 37.0 ºC for 72 h. At selected time intervals, size and zeta potential were evaluated. Micelle stability was also evaluated by FRET technique by co-encapsulating two different fluorescence probes into micelle core.[27] The hydrophobic dye

Nile Red (NR) was chosen as the fluorescent donor and VP as acceptor molecule. VP/NR micelles were prepared as described above for SRB/VP micelles (Preparation of drug-loaded micelles section). The concentration of NR in the micelles was 0.8 μg mL^{-1} and VP equal 4.0 μg mL^{-1} which gives a VP:NR ratio of 5:1 by weight. The ratio between the maximum intensity of emission bands for VP and NR was monitored as function of time. Decrease of this ratio and/or micelle size increase was considered indicative of micelle aggregation or disassembly in cell culture medium. DMEM medium without FBS was also evaluated as a control experiment. Results are reported as mean of three separate measurements (n=3) ±SD.

For release studies in PBS or in cell culture medium, the formulation (10 mg of Pluronic; [SRB] = 100 μg mL^{-1} and [VP] = 10.0 μg mL^{-1}) was dispersed in 1 mL of DMEM with 10% FBS and placed in a dialysis bag (MWCO=3500 Da, Spectra/Por®). The sample was plunged in 5 mL of PBS containing 5% v/v of polysorbate 80 (sink condition) and kept at 37 ºC up to 72 h. At selected time intervals, 1 mL of release medium was withdraw and replaced with an equal volume of fresh medium. SRB and VP quantitative analyses were carried out as described above. As control, release profile of free drugs diluted in PBS or DMEM with 10% FBS medium are reported for comparison. Results are expressed as release % over time (n=3) ±SD.

2.7 In vitro experiments

2.7.1 Cell culture

Human breast cancer cell line MDA-MB231 was purchased from American Type Tissue Culture Collection (ATCC, Rockville, Maryland). The cells were grown in DMEM with GlutamaxTM supplemented with 10% FBS, 100 U/ml streptomycin and 100 μg/ml penicillin G (Life Technologies, Milan, Italy), and maintained at 37 °C in a humidified atmosphere containing 5% CO_2.

2.7.2 Dark and photo toxicity (PDT) in vitro

The cytotoxicity in the dark of MDA-MB231 cells incubated with VP, SRB as well as their combination (free or loaded in Pluronic F127/P123 Micelles) was measured with the MTS assay after 24 h of

incubation (24 h) as well as after additional 24 h of cell growth in drug-free medium (24 + 24 h). Cells (6 x 10^3) were seeded in 96-well plates (24 h of growth) and then incubated with the drug formulations for 24 or 24 + 24 h. Lyophilized NP formulations containing 10 mg of micelles (loaded with 10 µg of VP and/or 100 µg of SRB) were solubilized in 2 ml DMEM and then further diluted in medium added with 10% FBS. For the MTS assay the medium was replaced with 100 µl of serum-free medium and 20 µl of CellTiter 96® Reagent (Promega Co., Madison, USA) and the wells were incubated for 1 h at 37 °C. The absorbance at 492 nm was measured with a Multiskan Go (Thermo Fischer Scientific, Waltham, USA) plate reader and the viability of treated cells was expressed as percentage of the absorbance of control cells that was taken as 100% viability. For the in vitro PDT experiments, cells were seeded as described above. After 24 h of incubation with the different drug formulations, the cells were washed once with PBS with Ca^{2+} and Mg^{2+}, and irradiated in PBS with 0.75 J cm^{-2} of red light (600-700 nm, fluence rate 25 mW cm^{-2}) from a Waldmann PDT 1200 lamp (Waldmann Medizintechnik, Germany). Immediately after irradiation the cells were brought back to the incubator after replacement of PBS with fresh medium. Cell viability was measured with the MTS test after additional 24 h.

2.7.3 Cellular uptake studies

Cells (5 x 10^4) were grown in 24-well plates for 24 h and incubated for 24 h with increasing concentrations of free VP, VP-loaded micelles or VP/SRB-loaded micelles diluted in cell medium added with 10% FBS. After incubation, the cells were washed twice with Versene™, detached from the plates with trypsin, which was neutralized by the addition of FBS. Cells were centrifuged and re-suspended in VerseneTM before measuring VP fluorescence by a BD FACSCanto™ II (Becton Dickinson, San Jose, USA) flow cytometer. The blue laser at 488 nm was used as the excitation source and wavelengths of 670-735 nm (PerCP channel) were selected for the detection of VP fluorescence. 10^5 events/sample were acquired and analyzed with the FACSDiva software.

2.7.4 Cell cycle analysis

Cells (10^6) were seeded in 100 mm culture dishes and incubated with 10 μM SRB free or loaded in Pluronic F127/P123 micelles for 24 or 24 + 24 h. Treated and control cells were harvested, fixed in 70% cold ethanol and stored overnight at 4 °C. Before analysis, cells were washed in distilled water, centrifuged and resuspended in 1 mL PBS containing 50 μg/mL propidium iodide (Sigma-Aldrich) and 100 μg/mL RNAse, for DNA staining. Samples were incubated for 1 h at 37 °C and then analyzed by flow cytometry. Data from 2 × 10^4 cells/sample were acquired with the FACSDiva software and analyzed with the ModFit LT 3.0 software (BD Biosciences) to determine alterations in cell cycle distribution.

2.7.5 Confocal microscopy

The intracellular localization of VP, free or loaded in pluronic F127/P123 micelles, was determined by confocal microscopy. Cells (8 x 10^4), seeded in special tissue culture dishes for fluorescence microscopy (μ-Dish 35mm, high, Ibidi GmbH, Planneg, Germany), were allowed to growth for 24 h and then incubated for 24 h with 2 μM Rho or 1 μM VP. Fifteen min before the end of the incubation, the cells were stained with MitoTracker® green FM (100 nM) or ER Tracker™ Green (1 μM) used as markers for mitochondria and endoplasmic reticulum, respectively. Cells were then washed twice with HBSS and analyzed with a Leica SP5 confocal laser-scanning microscope (Leica Microsystems Srl, Milan, Italy); the images were elaborated with the ImageJ software.

2.7.6 Statistical analysis

The Primer software for biostatistics (McGraw-Hill, Columbus, USA) was used for statistical analysis of the data. The data are expressed as means ±SD for at least 3 independent experiments. The difference between groups was evaluated with the Student‘s t-test or with Bonferroni‘s test and was considered significant for $p<0.05$.

3. Results and Discussions

3.1 Properties of drug-loaded micelles

A preliminary study was devoted to evaluate the optimal conditions to obtain micelles with good encapsulation efficiencies of SRB alone and in combination with VP. In a previous work we demonstrated that the thin film method followed by freeze-drying (with trehalose as cryoprotectant) allows preparation of Pluronic P123/F127 mixed micelles loaded with VP.[7] Results of this previous study demonstrated that, the optimal ratio between P123 and F127 was at 2:1 (w/w). This ratio was maintained in micelles explored here. Table 1 summarizes the physicochemical characteristics and drug-loading parameters of Pluronic P123/F127 micelles loaded with SRB (and SRB/VP combination).D_H of empty and drug-loaded micelles demonstrated that Pluronic P123/F127 form micelles with a size ranging between 25–43 nm and satisfactory PI. SRB entrapment was very efficient up to 2% drug/polymer by weight without any change in term of size and PI. Loading a combination of SRB and VP was feasible and mainly controlled by the initial amount of SRB employed, which is the most abundant drug in formulations. Considering that both drugs have low water solubility, it can be reasonably hypothesized that when entrapped together a mutual interference in micelle core may occur. As generally observed for polymeric micelles, drug-Pluronic ratio was found as a critical parameter to control encapsulation efficiency.[28] In fact, the lipophilic drugs accommodate inside the PPO core of Pluronic P123/F127 mixed micelles and, once these domains are saturated, a decrease in encapsulation efficiency is experienced.[29] The size increase after entrapment of drug combination can be ascribed to an increase of PPO core size probably due to the presence of entangled drugs. Nevertheless, the micelle size was still small enough for tumor-specific accumulation via the EPR effect.[4] Thus, optimal encapsulation efficiencies were found at 100 μg mL^{-1} for SRB and 4.0 μg mL^{-1} for VP. Under this condition, both loading values can be considered satisfactory for a therapeutically relevant system. All formulations presented slight negative zeta potential values as generally found for PEGylated nanocarriers made of uncharged polymers.

Table 1. Composition and properties of Pluronic P123/F127 2:1 w/w mixed micelles (total of 10 mg, where 6.67 mg of P23 and 3.33 mg of F127) Results reported as mean of three separated measurements on three different batches (n=9) ± SD.

SRB (µg)	VP (µg)	SRB loading[a] (EE %)[b]	VP loading[a] (EE%)[b]	Mean D_H[c](nm)	P.I.[d]	Zeta Potential (mV)
--	--	--	--	25.3 ± 1.8	0.16	--4.37 ± 0.96
--	4.0	--	0.038± 0.002 (95.3 ±1.7)	26.3 ± 1.8	0.18	-6.69± 0.78
--	6.0	--	0.053 ± 0.004 (89.2 ±2.4)	30.6 ± 2.7	0.22	-5.27 ± 1.92
--	10.0	--	0.076 ± 0.009 (76.1± 3.9)	36.8 ± 5.1	0.37	-3.13 ± 1.88
100	--	95.0 ± 0.1 (95.0 ± 1.2)	--	24.0 ± 1.9	0.13	-3.55 ± 0.65
200	--	187.0 ± 0.5 (93.5 ± 4.0)	--	26.5 ± 3.2	0.22	-4.12 ± 1.01
100	4.0	93.1 ± 1.5 (93.1 ± 1.92)	3.8 ±0.7 (95.0 ±2.4)	29.4 ± 3.8	0.18	-3.63 ± 0.69
200	4.0	149.0 ± 12 (74.8 ± 2.1)	3.6 ±0.3 (89.8 ±1.5)	34.0 ± 4.9	0.27	-5.06 ± 1.40
100	6.0	88.2 ± 10 (88.2 ± 1.1)	5.0 ±0.2 (83.3 ±1.7)	32.7 ± 3.1	0.25	-2.76 ± 1.44
200	6.0	131 ± 07 (65.3 ± 3.1)	3.3 ±0.6 (54.9 ±2.7)	40.1 ± 3.5	0.343	-6.08 ± 2.10
100	10.0	88.2 ± 0.1 (88.2 ± 2.3)	7.8 ±0.9 (78.2 ±1.5)	43.0 ± 5.5	0.281	-3.88 ± 0.64

[a] Actual loading is expressed as the amount (µg) of drug encapsulated per 10 mg of Pluronic P123/F127. [b] Entrapment Efficiency = Ratio between experimental and theoretical loading ×100. [c] D_H = Hydrodynamic Diameter. [d] P.I. = Polydispersity index.

Thin film rehydration methodology provided a fluffy lyophilized product, readily reconstituted in water within 20–30 s of manual shaking as already demonstrated in our previous work.[7] Storage stability of the lyophilized formulations (Fig. 1) demonstrated small decrease of drug content with a slight size increase (about 5-6 nm) after reconstitution of the product stored for 6 months. The high recovery yield observed highlighted that neither drug nor micelle precipitation occurred during the preparation.

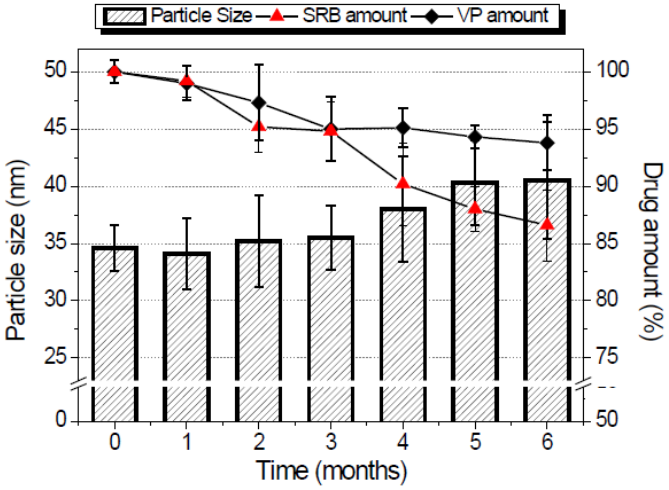

Fig.1. Stability to storage of lyophilized micelles.

3.2 Spectroscopic and photodynamic properties

Fig. 2 shows the absorption and emission spectra of VP free and loaded in the micelles under various experimental conditions. VP is poorly soluble in water media where it is mostly present as aggregated and non-fluorescent form (a and e in Fig. 2). In contrast, Pluronic P123/F127 mixed micelles are able to entrap VP in the monomeric form, as confirmed by the sharpening of VP absorption bands and the intense fluorescence emission (b and f in Fig. 2), similarly to VP in methanol where it is present as monomer (d and h in Fig. 2). Co-entrapment of SRB and VP did not influence the absorption and emission behavior of this latter (c and g in Fig. 2). In fact, only negligible changes were noted in the absorption region beyond 330 nm, being the SRB absorption dominating below this region. Besides, also the fluorescence emission was not affected, being the fluorescence quantum yield ca 0.06, basically the same value observed in methanol ($\Phi_F = 0.051$[30])

In order to gain insights into the efficiency of population of the triplet state we measured the laser intensity dependence of the transient

absorbance under different experimental conditions. Fig. 3B shows the top ΔA of the triplet absorption observed for VP incorporated in the micelles in the absence and in the presence of SRB and, for comparison, for VP in methanol. The behavior observed is typical of a one-photon process, such as the generation of the lowest excited triplet state. In this case, the initial part of each set of data points is proportional to the product $\Phi_T \times \varepsilon_{T\text{-}T}$, where Φ_T and $\varepsilon_{T\text{-}T}$ are the quantum yield of the triplet state and its molar absorption coefficient, respectively.

By taking into account that all solutions are almost optically matched at the excitation wavelength (only slight differences in the absorption at 532 nm are observed in the whole range of ratios explored) and that large changes in the $\varepsilon_{T\text{-}T}$ are fairly unlikely, being substantially unchanged the band profiles, the very similar set of points obtained suggests that the efficiency of population of the triplet state of VP in the Pluronic micelles is not affected by the presence of SRB and is very close to that observed in methanol solution.

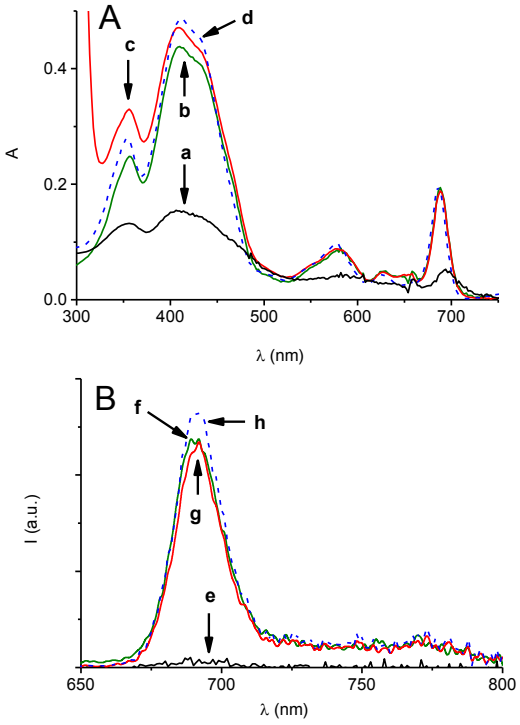

Fig. 2. Absorption spectra of VP in different media. (A) VP in water (a), methanol (d) and in Pluronic P123/F127 mixed micelles (10 mg) dispersed in water solution in the absence (b) and in the presence of SRB (100 μg mL^{-1}) (c). (B) Fluorescence emission spectra (λ_{exc} = 580 nm) of VP in water (e), methanol (h) and in Pluronic micelles dispersed in water solution in the absence (f) and in the presence of SRB (g).VP and SRB concentrations were 4.0 and 100 μg mL^{-1}, respectively.

Energy transfer from the triplet of VP to molecular oxygen results in the concomitant photogeneration of $^1O_2$. Near-infrared luminescence is the most suitable technique to unequivocally demonstrate the generation $^1O_2$. This species, in fact, exhibits a typical phosphorescence signal with maximum at 1270 nm.[34] Fig. 4 shows the diagnostic phosphorescence

spectrum for the Pluronic micelles loaded with VP alone and in the presence of SRB in D_2O solutions, this solvent being used to take advantage of the larger radiative constant and longer lifetime with respect to H_2O.

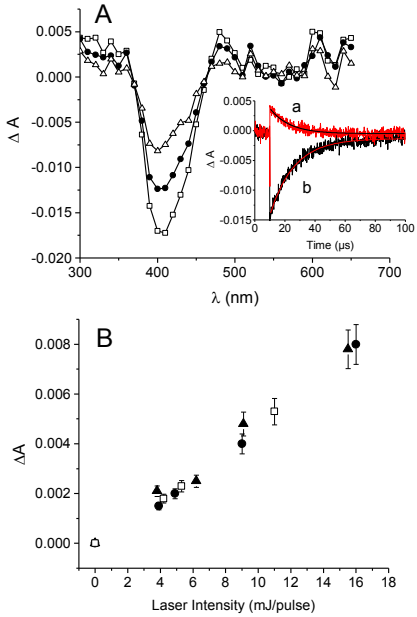

Fig.3. Triplet state features of VP in different conditions. (A) Transient absorption spectra observed 0.8 μs (□), 3.8 μs (●) and 8.7 μs (△) after 532 nm laser excitation (E_{532} ~ 10 mJ/ pulse) of Ar-saturated, aqueous solution of Pluronic micelles co-loaded with VP and SRB. The inset shows the decay trace monitored at 480 nm (a) and 400 nm (b) and the related first-order fittings. (B) Laser intensity dependence of the DA at 480 nm taken 0.1 μs after the laser pulse for VP in methanol(●) and in Pluronic micelles dispersed in water solution in the absence (▲) and in the presence (□) of SRB. VP and SRB concentrations were 4.0 and 100 μg mL^{-1}, respectively.

Since all solutions are optically matched at the excitation wavelength, the very similar area of the spectra obtained for micelles containing either VP or VP co-encapsulated with SRB, lead us to conclude that the $^1O_2$ quantum yield of the PS is basically independent of the presence of

the chemotherapeutic, according to what observed for the precursor excited triplet state (see above).

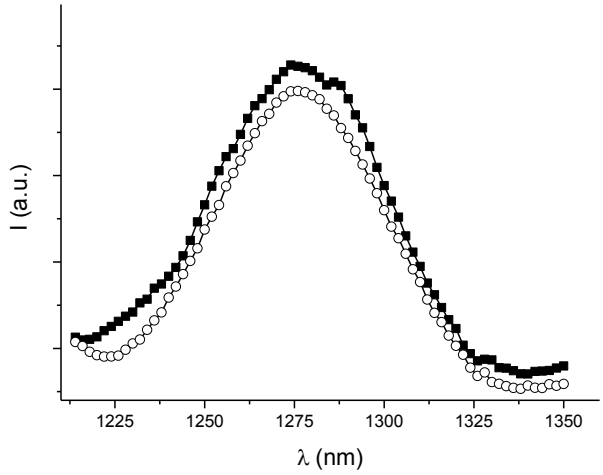

Fig.4. Singlet oxygen luminescence detected in D_2O solutions of Pluronic micelles loaded with VRB in the absence (■) and in the presence (○) of SRB.λ_{exc} = 405 nm.

3.3 Micelle behavior in cell culture medium

Interaction of micelles with proteins is regarded as a critical factor since it has been demonstrated that micelles can aggregate/dissociate in complex media altering the interpretation of biological results.[35] Therefore, the behavior of Pluronic P123/F127 micelles in DMEM enriched with 10% v/v of FBS was assessed by DLS and fluorescence measurements. However, monitoring only one fluorescent probe in the medium can lead to a false positive result because, even if the micelle is disrupted, the fluorescent tag could bind to FBS proteins resulting in no significant change of fluorescence properties, as demonstrated for VP.[36] FRET represents an efficient tool to track NPs stability in biological relevant media.[27;37] For FRET evaluation it was necessary to co-encapsulate into the micelle core two fluorescent probes, an energy donor and an energy acceptor, with appropriate spectroscopic

characteristics. The acceptor molecule in this work was VP. As donor, we choose the hydrophobic dye NR since its emission spectrum well overlaps with VP absorption spectrum, one of the indispensable requisites for FRET to be observed. (Fig.5) NR presents a strong association constant with Pluronic P123/F127 micelles and is located inside Pluronic hydrophobic core. DLS measurements showed no significant change in size and zeta potential after co-encapsulation of VP and NR under the present conditions (data not shown).

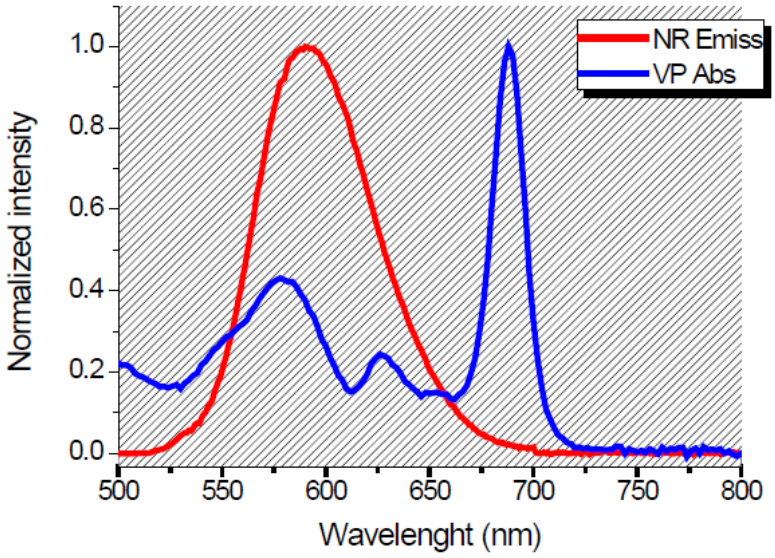

Fig.5. Normalizes absorption spectrum of Verteporfin and emission spectrum of nile red co-loaded in micelles

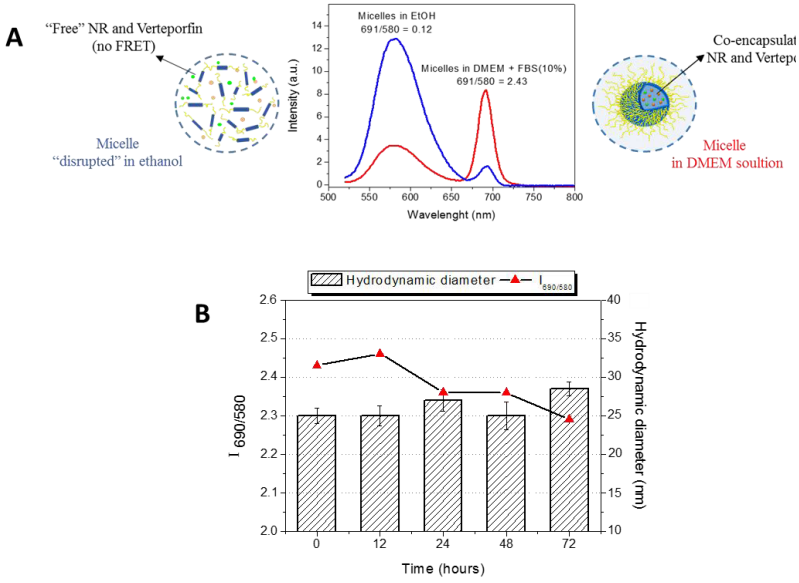

Fig.6. Behavior of Pluronic P123/F127 2:1 w/w mixed micelles (10 mg) loaded with NR (0.8 μg mL^{-1}) and VP (4.0 μg mL^{-1}) in DMEM enriched with FBS 10% (v/v). (A) Fluorescence emission spectra of co-encapsulated dyes in DMEM (red line) and diluted in ethanol (blue line) at λ_{exc} = 480 nm. (B) Hydrodynamic diameter (bars) and fluorescence intensity ratio between VP emission at 690 nm and NR emission at 580 nm (symbols). Data are reported as mean of three independent experiments (n=3) ±SD.

Excitation at 480 nm of the micelle systems co-encapsulating the two chromofluorogenic components and dispersed in cell culture medium shows that the emission of the VP (λ_{em} = 690 nm) dominates over the emission of the NR (λ_{em} = 580 nm) despite NR absorbs most of the incident light and its fluorescence quantum yield is higher than that of VP (Fig. 6A). The intense fluorescence of VP (less fluorescent probe) demonstrates that an efficient energy transfer occurred, due to the close proximity of the co-encapsulated molecules.

Solubilizing the same formulation in organic solvents disrupts its core-shell structure releasing the fluorophores to the external medium. This lead to an increase of the distance between the molecules and thus, a dramatic reduction in FRET efficiency ($I_{690}/_{580}$ is reduced from 2.4 to

0.15, Fig. 6A). Similar results were observed when the dyes are solubilized directly in cell culture medium without micelles. This design allows to monitor micelle stability in different conditions.[27]No significant difference in FRET signal and size were observed for up to 72 h for Pluronic P123/F127 mixed micelles incubated in cell culture medium (Fig. 6B), suggesting that the steric hindrance conferred by the PEO corona offers efficient protection against protein adsorption on micelle surface and following disassembly.[38]Release profile of dual-drug loaded Pluronic P123/F127 mixed micelles dispersed in PBS at pH 7.4 and 37.0 °C were evaluated by dialysis method (Fig.7). Polysorbate 80 in the external medium ensured both sink conditions and prevention of drug aggregation. SRB/VP-loaded micelles displayed lower rate of release as compared to free SRB and VP (Fig.7A) . The incomplete release of free VP was likely due to due to extensive aggregation in water which hindered transport through the dialysis membrane. Since the amount of drug free to diffuse through cell membranes cannot be derived directly from release studies in PBS,[39] the release behavior was followed after micelle dispersion in DMEM enriched with FBS 10% v/v (Fig. 7B). SRB presented a sustained released pattern while VP remained substantially entrapped in the micelle core. Similarly to PBS, SRB/VP-loaded micelles displayed lower rate of release as compared to free SRB and VP. Furthermore, release in DMEM with FBS occurred at slower rates than in PBS (Fig. 7,8 and 9). Once assumed that micelles are stable in DMEM as demonstrated by FRET, the interaction of SRB and VP with FBS proteins, especially albumin, [36]is likely contributing to a decreased release rate. This hypothesis is supported by the fact that also therelease rate of free drug in DMEM is slower as compared to PBS. Thus, the fraction of drugs released from micelles can interact with medium proteins contributing to albumin-mediated transport inside cells.[40]

Release profile from SRB/VP-loaded micelles in all the media was faster than that from micelles loaded with single drug (Fig. 8 and 9). This result together with the slight increase of micelle size when both drugs are co-loaded is indicative of the looser packing of hydrophobic PPO chains, which can leads to a faster release rate.

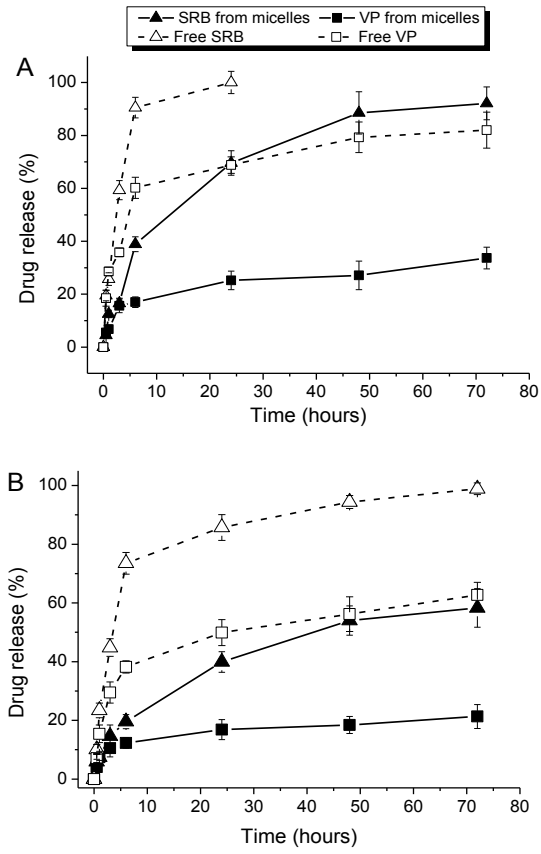

Fig. 7. Release profile of SRB and VP as free or loaded in SRB/VP Pluronic P123/F127 micelles dispersed in (A) PBS or (B) DMEM with FBS 10%. The external medium used for dialysis was PBS buffer with polysorbate 80 (5% v/v) at pH 7.4; T = 37 °C. SRB and VP concentrations were 100 and 10.0 μg mL^{-1}, respectively. Data are reported as mean of three independent experiments (n=3) ±SD.

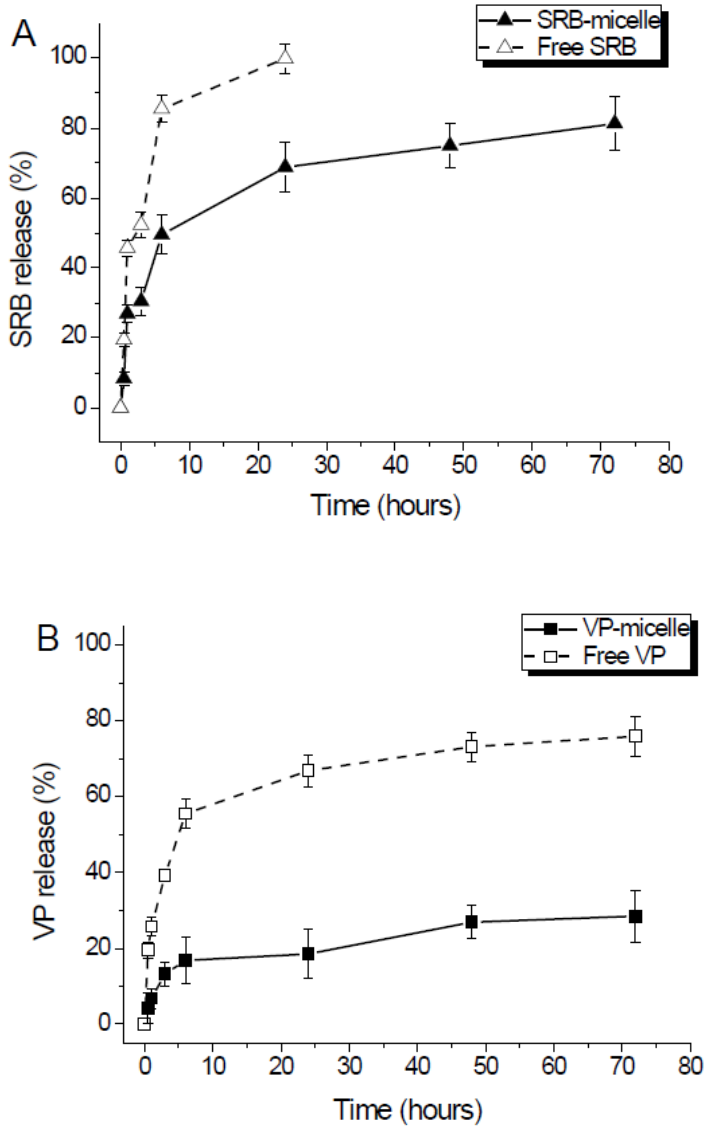

Fig.8. Release profile of free and micelle-loaded SRB (A) and VP (B)in PBS pH 7.4

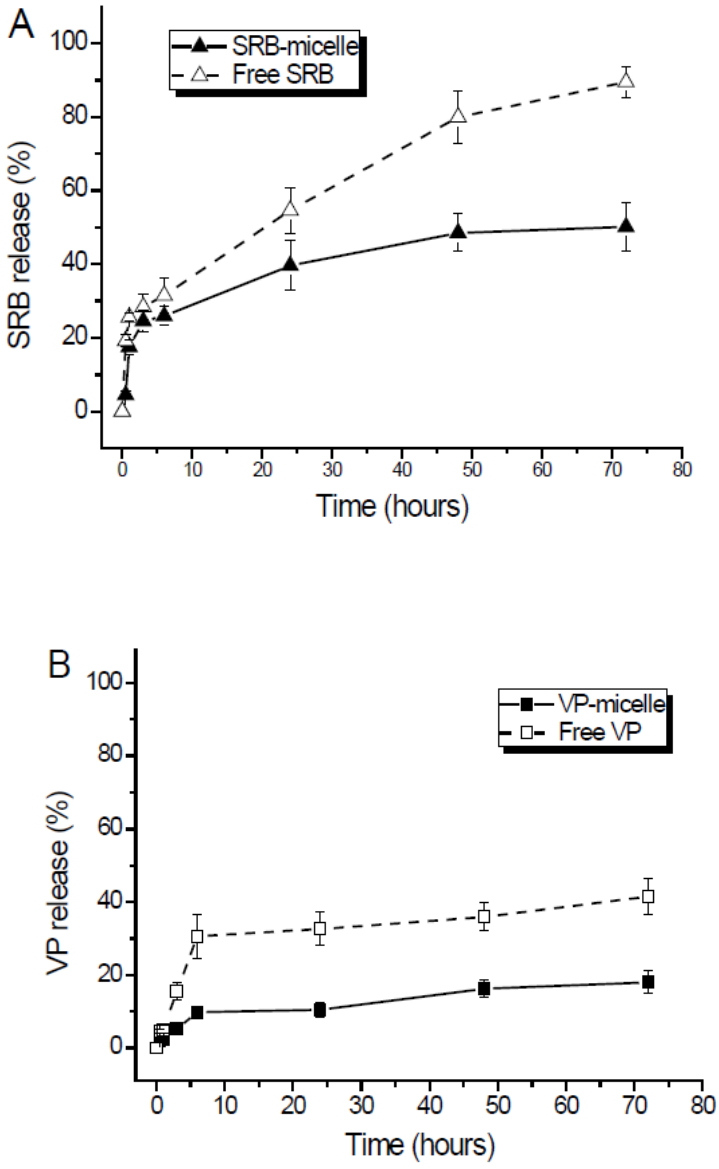

Fig.9. Release profile of free and micelle-loaded SRB (A) and VP (B)in DMEM enriched with FBS 10%

3.4 Cytotoxicity of SRB

The concentration-dependent cytotoxicity of SRB loaded in Pluronic P123/F127 micelles was measured in MDA-MB231 cells after 24 h of exposure and compared to that of the free drug. Cell death measured with the MTS assay immediately after the drug exposure was significantly higher for free SRB incubated at 15 o 20 μM with respect to SRB micelles, which in contrast demonstrated higher efficacy only at very low drug concentration (ie 1 μM) (Fig. 10A). However, the cytotoxicity of SRB delivered in Pluronic micelles was significantly higher with respect to free SRB 24 h after drug exposure (24 + 24 h) with an IC_{50} of 7.7 and 14.8 μM for SRB micelles and free SRB, respectively. The data suggest that after the removal of free SRB the cells resume to proliferate, at least in the lower range of concentrations used in these experiments, while SRB in micelles exerted a delayed but stronger and prolonged cytotoxic effect that might be associated to slow but sustained release of the drug from micelles. Accordingly, free SRB did not perturb to a great extent the progression through the various phases of the cell cycle nor caused the appearance of a hypo-diploid cell population indicative of apoptosis (Fig. 10B and C). On the contrary, SRB in Pluronic P123/F127 mixed micelles caused an accumulation of the cells in the S phase already at 24 h, with a further increase at 24 + 24 h (Fig. 10C) and the appearance of hypo-diploid events in the flow cytometry histograms relative to cell DNA content (Fig.10B). In any case, the induction of an apoptotic response was not ascribable to the presence of the delivery system, since empty Pluronic P123/F127 mixed micelles did not induce cytotoxicity or cell cycle alterations in the same concentration range of SRB micelles (data not shown). Similarly to our results with MDA-MB231 cells, the induction of apoptosis was reported also for in BGC-823 gastric cancer cells after incubation with SRB loaded in salicylic acid-chitosan/heparin coated Pluronic NPs.[41]

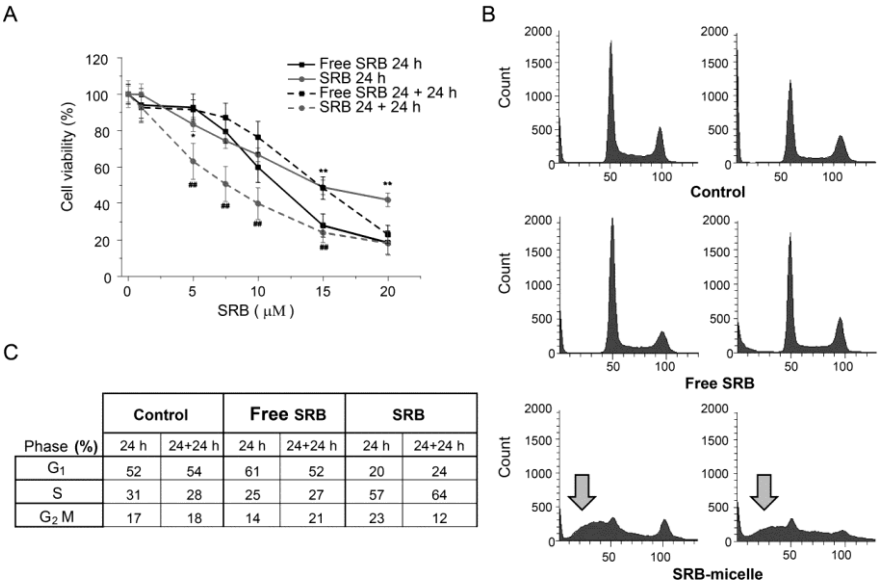

C

	Control		Free SRB		SRB	
Phase (%)	24 h	24+24 h	24 h	24+24 h	24 h	24+24 h
G_1	52	54	61	52	20	24
S	31	28	25	27	57	64
G_2 M	17	18	14	21	23	12

Fig. 10. Cytotoxicity of SRB-loaded Pluronic P123/F127 mixed micelles vs. free SRB. (A) Cell viability measured with the MTS assay in MDA-MB231 cells incubated with increasing concentrations of SRB free or loaded in micelles for 24 or 24 + 24 h. Data are mean ±SD of at least three independent experiments carried out in triplicate. * $p< 0.05$, ** $p<0.001$ SRB-micelle vs. free SRB 24 h; ## $p< 0.001$ SRB-micelle vs free SRB 24 + 24 h (t test). (B) Representative cell cycle histograms showing the appearance of a hypo-diploid populations (gray arrows) in the samples treated with SRB-micelles. C) Summary table of cell cycle analysis.

3.5 Cytotoxicity of the combination SRB plus VP-mediated PDT

Based on the results reported above, showing a benefit by delivering SRB in Pluronic micelles, and those reported previously by our group[7] on the delivery with the same micelles of the photosensitizer VP, we investigated on the possibility of further improving the cytotoxic effect on MDA-MB231 cells by treating them with the combination of SRB and PDT with VP.

Fig.11 shows that the reduction of viability of cells treated with PDT (irradiated with 0.75 J cm^{-2} of red light) after 24 h-incubation with the combination of free SRB + free VP was very similar to that measured after cell incubation and irradiation with free VP only. The absence of

any increased cytotoxicity of the combination with respect to free VP alone is very likely explained by the negligible cytotoxicity of free SRB at 24 + 24 h (Fig.10) i.e. the same time point at which the viability of PDT-treated cells was measured.

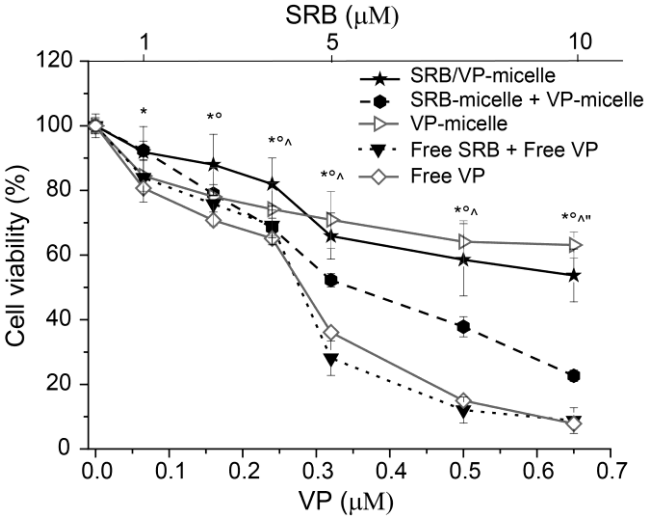

Fig. 11. Photo-toxicity in MDA-MB231 cells exposed to the photosensitizer alone (VP) or to the drug combination (VP + SRB) delivered or not by Pluronic P123/F137 micelles (24 h) and irradiated with 0.75 J cm^{-2} of red light. Cell viability was measured with MTS assay 24 h post-irradiation. Data are mean ±SD of at least three independent experiments carried out in triplicate. Bonferroni test ($p<0.05$); SRB/VP-micelle significantly different from * free VP, free SRB + free VP, ^ VP-micelle + SRB-micelle, VP-micelle.

The experiments carried with the combination in the dark confirmed that free SRB was poorly cytotoxic at concentrations lower than 10 μM (Fig. 12). These latter experiments also confirmed that VP alone is devoid of any toxicity in the absence of light independently from delivery modality. Contrary to our expectation, the combination of SRB and VP formulated in separate micelles was less photo-to toxic than the combination of the free drugs. This is very likely caused by the reduced photo-toxicity of VP-loaded micelles in comparison to free VP. In any case, the treatment with the combination of VP Pluronic-mediated PDT and SRB-loaded micelles was slightly more efficient in reducing cell viability than the single treatments. This positive interaction appeared however disturbed by the encapsulation of the two drugs in the same

micelle for their co-delivery to MDA-MB231 cells. In fact the reduction of viability in cells treated with VP/SRB-loaded Pluronic micelles was less than that caused by VP-micelles plus SRB-micelles added separately.

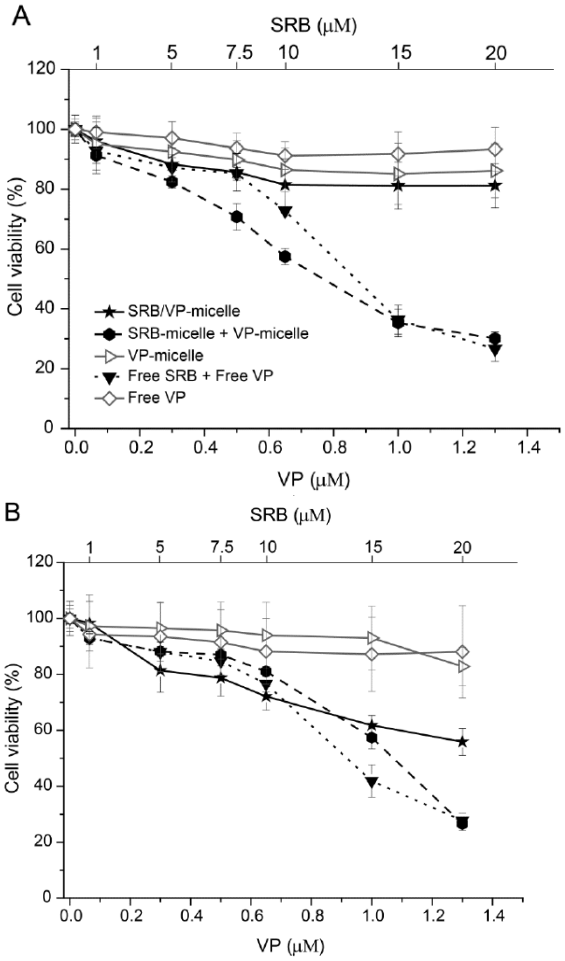

Fig. 12. Cytotoxicity of MDA-MB231 cells incubated in the dark with VP alone or drug combination (VP + SRB) delivery or not whit micelles at 24 h (A) and 24 + 24 h (B).

One possible explanation of the reduced efficacy of the combination of co-loaded VP/SRB is the increased size of micelles associated with drug co-encapsulation, as shown by the DLS measurements of Table 1 that might have reduced the efficiency of cell internalization and drug bioavailability.

3.6 Uptake and cellular localization of BPDMA in MDA-MB231 cells

The hypothesis of a reduced cellular uptake of drugs encapsulated in micelles as compared to the free forms was confirmed for VP. The red fluorescence of VP was exploited to easily investigate both the cellular uptake by flow cytometry and cellular localization by confocal microscopy.

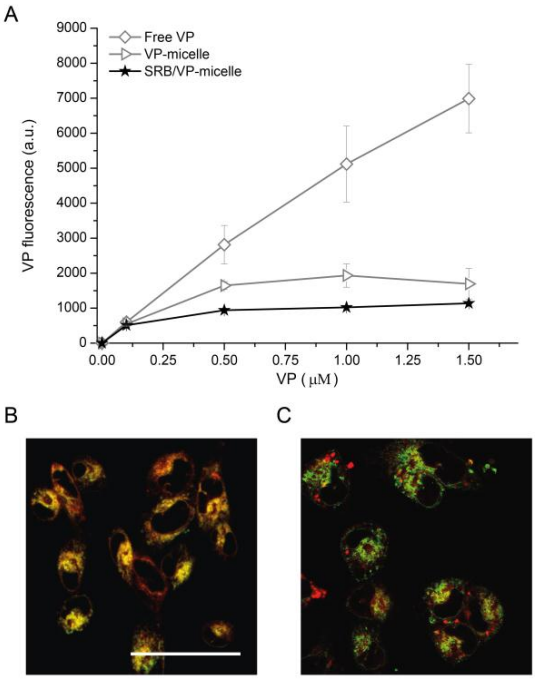

Fig.13. Uptake and intracellular localization of VP formulations. (A) Flow cytometry measurements of VP uptake after 24 h of cell incubation with increasing concentrations of free VP, VP-micelles or VP/SRB-micelles. Confocal microscopy images of MDA-MB231 cells incubated with free (B) or VP-loaded micelles (C) (red fluorescence) for 24 h and stained with the endoplasmic reticulum probe ER Tracker green (green fluorescence). Clear co-localization between the probe and VP fluorescence is visible exclusively in B. Scale bar = 50 μm.

We found that the uptake of free VP in MDA-MB231 cells incubated for 24 h increased linearly at least up to 1.5 μM (Fig. 13A). On the contrary, the uptake of VP loaded in Pluronic micelles reached a plateau at approx. 0.5 μM. Of interest is the fact that co-loaded VP/SRB micelles showed a decreased uptake at the plateau with respect to VP-loaded micelles.

Note that, the reduced cellular uptake of the micelles cannot be trivially ascribed to a lower fluorescence of the VP when encapsulated in the carrier. In fact, we demonstrated that the fluorescence quantum yield of this fluorophore is not affected by its compartmentalization in the Pluronic micelles and is also independent by the presence of SRB. Thus, reduced uptake of VP when loaded in micelles parallels the poor internalization of PEO-coated nanocarriers.[42]The observations on the decreasing uptake of VP well correlate with the decreasing of cell photosensitisation efficiency that is higher for free VP with respect to VP-loaded micelles (Fig. 11). For VP/SRB-loaded micelles we can safely assume that, based on the uptake experiments, the contribution of PDT to the overall effect of the combined treatment is less than in the combination VP-loaded micelles + SRB-loaded micelles with a consequent decreased cell mortality. The fluorescence microscopy analyses (Fig. 13B,C) confirmed the lower uptake of VP-loaded micelles with respect to free VP and showed cytoplasmatic localisation of both formulations, with exclusive accumulation of free VP in the endoplasmic reticulum.

Moreover, together with the reduced uptake, the different intracellular localization of the two formulations can be responsible of the reduced photo-toxic profile measured for VP-loaded micelles at least in MDA-MB 231 cells. In our previous work we reported a mitocondrial localization of both free and micelle VP in HeLa cells and significantly increased photo-toxicity of VP with the delivery by Pluronic P123/F137 micelles at least for PS concentrations lower than 0.1 μM.[7] It must however be considered that, the latter results were obtained in HeLa cells incubated with VP for 4 h only before performing PDT. Therefore, to exclude any timing effects that might negatively affect cell photosensitation and/or drug combination sequence, we performed experiments in which MDA-MB231 cells were incubated for 4 h with

VP, irradiated with 0.75 J cm^{-2} of red light and incubated for further 24 h with SRB (Fig.14).

The changing of incubation time and schedule of delivery of the treatments, however, did not improve the cytotoxic effects of the

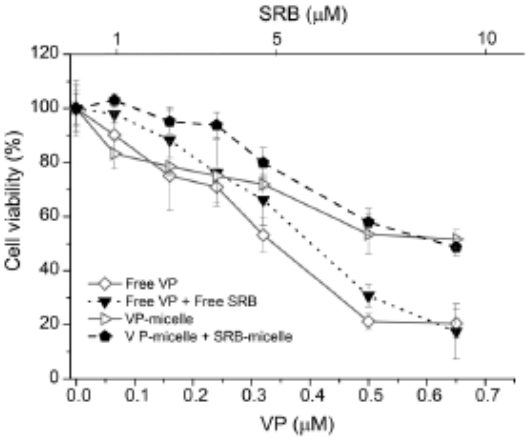

Fig.14.Cytotoxicity of MDA-MB231 cells incubated in the dark at 4 h and with o.75 J cm 2 of red light

combination VP-PDT and SRB, did not show any synergism or additive effects for the drugs delivered free nor in Pluronic P123/F127 mixed micelles.

4. Conclusions

The present study demonstrates that Pluronic P123/F127 mixed micelles do not suffer neither disassembling nor size changes in biological media and are very suited to entrap effectively the poorly water soluble SRB, VP and their combination. While cytotoxicity of SRB delivered by Pluronic micelles is significantly higher than that observed for the free drug, the effect is the opposite for VP. Furthermore, micelles co-delivering the two active components do not improve the anticancer performances. These findings cannot be attributable to reduced photodynamic properties of VP when encapsulated in the micelles, being its capability to photogenerate $^1O_2$ basically the same to that observed in organic solvent and in the micelles co-encapsulating SRB. One possible explanation of the reduced efficacy of the combination VP/SRB is the different cell uptake and localization of the micelles, which result in a reduced efficiency of cell internalization and drug bioavailability. In view of previous study reporting enhanced cytotoxic effects on systems based on photo-chemotherapeutic combination, the present contribution provides a clear example that no generalizations are possible at this regard and then each system must be investigated in detail. Co-encapsulation of a PDT agent and a chemotherapeutic in a single nanodelivery system cannot be proposed as a general strategy to observe amplified cell mortality effects, even under the complete preservation of the photodynamic properties of the PS in the co-presence of the chemotherapeutic agent, which, in any case, remain always a key pre-requisite to be fulfilled.

References

1. Aw MS, Kurian M, Losic D. Polymeric micelles for multidrug delivery and combination therapy. Chemistry. 2013;19:12586-12601.

2. Sanna V, Pala N, Sechi M. Targeted therapy using nanotechnology: focus on cancer. Int J Nanomedicine. 2014;9:467-483.
3. Xu X, Ho W, Zhang X, Bertrand N, Farokhzad O. Cancer nanomedicine: from targeted delivery to combination therapy. Trends Mol Med. 2015;21:223-232.

4. Batrakova EV, Kabanov AV. Pluronic block copolymers: evolution of drug delivery concept from inert nanocarriers to biological response modifiers. J Control Release. 2008;130:98-106.

5. Jung YW, Lee H, Kim JY, Koo EJ, Oh KS, Yuk SH. Pluronic-based core/shell nanoparticles for drug delivery and diagnosis. Curr Med Chem. 2013;20:3488-3499.

6. Attia ABE, Ong ZY, Hedrick JL, et al. Mixed micelles self-assembled from block copolymers for drug delivery. Curr Opin Coll Interf Sci. 2011;11(3):182-184.
7. Pellosi DS, Tessaro AL, Moret F, et al. Pluronic® mixed micelles as efficient nanocarriers for benzoporphyrin derivatives applied to photodynamic therapy in cancer cells. J Photochem Photobiol A: Chem. 2016;314:143-154.
8. Wilhelm S, Carter C, Lynch M, et al. Discovery and development of sorafenib: a multikinase inhibitor for treating cancer. Nat Rev Drug Discov. 2006;5:835-844.

9. Bolondi L, Craxi A, Trevisani F, et al. Refining sorafenib therapy: lessons from clinical practice. Future Oncol. 2015;11:449-465.

10. Lin T, Gao DY, Liu YC, et al. Development and characterization of sorafenib-loaded PLGA nanoparticles for the systemic treatment of liver fibrosis. J Control Release. 2016;221:62-70.

11. Craparo EF, Sardo C, Serio R, et al. Galactosylated polymeric carriers for liver targeting of sorafenib. Int J Pharm. 2014;466:172-180.

12. Bondi ML, Botto C, Amore E, et al. Lipid nanocarriers containing sorafenib inhibit colonies formation in human hepatocarcinoma cells. Int J Pharm. 2015;493:75-85.

13. Thapa RK, Choi JY, Poudel BK, et al. Multilayer-Coated Liquid Crystalline Nanoparticles for Effective Sorafenib Delivery to Hepatocellular Carcinoma. ACS Appl Mater Interfaces. 2015;7:20360-20368.

14. Xie B, Wang DH, Spechler SJ. Sorafenib for treatment of hepatocellular carcinoma: a systematic review. Dig Dis Sci. 2012;57:1122-1129.

15. Weiss A, den BH, Griffioen AW, Nowak-Sliwinska P. Angiogenesis inhibition for the improvement of photodynamic therapy: the revival of a promising idea. Biochim Biophys Acta. 2012;1826:53-70.

16. Dolmans DE, Fukumura D, Jain RK. Photodynamic therapy for cancer. Nat Rev Cancer. 2003;3:380-387.

17. Lucky SS, Soo KC, Zhang Y. Nanoparticles in photodynamic therapy. Chem Rev. 2015;115(4):1990-2042.
18. Huggett MT, Jermyn M, Gillams A, et al. Phase I/II study of verteporfin photodynamic therapy in locally advanced pancreatic cancer. Br J Cancer. 2014;110:1698-1704.

19. Nowak-Sliwinska P, Weiss A, van Beijnum JR, et al. Angiostatic kinase inhibitors to sustain photodynamic angio-occlusion. J Cell Mol Med. 2012;16:1553-1562.

20. Bennet D, Marimuthu M, Kim S, An J. Dual drug-loaded nanoparticles on self-integrated scaffold for controlled delivery. Int J Nanomedicine. 2012;7:3399-3419.

21. Mignani S, Bryszewska M, Klajnert-Maculewicz B, Zablocka M, Majoral JP. Advances in combination therapies based on nanoparticles for efficacious cancer treatment: an analytical report. Biomacromolecules. 2015;16:1-27.

22. Batist G, Gelmon KA, Chi KN, et al. Safety, pharmacokinetics, and efficacy of CPX-1 liposome injection in patients with advanced solid tumors. Clin Cancer Res. 2009;15:692-700.

23. Feldman EJ, Lancet JE, Kolitz JE, et al. First-in-man study of CPX-351: a liposomal carrier containing cytarabine and daunorubicin in a fixed 5:1 molar ratio for the treatment of relapsed and refractory acute myeloid leukemia. J Clin Oncol. 2011;29:979-985.

24. He C, Liu D, Lin W. Self-assembled core-shell nanoparticles for combined chemotherapy and photodynamic therapy of resistant head and neck cancers. ACS Nano. 2015;9:991-1003.

25. Maiolino S, Moret F, Conte C, et al. Hyaluronan-decorated polymer nanoparticles targeting the CD44 receptor for the combined photo/chemo-therapy of cancer. Nanoscale. 2015;7:5643-5653.

26. Zhang X, Jackson JK, Burt HM. Development of amphiphilic diblock copolimers as micellar carriers of taxol. Int J Pharm. 1996;132(1-2):195-206.
27. Chen H, Kim S, He W, et al. Fast release of lipophilic agents from circulating PEG-PDLLA micelles revealed by in vivo forster resonance energy transfer imaging. Langmuir. 2008;24:5213-5217.

28. Wei Z, Hao J, Yuan S, et al. Paclitaxel-loaded Pluronic P123/F127 mixed polymeric micelles: formulation, optimization and in vitro characterization. Int J Pharm. 2009;376:176-185.

29. Park S, Jeong K, Lee E, et al. Amphiphilized poly(ethyleneimine) nanoparticles: a versatile multi-cargo carrier with enhanced tumor-homing efficiency and biocompatibility. J Mater Chem B. 2015;3:198-206.
30. Aveline BM, Hasan T, Redmond RW. The effects of aggregation, protein binding and cellular incorporation on the photophysical properties of benzoporphyrin derivative monoacid ring A (BPDMA). J Photochem Photobiol B. 1995;30:161-169.

31. Pandey R, Zheng G. The Porphyrin Handbook. Smith KM, Kadish K, Guilard R, ed. San Diego: Academic Press; 2000.

32. Montalti M, Credi A, Prodi L, Gandolfi MT. Handbook of Photochemistry. 3 ed. Boca Raton: CRC Press; 2006.

33. Nowak-Sliwinska P, Karocki A, Elas M, Pawlak A, Stochel G, Urbanska K. Verteporfin, photofrin II, and merocyanine 540 as PDT photosensitizers against melanoma cells. Biochem Biophys Res Commun. 2006;349:549-555.

34. Wilkinson F, Hlman WP, Ross AB. Quantum Yields for the Photosensitized Formation of the Lowest Electronically Excited Singlet State of Molecular Oxygen in Solution. J Phys Chem Ref Data. 1993;22:113.

35. Conte C, Ungaro F, Maglio G, et al. Biodegradable core-shell nanoassemblies for the delivery of docetaxel and Zn(II)-phthalocyanine inspired by combination therapy for cancer. J Control Release. 2013;167:40-52.

36. Chowdhary RK, Shariff I, Dolphin D. Drug release characteristics of lipid based benzoporphyrin derivative. J Pharm Pharm Sci. 2003;6:13-19.

37. Swaminathan S, Garcia-Amoros J, Fraix A, Kandoth N, Sortino S, Raymo FM. Photoresponsive polymer nanocarriers with multifunctional cargo. Chem Soc Rev. 2014;43:4167-4178.

38. Shubhra QTH, Tóth J, Gyenis J, Feczkó T. Poloxamers for Surface Modification of Hydrophobic Drug Carriers and Their Effects on Drug Delivery. Poly Rev. 2014;54:122-138.

39. Gullotti E, Yeo Y. Beyond the imaging: limitations of cellular uptake study in the evaluation of nanoparticles. J Control Release. 2012;164:170-176.

40. Palma G, Conte C, Barbieri A, et al. Antitumor activity of PEGylated biodegradable nanoparticles for sustained release of docetaxel in triple-negative breast cancer. Int J Pharm. 2014;473:55-63.

41. Yang YC, Cai J, Yin J, Zhang J, Wang KL, Zhang ZT. Heparin-functionalized Pluronic nanoparticles to enhance the antitumor efficacy of sorafenib in gastric cancers. Carbohydr Polym. 2016;136:782-790.

42. Conte C, d'Angelo I, Miro A, Ungaro F, Quaglia F. PEGylated polyester-based nanoncologicals. Curr Top Med Chem. 2014;14:1097-1114.

ANNEX-II
In vitro/in vivo investigation of the potential of Pluronic mixed micelles for pulmonary drug delivery

1 Introduction

Pulmonary delivery systems are in the limelight for local release of active agents in severe lung diseases, including cancer, asthma, cystic fibrosis and chronic lung infections[1,2]. In fact, direct delivery of the drug to the site of action is feasible by this way, thus improving therapeutic potential while reducing drug-related systemic side effects. However, a number of obstacles must be considered before the administered drugs reaches the site of action [3]. For example, mucociliary clearance can eliminate drugs and foreign particles from the airways reducing residence time and the drug amount reaching the target. In addition, undesirable interactions of the formulation with lung lining fluids, airway macrophages and lung epithelial cells may be detrimental for drug therapeutic efficacy [4].

To overcome these drawbacks, controlled and targeted delivery of drugs to the lungs by means of biodegradable polymeric nanoparticles (NPs) is under investigation. Indeed, NPs may, at least in principle, assist the drug getting through extracellular and cellular barriers [5]Additionally, NP composition and surface properties can be adequately manipulated to reduce mucoadhesive tendency or to improve NP targeting ability [5]. Nevertheless, nanocarriers cannot be administered as such since they suffer from the disadvantage of being exhaled from the respiratory tract. To reach smaller airways (bronchus and bronchioles), inhalable NPs must be appropriately engineered in order to meet optimal aerodynamic properties [6].

Although a huge number of studies have been recently focused on the development of polymer NPs for lung delivery [5], only few works have exploited the potential of polymeric micelles as drug delivery systems for local therapies of lung diseases [7]. One representative of such nanocarriers are poloxamer, or Pluronic ®, micelles, having the ability to load and to stabilize a great variety of drugs [8]. The very small size (<100 nm) and the hydrophilic surface properties (i.e., polyethylene oxide shell) of Pluronic micelles make them very intriguing to facilitate drug diffusion through human airway mucus [9]. In addition, Pluronic micelles can be modified at unimer terminus to bind functional molecules in order to gain surface decorated micelles with improved targeting properties. Finally, recent studies

demonstrated that Pluronic micelles are safe and may efficiently promote drug release in different lung cells both in vitro and in vivo [10,11].

Despite their great potential, Pluronic has been mainly used as excipient or helper polymer in drug delivery systems for inhalation [12,13]. To our knowledge just two papers developed nanostructured self-assembled Pluronic micelles as vehicle for drug release to the lung through spray-dried microparticles technology [7,14].

Thus, the objective of this work is to test pluronic micelles as a platform for pulmonary drug delivery. To this purpose, multimodal Pluronic mixed micelles (PMM) in form of aqueous liquid suspension and solid nano-embedded microparticles (NEM) were developed and tested. PMM stability in different pulmonary-relevant media, their interaction with mucin and penetration through artificial mucus were evaluated. PMM-based NEM engineered for inhalation were produced by spray-drying using lactose as carrier and evaluated in term of stability, flow and aerosolization properties. Finally, PMM biodistribution after administration in mice was assessed.

2 Materials and Methods

Pluronic s® P123 (EO_{20}–PO_{65}–EO_{20}, MW = 5750 g mol^{-1}) and F127 (EO_{100}–PO_{65}–EO_{100}, MW = 12600 g mol^{-1}) were purchased from Sigma-Aldrich and the solutions were prepared by weighting materials previously desiccated under vacuum for 24 h. European Pharmacopoeia 7th Ed. (Ph.Eur.) grade lactose was used (NEW.FA.DEM., Italy). Calcium chloride dihydrate, magnesium chloride, potassium chloride, potassium phosphate dibasic, sodium acetate, sodium bicarbonate, sodium chloride, sodium citrate dihydrate, sodium phosphate dibasic, sodium sulfate,nile red, gelatin from bovin skin type B, diethylenetriaminepentaacetic acid (DTPA), RPMI amino acid solution, type II mucine from porcin stomach, Egg Yolk Emulsion were purchased from Sigma Aldrich (Italy). Verteporfin was kindly supplied by Professor D. Dolphin (University of British Columbia, Vancouver, Canada).

2.1 Synthesis of biotin-conjugated and rhodamine-conjugated Pluronics

The synthetic procedure was similar for both Pluronics. For biotin-conjugated Pluronic, F127 (5.0 g, 0.40 mmol) was dissolved in 75 mL of dichloromethane followed by the addition of biotin (0.12 g, 0.48 mmol). For Rhodamine-conjugated Pluronic, P123 (3.0 g, 0.40 mmol) was dissolved in 75 mL of dichloromethane followed by the addition of rhodamine B (0.44 g, 0.48 mmol). After that, DMAP (0.004 g, 0.03 mmol) was added to each reaction flask and the solution cooled to 0°C. DCC (0.08 g, 0.40 mmol) was added dropwise *via* a dropping funnel over 30 min, and the reactions were carried out for 48 h at room temperature under agitation. The reaction mixtures were then extracted with a $NaHCO_3$ water solution (10% v/v). After this step, the organic phases were frozen overnight and the insoluble substances were removed by filtration. The organic solutions were then precipitated twice in cold diethyl ether. The functionalized polymers were filtered and dried overnight under vacuum.

Biotin-F127 reaction yield = 82%. ^{1}H-NMR (300 MHz, DMSO-d6, TMS), δ (ppm): 1.000-1.485 (s, -CH_3 b), 1.493 (m, H_5, 2H), 2.200 (m,

H_3, 2H), 2.821 (m,H_5, 2H), 3.105 (m, H_4, 2H), 3.260-3.619 (m, -O-CH_2-CH_2- a), 4.138 (m, $H_{6'}$, 1H), 4.300 (m, H_6, 1H), 6.363 (s, H_{N2}, 1H) e 6.437 (s, H_{N1}, 1H).

Rhodamine-P123 reaction yield = 68%. ^{1}H-NMR (300 MHz, DMSO-d6, TMS), δ (ppm): 1.000-1.126 (s, -CH3 b), 1.209 (t, N-CH_3, 12H), 3.260-3.549 (m, -O-CH_2-CH_2- a), 3.641 (d, N-CH_2, 8H), 6.980 (m, H_2-H_7-H_4-H_5, 4H), 7.094 (d, H_8-H_1, 2H), 7.473 (dd, $H_{6'}$, 1H), 7.842 (m, $H_{4'}$-$H_{5'}$, 2H), 8.320 (dd, $H_{3'}$, 1H).

2.2 PMM preparation

PMM were prepared by the thin-film hydration method [15]. Briefly, 100 mg of the Pluronic P123/F127 mixture (2:1 w/w ratio) were dissolved in 10 mL of ethanol in a round-bottom flask. Then, the solvent was evaporated by rotary evaporation at 50 °C for about 20 minutes. Residual solvent in the film was removed under vacuum overnight. Thereafter, the dried film was hydrated with 10 mL of filtered distilled water and the material was sonicated for 5 minutes to obtain a limpid solution. This solution was filtered through 0.22 μm filters (RC Chemtek, Italy) to remove possible large cylindrical aggregates formed by P123. When indicated, the resulting solution was lyophilized for 24 h.

For Biotin-decorated PMM (Bio-PMM), biotin-conjugated F127 was added at 20% of total F127 weight. For Rhodamine B-tagged PMM (Rho-PMM or Bio/Rho-PMM) rhodaminated-P123 was added in order to give rhodamine B concentrations of 5.0 μM. For Bio/Rho-PMM micelles at 10 mg mL^{-1}, for example, 2.66 mg of F127 and 0.66 mg of biotin-conjugated F127, 6.60 mg of P123 and 0.066 mg of rhodamine B-conjugated P123 (a stock solution in ethanol of all the components) were used.

Hydrodynamic diameter (D_H), polydispersity index (PI) and zeta potential (ζ) of micelles were determined using a Zetasizer Nano ZS (Malvern Instruments Ltd, UK). On the freeze-dried formulations dispersed in water. Results are reported as mean of three measurements on three different micelle batches (n=9) ±SD.

2.3 Micelle stability in pulmonary-relevant media

Micelle stability in saline solution, mucin aqueous solution, artificial mucus and simulated interstitial lung fluids (SILF) was evaluated. For mucin aqueous solution, mucin powder was dispersed in water (0.08% w/v) and stirred overnight. Then, the dispersion was centrifuged at 6000 rcf for 20 min to collect the mucin-containing supernatant. Artificial mucus was prepared adding 250 μL of sterile egg yolk emulsion, 250 mg of mucin, 0.295 mg DTPA, 250 mg NaCl, 110 mg KCl, 1 ml of RPMI to 50 mL of water. SILF was prepared following the preparation instructions dictated by [16]. Briefly, 1 L of SILF contains 0.095 g of magnesium chloride, 6.019 g of sodium chloride, 0.298 g of potassium chloride, 0.126 g of sodium phosphate dibasic, 0.063 g of sodium sulfate, 0.368 g calcium chloride dihydrate, 0.574 g of sodium acetate, 2.604 g of sodium bicarbonate, and 0.097 g of sodium citrate dehydrate. Stability was assessed by fluorescence resonance energy transfer (FRET) technique by co-encapsulating Nile Red (NR) and Verteporfin (VP) into micelles (FRET-PMM). The concentrations of NR and VP in FRET-PMM were 0.8 μg and 4.0 μg mL^{-1}, respectively. For the analyses, 20 mg of lyophilized FRET-PMM were added to 2 mL of each medium and incubated at 37.0 ºC for 72 h. At selected time intervals, the ratio between the maximum intensity of emission bands for Verteporfin and NR size and micelle size were monitored. A decrease of this ratio and/or micelle size increase was considered indicative of micelle aggregation or disassembly. The fluorescence measurements were made on a Shimadzu RF-1501 spectrofluorometer using a 1.00 cm path-length quartz cuvette. Results are reported as mean of three separate measurements (n=3) ±SD.

2.4 In vitro assessment of micelle interactions with mucus

2.4.1 Mucoadhesive tendency

Mucoadhesive tendency of PMM was assessed by turbidimetric measurement of their interaction with mucin [16]. Equal volumes of mucin and PMM dispersions (20 mg/mL) were mixed by vortexing for 1 min. The turbidity of the mixtures was measured at time 0 and after incubation at 37 °C (30–60 min). The ABS at 650 nm was recorded by

electronic spectrophotometry on a Shimadzu UV-1800 spectrophotometer. Reference ABS of mucin and PMM dispersions was also evaluated. Experiments were run in triplicate. Results are expressed as ABS at 650 nm±SD over time.

The ζ potential of PMM dispersions in mucin was also measured. The mucin dispersion was first diluted in water (1:4 v/v) and analyzed. Afterwards, a drop of micelle dispersion was added to mucin and the ζ potential of the samples recorded.

2.4.2 Penetration of fluorescent micelles through artificial mucus

The penetration of fluorescent Rho-PMM through artificial mucus was followed in an artificial mucus model as previously reported [17]. Briefly, 50 ml of artificial mucus solution was prepared as described above. A 10% (w/v) gelatin solution was prepared in hot water. One milliliter of gelatin solution was placed in each well of a 24-well plate, hardened at room temperature and stored at 4 °C until use. One milliliter of artificial mucus was placed on the hardened gelatin gel. Then, 500 µl of a Rho-PMM water dispersion fluorescent-tagged micelles (10 mg/ml) were placed on the artificial mucus layer and maintained at room temperature for 24 h. At regular time intervals, artificial mucus was withdrawn from 3 plates, gelatin washed with water (2 ml×6) and subsequently melted at 60 °C. Mean while, micelle dispersions in mucus were centrifuged at 6000 rcf and 4 °C for 20 min. The amount of micelles permeated in the gelatin layer was evaluated by spectrofluorimetry (EX= 480 nm, EM= 520 nm). Results are reported as percentage of Rhodamine penetrated through artificial mucus (amount of Rhodamine in gelatin plates/total amount of Rhodamine in micelles ×100) ±SD.

2.5 Production and characterization of NEM

NEM were produced by co-spray drying PMM and lactose as inert carrier. Briefly, PMM were dispersed in a 100 mL of lactose aqueous solution (2% w/v) in order to achieve Pluronic /lactose ratio 1:1, 1:10 and 1:20 in weight. Dispersions were processed in a Mini Spray Dryer Büchi 190 (Flawil, Switzerland) equipped with a high-performance cyclone for the recovery of small powder amounts. PMM and Bio-PMM

dispersions in lactose were individually spray-dried with the following process parameters: feed rate 4 ml/min; aspirator setting 20; spray-flow 400 Nl/h; inlet temperature 150 °C (resulting outlet temperature = 95 °C). A 0.5 mm nozzle was used throughout the experiments. Powders were collected and stored in a glass dryer under vacuum at room temperature until use.

The mean geometric diameter and size distribution of NEM were determined by laser light scattering (Coulter LS 100Q, USA) on a NEM suspension in chloroform/span 80 (2% w/w) solution. Size is expressed as volume mean diameter ±S.D. of values collected from three different batches (n = 6). Powder tapped density (ρ) and flowability (Carr's Index) were evaluated according to European Pharmacopoeia 7th Edition (Ph.Eur.) The theoretical mass mean aerodynamic diameter ($MMAD_t$) of particles was estimated as previously reported [18].

2.6 In vitro aerosolization properties of NEM

The aerosolization properties of NEM were tested in vitro after delivery from Turbospin® (PH&T Pharma, Milano, Italy), a breath-activated, reusable DPI working with single unit gelatin capsule containing the dry powder, as previously reported [18].

Mean geometric diameter and size distribution of NEM were determined by laser light scattering (Coulter LS 100Q, USA) on NEM suspensions in chloroform containing sorbitan monooleate (2% w/v) as dispersing agent. Size is expressed as volume mean diameter ± SD of values collected from three batches.

Powder tapped density (ρ) and flowability (Carr‘s Index) were assessed according to European Pharmacopoeia (Ph.Eur. 8 Ed) by a tapped density tester (Mod. IG/4, Giuliani, Italy).

The theoretical mass mean aerodynamic diameter ($MMAD_t$) of particles was estimated on the basis of the definition (1):

$$MMADt = d\,(\rho/\rho_0 X)^{1/2} \quad (1)$$

where d is the mean geometric diameter, $\rho_0$is a reference density of 1 g/ml and X is the dynamic shape factor, which is 1 for a sphere. An approximate bulk measure of ρ is provided by tapped density measurements.

The aerosolization properties of powders were tested in vitro after delivery from Turbospin®(PH&T Pharma, Milano, Italy), a breath-activated reusable DPI, ina Next Generation ImpactorTM(NGI) (Copley Scientific, UK) according to European Pharmacopeia (Ph.Eur. 8 Ed). The NGI was coupled with a DFM critical flow controller (Copley Scientific, Nottingham,UK), which was connected to an HCP5 vacuum pump (Erweka, USA).The airflow rate was measured and adjusted prior to each experiment to a constant value of 60 L min^{-1}.

The powder amount deposited on the seven NGI collection cups was quantitatively collected by dissolution in 2 mL of water. The amount deposited in the induction port and remaining inside the nebulizer chamber was also determined by washing with an appropriate amount of water. To quantify powder deposition, Rho-PMM were used to produce NEM and rhodamine-B absorption evaluated by spectrofluorometry as reported in 2.5.2.

The emitted dose (ED) was calculated by accurately weighing the capsule before and after Turbospin® actuation. The fine particle fraction (FPF), the experimental mass median aerodynamic diameter ($MMAD_{exp}$) and the geometric standard deviation (GSD) were calculated according to Ph.Eur. deriving a plot of cumulative mass of powder detained at each stage (expressed as percent of total mass recovered in the impactor) versus cut-off diameter of the respective stage. The FPF was calculated by interpolation from the plot as the percentage of powder emitted from the inhaler with an aerodynamic diameter less than 5μm. The $MMAD_{exp}$ of the particles was determined from the same graph as the particle size at which the line crosses the 50% mark and the GSD was defined as

$GSD = (Size\ X / Size\ Y)^{1/2}$

where size X was the particle size at which the line crosses the 84% mark and size Y the size at which it crosses the 16% mark.

2.7 In vivo biodistribution of PMM

2.7.1 Animals

Male Wistar rats (200-220 g; Charles River, Lecco, Italy) were used. All the experimental procedures were performed following the specific guidelines of the Italian and the European Council law for animal care

and were approved by the Animal Ethics Committee of the University of Naples "Federico II" (Italy).

2.7.2 Treatments

Rats were anesthetized using ketamine (80-100mg/kg, i.p.) and xilazine (10mg/kg, i.p.) and the depth of anesthesia was continuously controlled. Rats were divided into different groups and treated with saline (100 µL, SHAM group), 10 mg mL^{-1} Rho-PMM dispersion in saline (100 µl, corresponding to 66 µg mL-1 of Rhodamine B-Pluronic P123 conjugate) or an aqueous solution containing an equivalent amount of free rhodamine B (100µl, 52 µg mL-1). The formulations were intra-tracheally administered by using a Microsprayer® (Model 1A-1B, PennCentury, USA).

At 5 min, 1 h, 3 h and 24 h 5 after treatment and under anesthesia, the carotid artery was cannulated for blood collection and, after euthanization, bronchoalveolar lavage (BAL) and lungs were obtained. Briefly, the trachea was cannulated with a polyethylene tube (1 mm inner diameter) to perform BAL as previously reported [19]. Lungs were washed (three times) by flashing sterile ice cold PBS. The BAL was centrifuged to separate cells (BALC) from fluid (BALF), while blood was withdrawn in a glass tube and left for 24 h at 4°C to obtain serum. BALC and lungs were homogenized in PBS containing Triton 0.1%

2.7.3 Quantitative determination of PMM amount in BALF, lung and serum

Fluorescence emission of rhodamine B in biological samples deriving from treated animals was evaluated and compared to that of SHAM group. To this purpose, BALF (500 µL), BALC (200 µL) and lung homogenate samples were freeze dried, while fresh serum was processed.

For BALF and BALC analysis, freeze-dried samples were dispersed in 200 µL of ethanol and centrifuged at 5.000 rpm for 5 min. After centrifugation, 100 µL of supernatant were analyzed.

For lung tissue analysis, 10 mg of freeze dried powder were treated with 300 µL of ethanol and samples centrifuged at 13.000 rpm for 5 min.

After centrifugation, 100 µL of supernatant were collected for quantitative analysis.

For serum analysis, fresh samples (200 µL) were treated with the same volume of a 1:1 water/acetonitrile mixture for protein precipitation. The samples were then centrifuged at 13.000 rpm for 5 min and 100 µL of supernatant were analyzed.

To evaluate recovery, known amounts of Rho-PMM or free Rhodamine B were added to biological samples deriving from SHAM animals before freeze-drying and analysis.

In each case, the fluorescence of the sample was measured in 96 multi-wells on an ENVISION apparatus at Ex/Em 480/520 nm. A calibration curve was obtained by plotting fluorescence intensity versus the concentration of fluorescently-tagged Pluronic P123 solutions in ethanol. The linearity of the response was verified in the Pluronic P123concentration range of (equivalent to 0.2-0.0002 µg mL^{-1} of rhodamine B free) ($r^2 \geq 0.99$).

3 Results and discussion

The technological development of drug-based respiratory therapies in humans runs into the need of specifically tailored inhalable formulations able: i) to protect the encapsulated drug from in vitro/in vivo degradation; ii) to promote drug transport through mucus barriers and iii) to facilitate drug uptake by lung cells, the target of action. To this end, we choose PMM as nano-vehicle for the delivery of hydrophobic drugs to the lungs, since they are easy to formulate, have a low cost of production and promising features for pulmonary delivery [20]. In water, Pluronic P123/F127 mixed micelles (PMM) self-assemble as core-shell nanostructures. The micelle core promotes the solubilization of very hydrophobic drugs with high encapsulation efficiency as previously demonstrated [11] while the shell contributes to high stability and biocompatibility both in vitro and in vivo [20].

3.1 PMM stability in pulmonary-relevant media

PMM based on Pluronic P123/F127 mixtures 2:1 by wt formed nanostructures with size of 22 nm (PDI = 0.12) and zeta potential of -3.6 mV [11]. PMM are stable upon dilution up to 1:100 and do not disassemble in protein-rich media (Annex I and Pellosi et al., 2016, in press).

Indeed, stability of a new formulation in complex media is regarded as a critical factor since it has been demonstrated that micelles can aggregate/dissociate in different conditions, with a consequent poor therapeutic outcome [21]. Conceiving PMM for lung delivery of active species, the behavior of PMM in pulmonary relevant media was assessed by size and FRET measurements as previous described (Annex I and Pellosi et al., 2016, in press).

To this purpose, PMM co-encapsulating the two fluorophores nile red (NR) and verteporfin (FRET-PMM) were prepared at the 2:1 P123/F127 ratio by wt. As pulmonary relevant media we choose saline, mucin, artificial mucus and SILF. As shown in Fig. 1 PMM size increased of about 6 nm in SILF and 10 nm (from 23.0 nm in water – control experiment) in artificial mucus probably due the high ionic strength of these solutions. Results for Bio-PMM were comparable to those obtained for PMM.

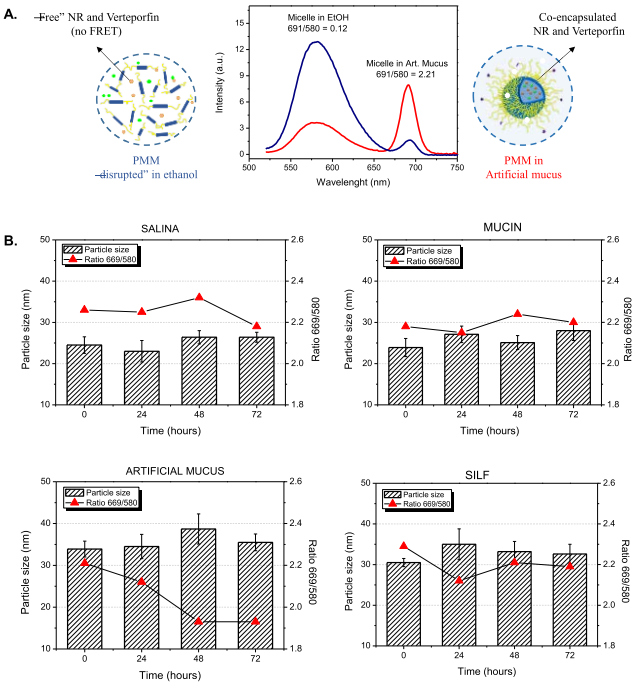

Fig. 1. Behavior of PMM loaded with NR (0.8 μg mL-1) and verteporfin (4.0 μg mL-1) in pulmonary relevant media. A) Fluorescence emission spectra of co-encapsulated dyes in artificial mucus solution (red line) and diluted in ethanol (blue line) at λex = 480 nm. B) Particle size (bars) and fluorescence intensity ratio between verteporfin emission at 690 nm and NR emission at 580 nm (symbols) for salina, mucin, artificial mucus and SILF solutions. Rhodamine B-conjugated P123 was not used to avoid spectral interferences. Data are reported as mean of three independent experiments (n=3) ±SD.

Independently of the medium, no significant difference in FRET signal and size was observed for up to 72 h for PMM. Of note, a similar tendency was observed for biotinylated PMM (data not shown) indicating that insertion of the target moiety at present condition did not alter PMM stability. Our results suggest that the steric hindrance and slight negative zeta potential conferred by the poly(ethylene oxide) (PEO) corona offers efficient protection and stability to PMM structure. Furthermore, PMM allow efficient entrapment and no significant release of the fluorophores utilized for FRET measurements. Taken all together, these data augur well for further development of PMM formulations for lung delivery of hydrophobic drugs.

3.2 PMM behavior in mucin-containing media

Micelle formulations will be released in vivo in the lung mucus, which could not only disassemble PMM, but may also prevent them from reaching the target. In this scenario, the assessment of mucoadhesive properties of the developed micelles is also fundamental to the development of clinically-relevant pulmonary drug delivery systems. Mucoadhesion studies were thus performed by measuring the turbidity at 650 nm (ABS) of PMM dispersions in mucin over time (Fig. 2A).

A.

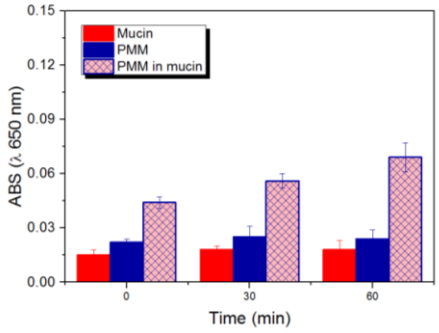

B.

Mucin	ζ potential (mV SD)	
-	-4.43	1.26
+	-5.20	0.87

Fig. 2. Mucoadhesive tendency of PMM: (a) turbidimetry at 650 nm of PMM dispersions either in water or in a saturated mucin solution as a function of time; (b) ζ potential of PMM in the presence (+) or not (−) of mucin (ζ potential of the control mucin dispersion was −8.73 ±0.69 mV). Data are mean ±SD of values calculated on 3 different batches (n=6).

The ABS values of reference mucin and PMM dispersions did not significantly differ (ranging from 0.01 to 0.02). Only a slight increase in turbidimetry was observed for PMM-mucin dispersions during time up to an absorption value as low as 0.09, which could not be considered indicative of PMM/mucin interactions. This hypothesis was supported by ζpotential values of PMM, which were not significantly different in the presence or not of mucin (Fig. 2B), confirming the poor mucoadhesive tendency of PMM. Of note, biotinylation did not result in a different PMM behavior in mucin (data not shown).

To go in depth into PMM tendency to interact with airway mucus, Rho-PMM underwent diffusion studies in a previously-developed in vitro model consisting of a layer of artificial airway mucus applied on solidified gelatin [17][12].Ascan be seen in Fig. 3, a high percent of Rho-PMM was found in gelatin after 24 h. Visual inspection (Fig. 3A) associated with quantitative data of permeation (Fig. 3 B) demonstrated a rapid and continuous penetration of the developed PMM through the mucus layer allowing a homogeneous dispersion of the formulation in the gelatin layer after 24 h. Again, biotinylation did not alter PMM penetration profile in artificial mucus model (data not shown).

In line with results of mucoadhesion tests, the facilitated transport of PMM through the artificial mucus model suggests poor PMM/mucin interactions and a consequent ability of PMM to penetrate inside mucus. Indeed, several literature data indicate that mucoinert NPs modified at surface with poly(ethylene glycol) may deeply penetrate a variety of human lung mucus secretions independently upon their viscosity. In particular, Pluronic F127-coated poly(lactide-co-glycolide) NPs rapidly penetrated fresh undiluted human mucus, with only a 10-fold reduced speed in mucus compared to their theoretical speeds in water. This effect is likely due to a reduction of hydrophobic and/or electrostatic interactions with mucus components.

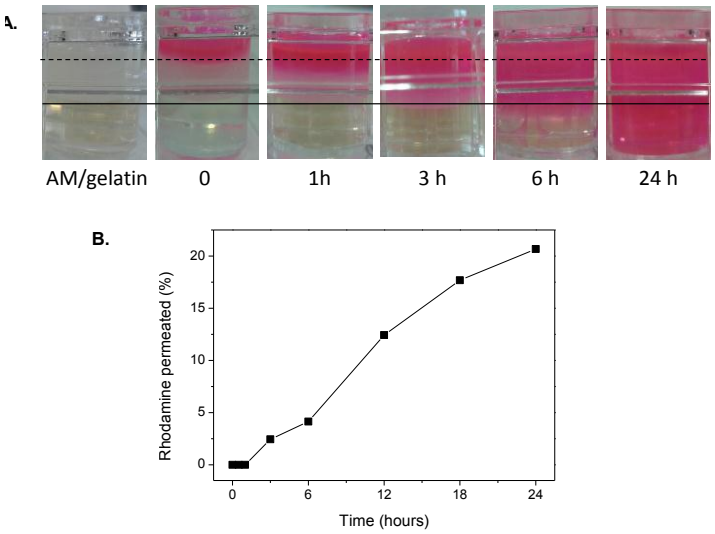

Fig. 3. In vitro assessment of Rho-PMM interaction with artificial airway mucus (AM). A) Visual inspection of penetration through an AM layer at different times (---- artificial mucus layer, — gelatin layer). B) kinetic profile of rhodamine B permeation inside gelatin (total percent of rhodamine B permeated after 24 h = 21.3%).

3.3 Developing dry powders for pulmonary delivery of PMM

NP aqueous liquid dispersions can be delivered through commercially available nebulizers to generate an aerosol with a 1-5 μm droplet size to achieve the desirable distribution in lungs [5].However, low delivery time efficiency and low formulation stability in water solutions are challenges for the practical applications of NP-based liquid formulation. To overcome these limitations, formulations can be engineered through the incorporation in an inert micron-scale dry powder. These particles, also termed as nano-embedded microparticles (NEMs), may be prepared by spray-drying with adequate technological properties to reach deep lung and to locally release NPs after the dissolution of inert carrier [12][22]. Thus, we developed NEM by co-spray drying of PMM and an inert sugar, lactose, with proved biocompatibility in pulmonary delivery and also with good properties for NEM production[23]. Both lactose and

Pluronics are soluble/dispersable in water media allowing the preparation of NEM without the use of organic solvents.

With the aim to optimize the production process, three aqueous dispersions, at different PMM/lactose ratios by weight (1:1, 1:10 and 1:20) were individually spray-dried. Rho-PMM were selected for formulation studies to permit the fully characterization of the system. The 1:1 Rho-PMM/lactose formulation produced a sticky dry powder unsuitable for inhalation purposes likely due the high concentration of the gel-type Pluronic P123 in the spray-dried mixture. Nevertheless, good powders with high recovery yields (78.0 and 81.9%, respectively) were achieved at the lower PMM/lactose ratios of 1:10 and 1:20.

Nanostructure integrity is a very important pre-requisite for NEM therapeutic application since NP disruption implies the loss of the encapsulated drug and a potential reduced therapeutic outcome [5]. In order to verify if the structure of PMM was not disrupted during spray-drying process. FRET-PMM were prepared and spray-dried with lactose at the selected PMM/lactose ratios. After production, the resulting dry powders were suspended in water to dissolve lactose without disrupting the PMM structure - if present - for size and FRET studies. Of note, both formulations presented very similar hydrodynamic diameters and FRET signal compared to the solutions pre-spray drying (data not shown), which clearly demonstrated that Pluronic s are assembled as PMM even after processing at high temperatures.

Micron-sized dry powders were achieved in both cases, with mean geometric volume diameters ranging between 7.2 and 8.1 μm. In addition, tapped density and Carr‘s index values along with the estimation of MMADt confirmed the good flow properties of the developed formulations likely suitable for lung deposition (Table 1). Indeed, a crucial factor to consider when developing inhalable dry powders relies on their aerosolization properties. In vitro aerosol performance of spray-dried formulation was assessed according to Pharmacopoeia test through NGI. The seven NGI stages produce cutoff diameters in the range 8.06-0.34 μm, with cup 3 to CMO (4.66-0.34 μm) representing deep lung airways. Results presented in Table 1 demonstrated that both formulations have good aerosolization properties, with approximately 95% of the capsule content being emitted during aerosolization, very high FPF and a suitable MMADexp.

Table 1. Flow and aerosolization properties of NEM based on Rho-PMM and lactose (value ±SD calculated on 3 different batches; n=6).

	Rho-PMM/lactose 1:10 (w/w)	**Rho-PMM/lactose 1:20 (w/w)**
Volume mean diameter[a] (µm ±SD)	8.08 ±1.85	7.24 ±2.70
Tapped density[b] (g/mL ±SD)	0.25±0.05	0.13±0.04
$MMAD_t$[c] (µm ±SD)	4.04 ±0.80	2.58 ±0.58
Carr's index[b]	15.3 ± 0.8	16.8 ±1.9
Emitted dose (% ±SD)	93.5 ±2.0	96.8 ±2.9
Fine particle fraction (% ±SD)	58.8 ±3.5	62.0 ±4.0
$MMAD_{exp}$[c] (µm ±GSD[d])	4.9 ±0.7	4.4 ±1.3

[a] Mean geometric diameter as determined by laser light diffraction analysis.

[b] Tapped density and flowability index (Carr's index) were estimated according to Ph.Eur. VII ed.

[c] Theoretical ($MMAD_t$) and experimental ($MMAD_{exp}$) Mass Mean Aerodynamic Diameter.

[d] Geometrical standard deviation.

In each case, the aerodynamic assessment of fine particles upon delivery from DPI confirmed that the developed formulation have a great potential for lung deposition of PMM, and consequently their drug cargo, in deep lungs.

Once again, functionalization of Pluronic micelles did not influence significantly the results (data not show).

3.4 PMM biodistribution after pulmonary delivery in rats

Since flow and aerosolization properties of PMM/lactose 1:10 and 1:20 formulations were very similar, we decided to work in the formulation condition ―1:10" because higher contents of PMM means a higher content of the drug and, subsequently, a higher dose.

To allow a proof of principle of the potential the developed PMM for in vivo drug delivery to the lung, biodistribution studies were performed upon intra-tracheal aerosolization of a micelle dispersion in saline. The amount of Rho-PMM in BALF, BALC and lung tissue during time was evaluated and results reported as fluorescence intensity (FI).

To fully understand the behavior of the PMM after intra-tracheal administration, the distribution in BALF, serum and lung at time 0 of the Rho-PMM dispersion was compared to that of a solution containing an equivalent amount of free rhodamine B. Results showed that the amount of free Rho B in BALF was much lower than that of micelles presumably due to its fast distribution in lung tissue and serum (Fig. 4A).Kinetics of micelle persistence in the BALF (Fig. 4B) showed that Rho-PMM are still present in the rat lung after 24 h and are able to reach dry lung tissue (Fig. 4C). Furthermore, no significant amount of PMM was found in BALC at each time interval (data not shown).

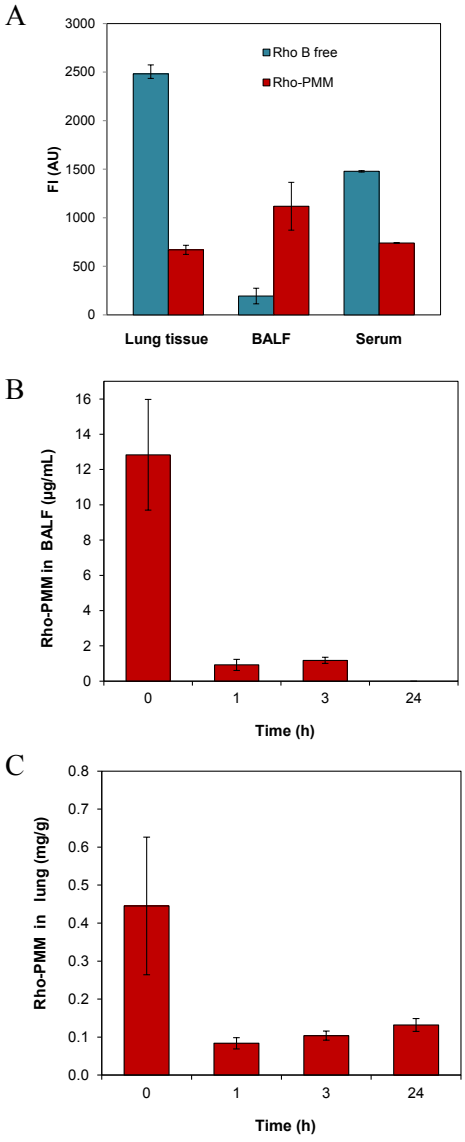

Fig. 4. Fluorescence in lung homogenate, BALF and serum after intratracheal administration of Rho-PMM (100 □L, 1 mg). Animal were sacrificed after 5 min (A). Amount of Rho-PMM in BALF (B) and dry lung (C) along time. For sample treatment see materials and methods. Data are mean ± SD of values calculated on 5 animals.

References

1. D'Angelo I, Conte C, La Rotonda MI, Miro A, Quaglia F, Ungaro F: Improving the efficacy of inhaled drugs in cystic fibrosis: Challenges and emerging drug delivery strategies.*Advanced Drug Delivery Reviews* 2014, 75: 92-111.

2. Loira-Pastoriza C, Todoroff J, Vanbever R: Delivery strategies for sustained drug release in the lungs.*Advanced Drug Delivery Reviews* 2014, 75: 81-91.

3. Ibrahim BM, Park S, Han B, Yeo Y: A strategy to deliver genes to cystic fibrosis lungs: A battle with environment.*J Controlled Release* 2011, 155: 289-295.

4. Pazetti R, Pego-Fernandes PM, Jatene FB: Adverse Effects of Immunosuppressant Drugs upon Airway Epithelial Cell and Mucociliary Clearance: Implications for Lung Transplant Recipients.*Drugs* 2013, 73: 1157-1169.

5. D'Angelo I, Conte C, Miro A, Quaglia F, Ungaro F: Pulmonary Drug Delivery: A Role for Polymeric Nanoparticles?*Current Topics in Medicinal Chemistry* 2015, 15: 386-400.

6. Carvalho TC, Peters JI, Williams RO: Influence of particle size on regional lung deposition - What evidence is there?*Int J Pharm* 2011, 406: 1-10.

7. Andrade F, das Neves J, Gener P, Schwartz S, Ferreira D, Oliva M *et al*.: Biological assessment of self-assembled polymeric micelles for pulmonary administration of insulin.*Nanomedicine-Nanotechnology Biology and Medicine* 2015, 11: 1621-1631.

8. Batrakova EV, Kabanov AV: Pluronic block copolymers: Evolution of drug delivery concept from inert nanocarriers to biological response modifiers.*J Controlled Release* 2008, 130: 98-106.

9. Yang Y, Tsifansky MD, Shin S, Lin QN, Yeo Y: Mannitol-Guided Delivery of Ciprofloxacin in Artificial Cystic Fibrosis Mucus Model.*Biotechnology and Bioengineering* 2011, 108: 1441-1449.

10. Chen R, Wang X, Yao X, Zheng X, Wang J, Jiang X: Near-IR-triggered photothermal/photodynamic dual-modality therapy system via chitosan hybrid nanospheres.*Biomaterials* 2013, 34: 8314-8322.

11. Pellosi DS, Tessaro AL, Moret F, Gaio E, Reddi E, Caetano W *et al*.: Pluronic (R) mixed micelles as efficient nanocarriers for benzoporphyrin derivatives applied to photodynamic therapy in cancer cells.*Journal of Photochemistry and Photobiology A-Chemistry* 2016, 314: 143-154.

12. Ungaro F, D'Angelo I, Coletta C, Bianca RDD, Sorrentino R, Perfetto B *et al*.: Dry powders based on PLGA nanoparticles for pulmonary delivery of antibiotics: Modulation of encapsulation efficiency, release rate and lung deposition pattern by hydrophilic polymers.*J Controlled Release* 2012, 157: 149-159.

13. Shi C, Khan SA, Wang KP, Schneider M: Improved delivery of the natural anticancer drug tetrandrine.*Int J Pharm* 2015, 479: 41-51.

14. Yang YT, Chen CT, Yang JC, Tsai TM: Spray-Dried Microparticles Containing Polymeric Micelles Encapsulating Hematoporphyrin.*Aaps Journal* 2010, 12: 138-146.

15. Zhang XC, Jackson JK, Burt HM: Development of amphiphilic diblock copolymers as micellar carriers of taxol.*Int J Pharm* 1996, 132: 195-206.

16. Moss OR: Simulants of lung interstitial fluid.*Health Phys* 1979, 36: 447-448.

17. Rossi S, Ferrari F, Bonferoni MC, Caramella C: Characterization of chitosan hydrochloride-mucin interaction by means of viscosimetric and turbidimetric measurements.*European Journal of Pharmaceutical Sciences* 2000, 10: 251-257.

18. Yang M, Lai SK, Wang YY, Zhong WX, Happe C, Zhang M *et al*.: Biodegradable Nanoparticles Composed Entirely of Safe Materials that Rapidly Penetrate Human Mucus.*Angewandte Chemie-International Edition* 2011, 50: 2597-2600.

19. Ungaro F, Giovino C, Coletta C, Sorrentino R, Miro A, Quaglia F: Engineering gas-foamed large porous particles for efficient local delivery of macromolecules to the lung.*European Journal of Pharmaceutical Sciences* 2010, 41: 60-70.

20. Costabile G, D'Angelo I, Rampioni G, Bondi R, Pompili B, Ascenzioni F *et al*.: Toward Repositioning Niclosamide for Antivirulence Therapy of Pseudomonas aeruginosa Lung Infections: Development of Inhalable Formulations through Nanosuspension Technology.*Molecular Pharmaceutics* 2015, 12: 2604-2617.

21. Chen LC, Sha XY, Jiang XY, Chen YZ, Ren QY, Fang XL: Pluronic P105/F127 mixed micelles for the delivery of docetaxel against Taxol-resistant non-small cell lung cancer: optimization and in vitro, in vivo evaluation.*International Journal of Nanomedicine* 2013, 8: 73-84.

22. Moore TL, Rodriguez-Lorenzo L, Hirsch V, Balog S, Urban D, Jud C *et al*.: Nanoparticle colloidal stability in cell culture media and impact on cellular interactions.*Chemical Society Reviews* 2015, 44: 6287-6305.

23. Li XJ, Vogt FG, Hayes D, Mansour HM: Design, Characterization, and Aerosol Dispersion Performance Modeling of Advanced Co-Spray Dried Antibiotics with Mannitol as Respirable Microparticles/Nanoparticles for Targeted Pulmonary Delivery as Dry Powder Inhalers.*Journal of Pharmaceutical Sciences* 2014, 103: 2937-2949.

24. Pilcer G, Amighi K: Formulation strategy and use of excipients in pulmonary drug delivery.*Int J Pharm* 2010, 392: 1-19.